MICROCOPY RESOLUTION TEST CHART

NATIONAL BUREAU OF STANDARDS 1963 A

AD A124072

12

DTIC
SELECTED
FEB 3 1983

B

SCIENCE APPLICATIONS, INC.

83 02 03 030

RADIATION SOURCES AT

ELECTRON CYCLOTRON HARMONIC FREQUENCIES

FINAL REPORT

SAI-83-134-WA

SCIENCE APPLICATIONS, INC.

Post Office Box 1303, 1710 Goodridge Drive, McLean, Virginia 22102, (703) 821-4300

RADIATION SOURCES AT

ELECTRON CYCLOTRON HARMONIC FREQUENCIES

SAI-83-134-WA

January 28, 1983

Prepared by:

Y.Y. Lau
D. Dialetis
A. Drobot
A. Palevsky

Prepared for:

The Naval Research Laboratory
4555 Overlook Avenue
Washington, D.C. 20375

DTIC
SELECTED
FEB 3 1983

B

Science Applications, Inc.

1710 Goodridge Drive
P.O. Box 1303
McLean, VA 22102
(703)821-4300

REPORT DOCUMENTATION PAGE		READ INSTRUCTIONS BEFORE COMPLETING FORM
1. REPORT NUMBER SAI-83-134-WA	2. GOVT ACCESSION NO. *AD-7124 C72*	3. RECIPIENT'S CATALOG NUMBER
4. TITLE *(and Subtitle)* Radiation Sources at Electron Cyclotron Harmonic Frequencies		5. TYPE OF REPORT & PERIOD COVERED Final 7/79 - 4/80
		6. PERFORMING ORG. REPORT NUMBER
7. AUTHOR(*s*) Y.Y. Lau A. Drobot D. Dialetis A. Palevsky		8. CONTRACT OR GRANT NUMBER(*s*) N00173-79-C-0450
9. PERFORMING ORGANIZATION NAME AND ADDRESS Science Applications, Inc. 1710 Goodridge Dr., P.O. Box 1303 McLean, VA 22102		10. PROGRAM ELEMENT, PROJECT, TASK AREA & WORK UNIT NUMBERS
11. CONTROLLING OFFICE NAME AND ADDRESS Naval Research Laboratory 4555 Overlook Avenue Washington, D.C. 20375		12. REPORT DATE January 28, 1983
		13. NUMBER OF PAGES 132
14. MONITORING AGENCY NAME & ADDRESS(*If different from Controlling Office*)		15. SECURITY CLASS. (*of this report*) Unclassified
		15a. DECLASSIFICATION/DOWNGRADING SCHEDULE

16. DISTRIBUTION STATEMENT *(of this Report)*

Distribution Unlimited

> DISTRIBUTION STATEMENT A
> Approved for public release;
> Distribution Unlimited

17. DISTRIBUTION STATEMENT *(of the abstract entered in Block 20, if different from Report)*

18. SUPPLEMENTARY NOTES

19. KEY WORDS *(Continue on reverse side if necessary and identify by block number)*

Radiation source, electron cyclotron frequency, gyrotron, travelling wave amplifier, numerical cold testing.

20. ABSTRACT *(Continue on reverse side if necessary and identify by block number)*

This work covers an initial investigation of gyrotron devices operating in cylindrical geometry. Specific topics include an analysis of oscillations in a gyrotron travelling wave amplifier, the study of the effects of velocity spread and wall resistivity on gain and bandwidth in a gyrotron travelling wave amplifier, an investigation of mode competition in a cylindrical gyrotron cavity, and finally, a numerical cold

DD FORM 1473 EDITION OF 1 NOV 65 IS OBSOLETE
1 JAN 73
S/N 0102-014-6601

TABLE OF CONTENTS

DISCUSSION

This final report covers the period of July 1979 through April 1980, and describes the work performed under contract N00173-79-C-0450, titled "Radiation Sources at Electron Cyclotron Harmonic Frequencies."

This work covers an initial investigation of gyrotron devices operating in cylindrical geometry. Specific topics include an analysis of oscillations in a gyrotron travelling wave amplifier, the study of the effects of velocity spread and wall resistivity on gain and bandwidth in a gyrotron travelling wave amplifier, an investigation of mode competition in a cylindrical gyrotron cavity, and finally, a numerical cold testing of cavity modes in cylindrical structures.

1.1 Analysis of Oscillations in the Gyrotron Travelling Wave Amplifier

This work was fully reported in NRL Memo Report 4303, which is included here as Appendix A to this report. It was found that the convective instability which forms the basis of the gyrotron travelling wave amplifier may become absolute (non-convective) at a sufficiently high current level. This results in oscillation rather than amplification. This threshold current for the transition depends sensitively on the applied magnetic field. The axial wavelength and the characteristic frequency of oscillation at the onset of

1

absolute instability are given. It is found that momentum
spread has virtually no effect on the threshold current.
A small amount of resistive wall loss, however, raises the
threshold current significantly. Oscillations due to
partical reflections at the ends of the system are also
examined. Preliminary experimental results on both type
of oscillations are reported and are found to be in agree-
ment with the theory.

1.2 Effects of Velocity Spread and Wall Resistivity on the Gain and Bandwidth of the Gyrotron Travelling Wave Amplifier

This work was fully reported in NRL Memo Report
4304, which is included as Appendix B. to this report.
In this report the small signal gain bandwidth of the
gyrotron travelling wave amplifier (gyro-TWA) operating
at the fundamental cyclotron harmonic is examined.

The analytical and numerical studies focus on the
effects of velocity spread in the electron beam and of a
distributed wall resistivity in the waveguide. It is
found that wall resistivity reduces the forward gain of
the amplifier only by an amount approximately equal to
1/3 of the corresponding cold tube loss. Significant
increase in bandwidth may result, under certain conditions,
from the presence of wall resistivity. A moderate amount
(5-10%) of velocity spread does not reduce the peak gain
significantly in general, but may reduce the bandwidth by

an amount depending on the applied magnetic field. Based on considerations of such factors as power, stability, gain, bandwidth, and efficiency, we tentatively conclude that the optimum operating parameters for the gyro-TWA would be a beam current on the order of 10 amps, a wall resistivity with a skin depth on the order of 5×10^{-3} of the wall radius, and a magnetic field about 2 percent below the grazing value.

A study has been made of mode competition in a cylindrical gyrotron cavity. The examined model is as follows: Before entering the cavity, the electron beam consists of equally spaced rings with radius r_L, equal to the Larmor radius. Their guiding centers lie at a distance r_0 from the axis of the cylindrical cavity. Each ring carries a discrete number of electrons (usually 16 to 32 electrons). Initially, all the electrons have the same axial and normal velocity. The mode frequencies and spatial structure are unperturbed by the presence of the beam, since the beam is tenuous. Space charge effects are neglected. Therefore, the equations of motion of each electron are independent of the other electrons.

The efficiency for each mode is computed by solving the equations of motion for all the electrons on the rings. In the nonlinear regime, each efficiency depends on all the amplitudes of the modes present in the cavity. It was shown that the efficiencies converge to a fixed value as the number of rings increases and all other parameters remain constant. In each case studied, a sufficient number of rings was chosen to ascertain convergence.

For given beam power, the amplitudes of the modes present in the cavity were computed by solving a nonlinear set of algebraic equations which express the balance of power for

4

each mode when the system is at a steady state. In this
case, the power deposited to each mode by the electron beam
is equal to the power radiated by the mode under consideration.
The following basic assumption for mode excitation was made:
For fixed beam voltage, as the beam current (or beam power)
is increased from zero to some value, the system traces a
sequence of steady states (as defined above). The mode with
the lowest threshold is excited first. As the beam current
is increased beyond the lowest threshold value, a new mode
is excited if this is allowed by the presence of the other
modes in the cavity (i.e. if the set of nonlinear algebraic
equations, mentioned above, does have a solution). This is
a valid assumption since the rising or decay time of the
fields is much smaller than the rising time of the beam current.
The basic results are presented as plots which express the
functional dependence of the efficiency and radiated power
of each mode versus beam power.

For given beam power, a nonlinear algebraic system may
have more than a single real solution and only one of these
solutions is physically acceptable. A different approach to
the one mentioned above (namely, the solution of the nonlinear
algebraic system) has been devised which provides the necessary
information in selecting the physically acceptable solution
for given beam power. The information is contained in contour

plots of certain functions which depend on the amplitudes
of the modes. These functions depend also on the parameters
of the electron beam and the cavity but they are independent
of the Q's of the modes. Therefore, the same contour plots
can be used for another cavity with different Q's for each
mode. This is an advantage of this approach over that of
solving the nonlinear set of algebraic equations which depend
on the specific Q values of the modes for the cavity under
consideration. The contour plots have been a valuable tool
in the determination of the physically acceptable solution
for given beam power, particularly in cases where a jump of
the radiated power occurs for a particular mode as the beam
power slightly increases.

Two cases were examined:

i) TE_{011}, TE_{012} modes present in the cavity and the
first cyclotron harmonic is excited.

ii) TE_{021}, TE_{022} modes present in the cavity and the
second cyclotron harmonic is excited.

The preliminary conclusions are as follows:

a) The Q's for each mode are important in the
determination of mode competition.

b) For modes with azimuthal symmetry, there is
indication that, as the beam power builds up, the
mode with axial eigennumber $\ell = 1$ will eventually
exclude all other higher order modes in the cavity.

c)   There is indication that a mode with infinite
      threshold beam power may be excited through the
      excitation of other modes first and subsequent
      mode conversion.

Details, and results are presented in Appendix C.

1.4 Numerical Cold Testing

The MASK electromagnetic particle in cell computer code is a flexible tool which has the ability to simulate a wide variety of physical systems. This section will describe the use of the MASK code for "cold testing" cavity structures. We give a brief description of the method and present some sample results.

Experimental cold testing of cavity structures to find both eigenfrequencies and mode patterns is a difficult problem. A numerical solution is free of practical hardware problems, and can indeed give a better answer, since the cavity is in no way perturbed.

The section of MASK relevant to this problem is the Maxwell field propagator. If a point disturbance, a delta function in both time and space, is introduced into the cavity, the code will properly evolve the resulting fields in time. Because of the completeness theorem, the initial delta function disturbance must contain all the eigenmodes of the structure.

As the time proceeds, the code saves a complete time history of both the electric and magnetic fields, produced by the disturbance, at a number of spatial locations. This information can be Fourier analyzed to find what frequencies exist at each location. This are the eigenmodes of the cavity.

Finally, the structure can be driven at each frequency of interest for a number of periods. The resulting field patterns can be used to identify the mode.

As an example, a simple structure, consisting of a right circular cylinder was driven by imposing a noise pulse at one spatial location, for one time step. The mode was then allowed to run for a number of cavity transit times, with field information saved at several spatial locations. The use of more than one spatial location ensures that the accidental placement of one sample point at a mode null, will not cause the cold test to miss a particular frequency.

When a Fourier transform is performed for the data stored at each spatial point, a cavity spectrum results. A sample of such a spectrum is shown in Figure 1. As can be seen from the figure, a number of modes exist for this cavity. Each peak can be identified by driving the cavity at that frequency.

A number of point "antennas" are placed into the cavity, and they are driven at the appropriate frequency for a number of cycles. The TE_{011} mode was driven, and the resulting field plots are shown in Figure 2. In each plot, the figure must be rotated about the center line (as marked) to obtain a three dimensional figure. Each plot is a contour plot of a particular field component.

9

The top one is the azimuthal electric field, the middle
one is the axial magnetic field, and the lower one is the
radial magnetic field.

When the same cavity is driven at one of the other
peaks, the frequency for the TE_{013} mode, Figure 3 results.
This is indeed the mode pattern for this second mode.

In summary, this technique is a straight forward
method for determining the resonant frequency and mode
patterns for arbitrary cavities. For a simple cavity,
as in the example, field patterns identical to text book
figures result. The real power of the technique is that
any arbitrary configuration can be tested with equal ease.

10

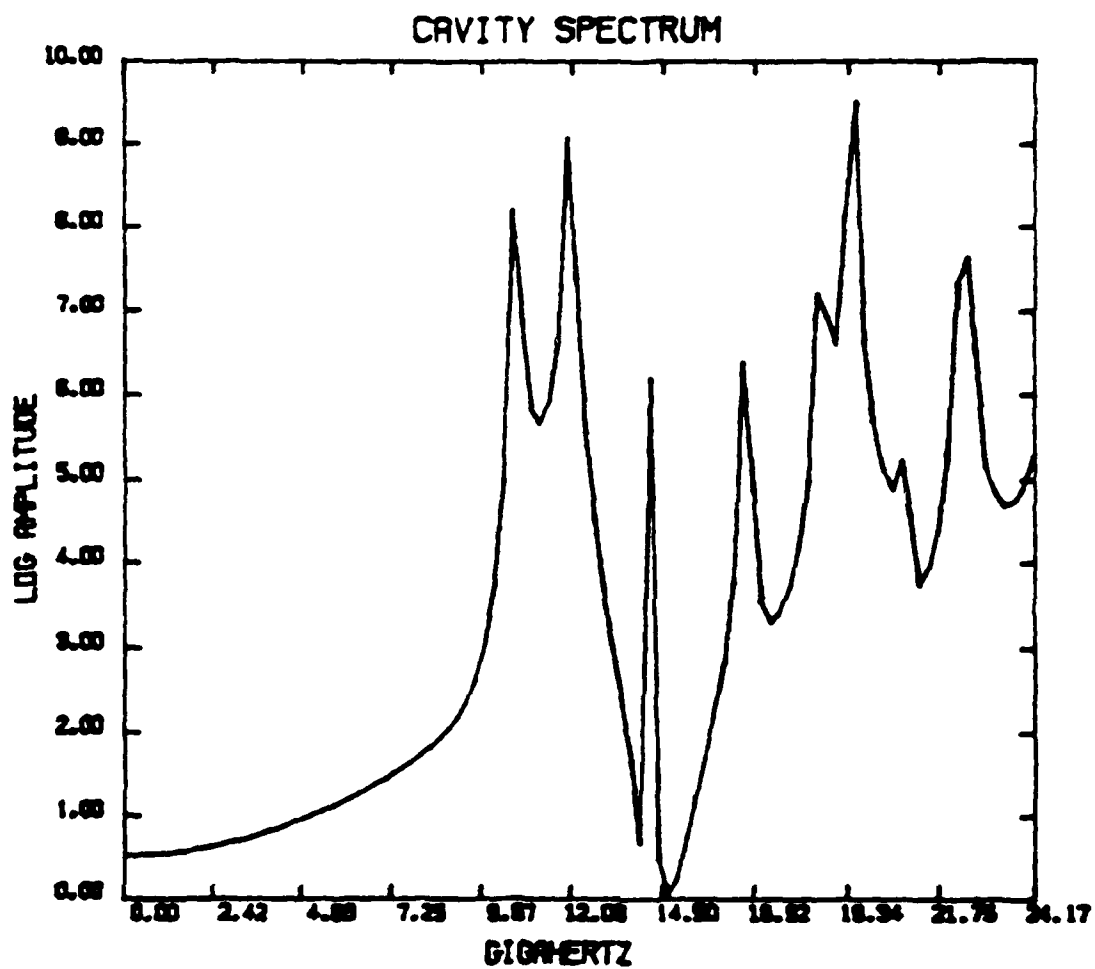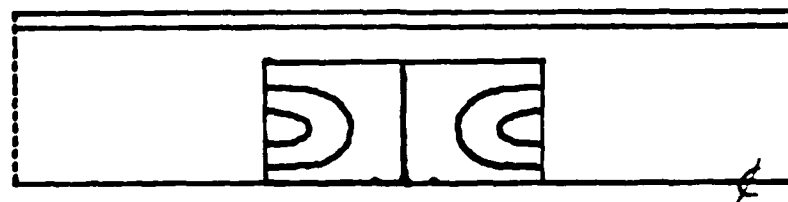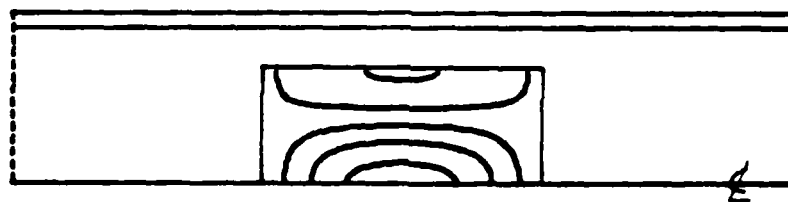Figure 1.   Cavity spectrum of right cylindrical
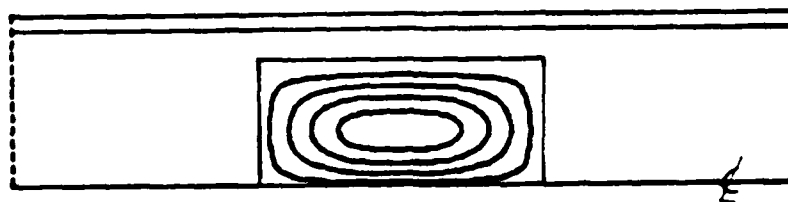cavity.

11

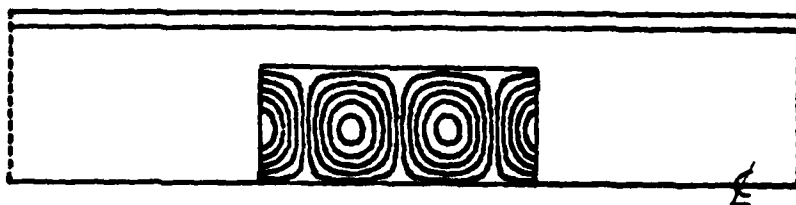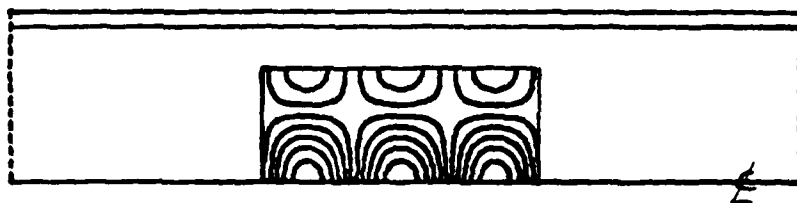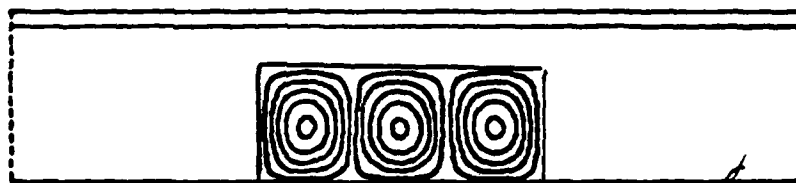Figure 2. Right cylindrical cavity with TE_{011} mode driven.

12

Figure 3.   Right cylindrical cavity with TE₀₁₃ driven.

13

APPENDIX A

ANALYSIS OF OSCILLATIONS IN THE GYROTRON
TRAVELLING WAVE AMPLIFIER

Y.Y. LAU
K.R. CHU
L. BARNETT
V.L. GRANATSTEIN

CONTENTS

ANALYSIS OF OSCILLATIONS IN THE GYROTRON TRAVELLING WAVE AMPLIFIER

I. INTRODUCTION

Current experiments performed at NRL on the gyrotron travelling wave amplifier (gyro-TWA) have yielded record power levels at millimeter wavelengths.[1,2] However, the presence of unwanted oscillations has thus far prevented the operations of the amplifier in the optimum regime[2]. Significant improvement in performance is anticipated with the suppression of these unwanted oscillations. The main purpose of the present work is to investigate the possible causes of these oscillations and thereby to suggest ways for their suppression.

Oscillations are generally caused by either an external or an internal feedback process. The external feedback is provided by reflections at both ends of the interaction region. If the amplitude of the reflected signal reaches a certain level that the loop gain exceeds unity, the wave amplification processes become regenerative and oscillation consequently takes place. The internal feedback is a result of the dispersiveness of the unstable medium. Under certain conditions, the wave may grow locally without propagating axially out of the system. As a result, large amplitude waves can simply grow from noise level perturbations. Unlike those caused by end reflections, oscillations produced by internal feedback processes received comparatively little attention. Their considerations have special importance for the gyro-TWA in that the optimum operating regime of a gyro-TWA happens to border on the transition from the convective instability (amplification) to the absolute instability (oscillation).[3] Careful study of the internal feedback processes can therefore provide a guide for acheiving optimum operation of the gyro-TWA without the excitation of absolute instabilities.

Experimentally, there is convincing evidence that both types of oscillations are excited in the gyro-TWA operated at NRL. The two types of oscillations have different characteristics. Toward the

end of this paper, we shall briefly describe the experimental results in the light of the present theoretical study. The details of these experiments have been reported elsewhere.[2]

We shall first [Sec. II] present a quantitative study of the threshold current above which an absolute instability would be excited as a result of internal feedback processes. The influence of velocity spread and resistive wall loss on the threshold current will also be examined. We next consider oscillations caused by external reflections in Section III, where experimental observations of both types of oscillations are reported.

II. INTERNAL FEEDBACK MECHANISMS—CONDITION FOR
THE ONSET OF ABSOLUTE INSTABILITY

When operated near the "grazing condition," the mildly relativistic electron beam of the gyro-TWA interacts most effectively with the waveguide.[4,5] This "grazing condition" is achieved when the longitudinal velocity of the beam is equal to the group velocity of the forward wave of the waveguide mode. If the beam-wave coupling (determined by the current strength and magnetic field match, etc.) is sufficiently weak, the beam will only couple to the forward waveguide mode. The gyro-TWA would then operate according to what is expected of a convective instability.[3] However, if the coupling is sufficiently strong, the backward wave of the guide mode would be excited. The excitation of these backward waves might then provide an internal feedback mechanism, resulting in an absolute instability which would manifest itself as a natural oscillation of the system. (Under these conditions, care must be exercised to intepret the gain curve of the "amplifier".[6])

The critical current which marks the transition to absolute instability depends sensitively on the magnetic field. It is obtained by using the stability criterion of Briggs and Bers.[3] The analysis is based on the assumption that the system is infinitely long. The characteristic frequency and wavenumber at the transition based on such an analysis would, however, shed light on the required length (starting length) of the system if it is to avoid these natural oscillations.

A-4

The result is summarized as follows. If both velocity spread and wall resistivity are absent, and if the applied magnetic field is maintained near the grazing condition, a convective instability sets in at a relatively low current. This convective instability becomes an absolute one if the current (beam strength) exceeds a certain critical value. This critical value is given analytically [cf. Eq. (10)] in terms of the waveguide dimension, electron parallel and perpendicular velocities, and the applied magnetic field. At the onset of the absolute instability, the oscillation frequency and the axial wavenumber are also given analytically. It is found that typically the oscillation frequencies are almost identical (but slightly less than) with the cut-off frequency of the waveguide. We found that velocity spread in the beam has virtually no effect on the threshold current for the transition to absolute instability. The presence of a small amount of distributed wall resistivity would, however, raise the threshold current significantly. It can be shown that such a distributed wall loss does not significantly reduce the gain of the amplifier.[7] In this regard, the presence of wall resistivity offers the best hope to render the amplifier stable at high current level.

In Section II-a, we present the details of the analysis for the case of a cold beam situated in a lossless waveguide. The method developed there has been extended to the studies of a beam with finite temperature in Section II-b. Finally, in Section II-c, we present the results for a lossy waveguide.

a. Cold Beam, Lossless Waveguide:

The typical configuration of a gyro-TWA (Fig. 1) consists of an annular electron beam propagating inside a waveguide of circular cross section of radius r_w. The electrons, guided by a uniform magnetic field $(B_0 \, e_z)$, move along helical trajectories. Ideally, all electrons have the same perpendicular velocity $v_{\perp 0}$, and the same parallel velocity (v_{z0}), with their guiding centers uniformly distributed on a surface of constant radius r_0 (Fig. 1). The dispersion relation for the interaction between this cold beam and the TE_{mn} waveguide mode (m, n being, respectively, the azimuthal and radial mode numbers) at the s-th cyclotron harmonic frequency has been derived in Ref. (5). It reads

$$\omega^2 - k_z^2 c^2 - k_{mn}^2 c^2 = \frac{-4\nu c^2}{\gamma_0 r_w^2 K_{mn}} \left[\frac{(\omega^2 - k_z^2 c^2) \beta_{\perp 0}^2 H_{sm} (k_{mn} r_0, k_{mn} r_{\perp 0})}{(\omega - k_z v_{z0} - s\Omega_c)^2} \right.$$

$$\left. - \frac{(\omega - k_z v_{z0}) Q_{sm} (k_{mn} r_0, k_{mn} r_{\perp 0})}{\omega - k_z v_{z0} - s\Omega_c} \right].$$ (1)

where ω is the frequency of the mode, k_z is the axial wavenumber, $\gamma_0 = (1 - v_{z0}^2 c^2 - v_{\perp 0}^2 c^2)^{-1/2}$, $\beta_{\perp 0} = v_{\perp 0}/c$, $\Omega_c = eB_0/\gamma_0 mc$, $r_{Lo} = v_{\perp 0}/\Omega_c$, $k_{mn} = X_{mn}/r_w$, X_{mn} is the n-th root of $J'_m(x) = 0$, $J_m(x)$ is the Bessel function of order m, $J'_m(x) = dJ_m(x)/dx$, $\nu \equiv Ne^2/mc^2$ is a dimensionless beam density parameter, N is the number of electrons per unit axial length, and the functions K_{mn}, H_{sm}, Q_{sm} are defined as follows:

$$K_{mn} = J_m^2(X_{mn}) [1 - m^2/X_{mn}^2],$$
$$H_{sm}(x,y) = \left[J_{s-m}(x) J'_s(y) \right]^2.$$

and

$$Q_{sm}(x,y) = 2H_{sm}(x,y) + y \left[J_{s-m}^2(x) J'_s(y) J''_s(y) + \frac{1}{2} J_{s-m-1}^2(x) \right.$$

$$\left. \cdot J'_s(y) J'_{s-1}(y) - \frac{1}{2} J_{s-m-1}^2(x) J'_s(y) J'_{s-1}(y) \right].$$

Instability occurs at wave frequency and axial wavenumber such that $\omega^2 - k_z^2 c^2 - k_{mn}^2 c^2 \cong 0$ and $\omega - k_z v_{z0} - s\Omega_c \cong 0$. Hence the second term on the right hand member of Eq. (1) can usually be ignored in comparison with the first term. We can further approximate $\omega^2 - k_z^2 c^2$ by $k_{mn}^2 c^2$ in the right hand side of (1). Thus, Eq. (1) is simplified to

$$(\omega^2 - k_z^2 c^2 - k_{mn}^2 c^2) (\omega - k_z v_{z0} - s\Omega_c)^2 = - \frac{4\nu c^2}{\gamma_0 r_w^2 K_{mn}} (k_{mn}^2 c^2) \beta_{\perp 0}^2 H_{sm}.$$ (2)

Henceforth, we shall concentrate on the stability analysis according to Eq. (2).

It is convenient to normalize the frequency ω with respect to the cutoff frequency $\omega_c \equiv k_{mn} c$ and k_z to k_{mn}. Then Eq. (2) is written in dimensionless form as

$$(\bar{\omega}^2 - \bar{k}^2 - 1)(\bar{\omega} - \bar{k}\beta_{\parallel} - b)^2 = - \epsilon,$$ (3)

where $\bar{\omega} \equiv \omega/\omega_c$; $\bar{k} \equiv k_z/k_{mn}$; $\beta_{\parallel} \equiv v_{z0}/c$; and the dimensionless parameters b and ϵ are defined by

$$b \equiv s\Omega_c/\omega_c$$ (4a)

$$\epsilon \equiv \frac{4\nu c^2 \beta_{\perp 0}^2 H_{sm}}{\gamma_0 r_w^2 K_{mn} \omega_c^2}.$$ (4b)

A-6

Note that b is proportional to the magnetic field and ϵ is a measure of the beam strength. Typically, ϵ is a very small number, on the order of 10^{-5} (or even less). As an example[2], take $m = 0$, $s = n = 1$, $\beta_{\perp 0} = .4$, $\beta_{\parallel 0} = .266$, $\omega_c/2\pi = 34.3$ GHz, $r_w = .533$ cm. Then

$$\epsilon = 3.78 \times 10^{-6} \, I \tag{4c}$$

where I is the beam current in units of ampere.

In the limit of zero beam strength ($\epsilon = 0$) the waveguide modes

$$\bar{\omega}^2 - \bar{k}^2 - 1 = 0, \tag{5a}$$

and the beam mode

$$\bar{\omega} - \bar{k}\beta_{\parallel} - b = 0, \tag{5b}$$

are decoupled [cf. Fig. (2)]. The coupling of these two modes is strongest when the dispersion curve of the beam mode is tangent to the waveguide mode [cf. Fig. (2)]. This occurs when the magnetic field is adjusted so that $b = b_0$, where

$$b_0 \equiv (1 - \beta_{\parallel}^2)^{1/2}. \tag{6}$$

In the following, we shall assume that $\beta_{\parallel}$ is fixed, and that b is in the vicinity of b_0. We shall then study the properties of the dispersion relation (3) as ϵ, the beam strength, is varied. This way of fixing parameters is suitable for comparison with experiments.[1,2]

We state here the principal results. The details of derivations of these results are given in the Appendices.

(i) If $b \geqslant b_0$, there is an instability whenever $\epsilon > 0$. This instability can either be convective or absolute. These statements are proven in Appendix A.

(ii) If $b = b_0$ (i.e., exact grazing condition), there is a convective instability if $0 < \epsilon < \epsilon_{cg}$. This instability becomes an absolute one when $\epsilon > \epsilon_{cg}$ where ϵ_{cg} is defined by

$$\epsilon_{cg}^{1/4} = (27)^{1/4} \sqrt{\beta_{\parallel}} \, \bar{k}_{sg}, \tag{7}$$

$$\bar{k}_{sg} = (\bar{\omega}_{sg} - b_0) / 4 \beta_{\parallel}, \tag{8}$$

$$\bar{\omega}_{sg} = \frac{(b_0 + 6\sqrt{2} \, \beta_{\parallel}^2)}{1 + 8\beta_{\parallel}^2}. \tag{9}$$

Furthermore, at the onset of the absolute instability, (i.e., $\epsilon = \epsilon_{cg}$), the characteristic wavenumber $\bar{k}_{sg}$ and frequency $\bar{\omega}_{sg}$ are given by Eqs. (8) and (9) respectively. Note that the wavenumber at the onset of absolute instability is purely real. This general result is demonstrated in Appendix B. The proof of the rest of the statements in this paragraph is given in Appendix C.

(iii) For $b \cong b_0$, the onset of the absolute instability occurs when $\epsilon = \epsilon_c$, where ϵ_c is defined by

$$\epsilon_c^{1/4} = (27)^{1/4} \sqrt{\beta_{||}} \, \bar{k}_s, \tag{10}$$

$$\bar{k}_s = \frac{1}{4\beta_{||}} (\bar{\omega}_s - b), \tag{11}$$

$$\bar{\omega}_s = \frac{b + [8\beta_{||}^2(1 - b^2) + 64\beta_{||}^4]^{1/2}}{1 + 8\beta_{||}^2} \tag{12}$$

Again, $\bar{k}_s$ and $\bar{\omega}_s$ are respectively the wavenumber and frequency of oscillation at the onset of the absolute instability. It is clear that Eqs. (10)-(12) reduce to (7)-(9) when $b = b_0$, i.e., when the gyro-TWA is operated exactly at the grazing condition.

The numerical values of the critical beam strength, as well as the corresponding frequency of oscillations and wavenumber, can readily be computed for various values of $\beta_{||}$ and b from Eqs. (7)-(12). Listed in Table 1 are the values generated from Eqs. (7)-(9) which physically correspond to the exact grazing condition. Note from the last column of this table that the threshold beam current (measured by ϵ_{sg}) increases with $\beta_{||}$. This result can readily be threshold beam current (measured by ϵ_{sg}) increases with $\beta_{||}$. This result can readily be understood by noting that at higher axial beam velocity, disturbances convect away at a higher rate. To couple the forward propagation of disturbances with the backward waveguide mode, a condition for the excitation of absolute instabilities[3], a stronger current is required. In Table 2, we fix $\beta_{||}$ at .266. We then calculate the threshold current at various values of magnetic field strength. We note that if the magnetic field is below the grazing value, a higher beam current is necessary in order to excite the absolute instability, because the beam mode and the waveguide mode are away from perfect synchronism. If the magnetic field is above the grazing value, the unstable spectrum readily extends to negative values of k_z and the absolute instability is easily excited. In the event that the beam mode (Fig. 2) intersects with the backward waveguide mode

the absolute instability sets in as long as the beam current is non zero. In the last two columns of Table 2, we have assumed that the threshold current I is related to ϵ by Eq. (4c). Note further that the oscillation frequency of these oscillations is slightly less than the cutoff frequency of the waveguide.

In the current gyro-TWA experiments at NRL[1,2], $\beta = .266$, $\omega_c/2\pi = 34.3$ GHz and $k_{mn} = 7.18$ cm^{-1} for the TE_{01} mode. If the magnetic field is maintained at the grazing condition $(b/b_0 = 1)$ then an oscillation at a frequency of 34.26 GHz is predicted to occur when the beam current is raised beyond .588 amps as a result of absolute instability [cf., Row (5) in Table II]. Experimentally, an oscillations at 34.27 GHz was indeed observed[8] at a beam current of 1 amp as the magnetic field is raised to the vicinity of the grazing condition. The actual threshold current observed should be somewhat higher than the predicted value as the latter was made for an infinitely long waveguide whereas in reality a finite length waveguide was used and coupling out the ends was not included in the present calculation. We shall discuss in greater detail the experimental results in Section III.

b. Warm Beam, Lossless Waveguide:

We have studied the effects of the velocity spread and energy spread on the threshold current above which an absolute instability is excited. In the NRL gyro-TWA experiments, the energy spread is minimal, of order 1% or less. The spread in the longitudinal velocity is considerably higher, on the order of 10 per cent. We found that, even if the velocity spread is as high as 20 percent, it has a negligible influence on the threshold current. In other words, momentum spread cannot stabilize the absolute instability. This seemingly surprising result can be understood as follows. The presence of an absolute instability requires the backward waveguide mode to be coupled to the forward beam mode[3]. The axial wavenumber k_z is thus constraint to a value in the vicinity of zero at the transition. [See also column 3 of Table II]. Now, the velocity spread $<\Delta v_z>$ modifies the dispersion relation by an amount on the order of $(k_z <\Delta v_z>)^2/\omega_c^2$, which is an exceedingly small quantity at the transition to the absolute instability by virtue of small value of k_z, leaving the threshold current calculated in the previous subsection essentially unchanged.

The above conclusions stem from our analysis of the dispersion relation which includes the effect of velocity spread and energy spread. measured respectively by $<\Delta v_z>/v_{z0}$ and $<\Delta \gamma>/\gamma_0$. Assuming that these quantities are small. we obtain the dispersion relationship

$$(\bar{\omega}^2 - \bar{k}^2 - 1)\left[(\bar{\omega} - \bar{k}\beta - b)^2 - \left(\bar{k}\beta \frac{<\Delta v_z>}{v_{z0}}\right)^2 - \left(\bar{\omega} \frac{<\Delta \gamma>}{\gamma_0}\right)^2\right] = -\epsilon. \qquad (13)$$

This equation can readily be compared with Eq. (3). where the symbols are defined. Equation (13) can be deduced from the one obtained by Uhm[9] who applied the idealized "water-bag" electron beam distribution function to the formulation developed earlier.[10]

Applying the techniques developed in the Appendices. we found that a velocity spread less than twenty percent has virtually no effect on the transition current. for reasons explained above. An energy spread less than half a percent actually slightly lowers the threshold current.

It should be emphasized that. while the momentum spread is not effective in suppressing the absolute instability. it can reduce the gain and bandwidth of the amplifier significantly[1]. Once the frequency of the input signal is above the cutoff frequency of the waveguide. k_z will increase significantly (in comparison with a value close to zero). The velocity spread will then have a significant effect on the gain [cf. Eq. (13)]. This observation is corroborated by the numerical studies on the gain and bandwidth of the amplifier reported in Refs. (1) and (7).

c. Cold Beam. Lossy Waveguide:

An attempt to stabilize the gyro-TWA is to coat the inner wall of the metallic waveguide with a layer of material of finite electrical conductivity. such as graphite.[8] A detail study of the effect of a resistive wall on the gain of the gyro-TWA is beyond the scope of this paper. Here we concentrate only on the dependence of threshold current on wall resistivity. It is found that even a small amount of wall loss increases the threshold current substantially.

Let δ be the skin depth of the wall material of the waveguide. Typically. $\delta/r_w << 1$ where r_w is the wall radius. In the limit of small δ/r_w. the dispersion relation reads[7]

$$\left\{\bar{\omega}^2 - \bar{k}^2 - \left[1 - \frac{\delta}{r_w}(i-1)\right]\right\}(\bar{\omega} - \bar{k}\beta - b)^2 = -\epsilon \tag{14}$$

which is again to be compared with Eq. (3). In obtaining Eq. (14), we have ignored the effect of velocity spread as it can hardly modify the threshold current. In passing, we remark that in the resistive wall experiments to be performed at NRL[8], $\delta/r_w \approx 2.6 \times 10^{-3}$, and that values of δ/r_w as high as 10^{-2} are reasonable in practice.

The analysis of Eq. (14) for the threshold current is more involved and will not be detailed here. Shown in Fig. (3) are the results. To obtain the data in this figure, we fix $\beta = .266$. The various curves correspond to different magnetic fields. They illustrate the threshold current as a function of δ/r_w (wall resistivity). It is seen that a small amount of wall resistivity can significantly increase the threshold current. That is, wall resistivity may render the gyro-TWA stable against the absolute instability. Shown in Table III are the data for $b/b_o = .98$ at the transition. Again, we have assumed that the beam current I is related to ϵ by Eq. (4c) in obtaining these results.

The increase of threshold current with wall resistivity may be understood qualitatively as follows. As the frequency of oscillation at transition is below the cutoff frequency of the waveguide, the backward wave of the waveguide mode attenuates in the *reverse* direction of beam propagation. This attenuation rate increases as wall resistivity (δ/r_w) increases. For an absolute instability to be excited, this attenuation rate must match the amplification rate of the forward beam mode. This matching requirement is just the alternative statement that a saddle point (i.e., merging of roots of k at a single frequency) must be present for the onset of absolute instability.[3] A higher beam current is thus needed to excite the absolute instability when wall resistivity is present. Note again that the oscillation frequency is just below the cutoff frequency of the waveguide at the transition, and that $\bar{k}_i$ is complex for reasons given above.

We point out that the internal feedback mechanism has recently been theoretically analyzed by Etlicher and Buzzi.[11] However, the main stabilizing influence of wall resistivity has not been included in their calculations. Their work, reported in a conference abstract[11], does not contain sufficient detail for a direct comparison with our work.

III. EXTERNAL FEEDBACK MECHANISMS AND EXPERIMENTAL OBSERVATIONS OF OSCILLATIONS.

Treating the length of the amplifier as infinite we study in the previous section the convective and absolute nature of the cyclotron maser instability. When an absolute instability first sets in. the frequency of oscillations is predicted to be just slightly less than the cutoff frequency of the waveguide. The axial wavenumber is typically 1/30 the transverse wavenumber of the waveguide. Thus. a short interaction length (as well as a resistive wall) may reduce the danger of exciting absolute instabilities.

In reality the gyro-TWA system is finite in length and an additional mechanism for oscillation is provided by partial reflections of the amplifying waves at the ends of the system. At high beam currents. the e-folding length of spatial amplification is very short. and a slight mismatch may convert an amplifier into an oscillator. Based on this argument. one can see that oscillations due to end reflection will inevitably set in at a high current level. regardless of how small a mismatch there is at the ends of the device. Oscillations induced by end reflections. as well as their suppressions. are well-known in the technology of travelling wave tubes. For the present case of the gyro-TWA. this type of oscillations will have frequencies higher than the cut-off frequency of the waveguide for only then would the gain of the amplifier be significant.[1] These statements appear to have been corroborated by the NRL experiments to be decribed below. Again. a resistive wall can (1) render the amplifier stable against this type of oscillations. and at the same time. (2) increase the bandwidth of the amplifier. without significantly sacrificing its gain.[7]

Instabilities have been routinely observed[2.8] during experimental operation of gyro-TWA operating in the TE_{01} circular-electric mode at 35.1 GHz at NRL. The physical design of the gyro-TWA uses a 0.533 cm radius. for a cutoff frequency of 34.30 GHz. copper waveguide 21 cm long. The parameters of the beam were designed to be v_{11} = .27 c and $v_\perp$ = .40 c. Typical linear (small signal) gains obtained were 24 db at a 3 ampere beam current and 32 db at 9 amps.

Typical oscillations occur at several discrete frequencies normally just above cutoff at 34.30 GHz. such as 34.38 GHz and 34.45 GHz. The power output of these oscillations is typically on the order of

the maximum saturated output during stable amplification. These oscillations can be induced from a stably operating amplifier by increasing the beam current and/or the magnetic field hence increasing the gain. These oscillations can be explained as follows.

The gyro-TWA is operated near the cutoff frequency of the interaction waveguide. The mechanism actually has considerable gain almost down to cutoff.[1] Even though the input and output couplers were carefully designed for low reflections throughout the useful bandwidth of the gyro-TWA, matching becomes impossible as the cutoff frequency is approached. Thus, reflection spikes are obtained near cutoff. Cold test reflection measurements indeed reveal reflections at the problem frequencies, namely, at 34.38 GHz and 34.45 GHz.

As the gyro-TWA beam current or magnetic field is increased the gain near cutoff is increased. The reflections constitute a feedback and when the net loop gain exceeds loop losses then oscillation sets in. This is evidenced by the oscillations at 34.38 GHz and at 34.45 GHz reported above.

Instability at just below empty waveguide cutoff has also been observed and is believed to be the absolute instability predicted in Sec. II. The conditions are as follows. At a beam current of 1 amp and cathode voltage of -70 kV, the magnetic field was scanned. The gain measured at 35.13 GHz peaked at 12.7 dB with 1230 watts output (unsaturated) at a magnetic field of 12.81 kG. As the magnetic field was increased the gain (at 35.13 GHz) dropped rapidly to ~0 db at 13.11 kG. Self-oscillation in the TE_{01}^0 mode at 34.45 GHz set in at a magnetic field of 13.15 kG at a power output level of 8.71 kW. This power level is on the order of maximum observed saturated amplifying power level. An observed (stable) maximum output power at saturation at 1 amp beam current was 5.75 kW with 4.3 db gain. As the magnetic field was raised the oscillations at 34.45 GHz continued. At 13.37 kG the 34.45 GHz oscillation ceased and another oscillation at 34.27 GHz was observed. This oscillation, slightly below the TE_{01}^0 cutoff, had an output power of 200 watts. At 13.41 kG the power output in this oscillation increased to 660 watts.

The experimental data reported here is limited. At the time the data was taken [1] we were unaware of potential absolute instabilities or their characteristics. Close attention will be made to absolute instabilities in future experiments. However, we tentatively interpret the above data as follows.

As the magnetic field is increased to the peak gain point measured at 35.13 GHz (corresponding to a grazing condition), the gain near cutoff, i.e., 34.30 GHz to 34.50 GHz, is too low to sustain reflection type oscillations. As the magnetic field is increased past the peak gain point (at 35.13 GHz) the gain is still increasing near cutoff until sufficient loop gain is attained for oscillation at 34.45 GHz. As the magnetic field is increased beyond grazing, the threshold current for the absolute instability rapidly decreases. When the absolute instability becomes dominate, then oscillation occurs in that mode. The calculations of the threshold indicate that the absolute instability should occur even at grazing, i.e., the calculated threshold current is 0.588 amp. However, the calculation was made for an infinitely long waveguide when realistically a finite length waveguide was used and coupling out the ends was not included. Thus we would expect the actual threshold to be somewhat higher than indicated in Table II. The lower power level output seems reasonable since the power is essentially coupled out the end rather than propagated out.

We then have several points supporting our belief in the observation of the absolute instability. (i) The oscillation was slightly below cutoff in TE_{01}^0 mode exactly at the predicted value; (ii) the power output level was substantially lower than the routinely observed reflective oscillations indicating a different type of instability; and (iii) as predicted, the absolute instability set in as the magnetic field was raised. Although the reflection type instability seems to be the most dominant, especially at higher current levels, this absolute instability could be important in gyro-TWA design with regard to methods of overall stabilization.

An attractive method to suppress both types of oscillations is to add loss to the circuit to decrease the loop gain. This also raises the threshold current for the excitation of absolute instabilities. Furthermore, calculations[7] show that the forward gain in a distributed loss waveguide circuit is only decreased by approximately one-third the cold tube loss in dB per unit length. Thus stability would be

obtained with only a slight decrease in forward gain. In addition, wall loss leads to bandwidth improvement.

ACKNOWLEDGMENT

REFERENCES

1. J.L. Seftor, V.L. Granatstein, K.R. Chu, P. Sprangle and M.E. Read, "The Electron Cyclotron Maser as a High-Power Travelling Wave Amplifier of Millimeter Waves," IEEE J. Quantum Electronics Vol. QE-15, pp. 848-853 (1979).

2. L.R. Barnett, K.R. Chu, J.M. Baird, V.L. Granatstein, and A.T. Drobot," Gain, Saturation, and Bandwidth Measurements of the NRL Gyrotron Travelling Wave Amplifier," IEDM Technical Digest, pp. 164-167, (Dec. 1979).

3. R.J. Briggs, *Electron Stream Interaction with Plasma*, MIT Press, Cambridge, Mass. (1964).

4. K.R. Chu, A.T. Drobot, H.H. Szu, and P. Sprangle, "Theory and Simulation of the Gyrotron Travelling Wave Amplifier Operating at Cyclotron Harmonics," IEEE Trans. MTT, Vol. MTT-28, pp. 313-317 (1980).

5. K.R. Chu, A.T. Drobot, V.L. Granatstein and J.L. Seftor, "Characteristics and Optimum Operating Parameters of a Gyrotron Travelling Wave Amplifier," IEEE Trans. Microwave Theory Tech., Vol. MTT-27, pp. 178-187 (1979)

6. See, e.g., Ref. 3, p. 38, 131,167.

7. Y.Y. Lau and K.R. Chu, and L. Barnett, "Effects of Velocity Spread and Wall Resistivity on the Gain and Bandwidth of the Gyrotron Travelling Wave Amplifier," to be published.

8. L. Barnet, et. al., to be published.

A-15

9.   H.S. Uhm and R.C. Davidson, "Influence of Energy and Axial Momentum Spreads on the Cyclo-tron Maser Instability in Intense Hollow Electron Beams," Phys. Fluids, Vol. 22, pp 1804-1810 (1979)

10.   K.R. Chu, "Theory of Electron Cyclotron Maser Interaction in a Cavity at the Harmonic Frequencies," Phys. Fluids, Vol. 21, pp. 2354-2364 (1978).

11.   B. Etlicher and J.M. Buzzi, "Study of the Synchrotron Maser Absolute Instabilities", Third International Topical Conference on High Power Electron and Ion Beam Research and Technology (July 3-6, 1979, Novosibirsk, USSR, p. 105).

12.   A.W. Trielpiece and R.W. Gould, "Space Charge Waves in Cylindrical Plasma Columns," J. Applied Phys: Vol. 30, pp. 1784-1793 (1959).

APPENDIX A

Presence of an Instability Whenever $b \geqslant b_0$.

In this Appendix, we prove that there is always an instability (which can either be absolute or convective) whenever the magnetic field is higher than that at the grazing condition. It suffices[3] to show that, whenever $\epsilon > 0$ and $b \geqslant b_0$, there is always a pair of complex roots of $\bar{\omega}$ for some real values of $\bar{k}$, say, at $\bar{k} = \beta_{11}/b$. With $\bar{k} = \beta_{11}/b$, Eq. (3) can be written as

$$(y^2 - 1)(y - a)^2 = -\epsilon_1, \tag{A1}$$

where

$$y \equiv \bar{\omega} b / (b^2 + \beta_1^2)^{1/2}, \tag{A2}$$

$$a \equiv (\beta_{11}^2 + b^2)^{1/2}, \tag{A3}$$

$$\epsilon_1 \equiv \epsilon \, b^4 / (b^2 + \beta_{11}^2)^2. \tag{A4}$$

Note that

$$a \geqslant 1 \tag{A5}$$

since

$$\beta_{11}^2 + b^2 = 1 + (b^2 - b_0^2) \geqslant 1 \quad \text{if} \quad b \geqslant b_0.$$

As a function of y, $f(y) \equiv (y^2 - 1)(y - a)^2$ is sketched in Fig. 4. As easily seen from this figure, the equation $f(y) = -\epsilon_1$ admits at least a pair of complex roots of y whenever $\epsilon_1 > 0$. From (A2) and (A4), we conclude that $\bar{\omega}$ has at least a pair of complex roots as long as $\epsilon > 0$.

APPENDIX B

Onset of Absolute Instability at Real Values of k.

In this Appendix, we prove that when an absolute instability first sets in, the wavenumber is always real. This result is useful because it considerably restricts our search in wavenumber space in the calculation of the critical beam strength that marks the transition to absolute instability.

At the transition, the frequency $\bar{\omega} = \bar{\omega}_s$ is real. For this value of $\bar{\omega}_s$, there is a double root[3] of $\bar{k}$. Below, we prove that this double root is real.

Since $\bar{\omega} = \bar{\omega}_s$ is real, and Eq. (3) is a fourth degree polynomial of $\bar{k}$ with *real* coefficients, all four roots $\bar{k}_1, \bar{k}_2, \bar{k}_3, \bar{k}_4$ of Eq. (3) must either be real or appear as complex conjugate pairs. We shall first assume that the above-mentioned double root has a nonvanishing imaginary part and then show that a contradiction results.

Denote the real and imaginary part of the double root $\bar{k}_1, \bar{k}_2$ to be k_{sr} and k_{si}. If $k_{si} \neq 0$, the other two roots $\bar{k}_3, \bar{k}_4$ must also be a double root since the roots occur in conjugate pairs. In this case, Eq. (3) may be written as

$$
\begin{aligned}
&(\bar{k} - \bar{k}_1)(\bar{k} - \bar{k}_2)(\bar{k} - \bar{k}_3)(\bar{k} - \bar{k}_4) \\
&= (\bar{k} - k_{sr} - i k_{si})^2 (\bar{k} - k_{sr} + i k_{si})^2 \\
&= \bar{k}^4 + \bar{k}^3 (-4k_{sr}) + \bar{k}^2 (6 k_{sr}^2 + 2 k_{si}^2) \\
&\quad + \bar{k} \left[-4k_{sr}(k_{sr}^2 + k_{si}^2)\right] + (k_{sr}^2 + k_{si}^2)^2 = 0.
\end{aligned}
\tag{B1}
$$

On the other hand, equation (3) may also be written as

$$
\begin{aligned}
&\bar{k}^4 + \bar{k}^3 \left[2\left(\frac{b - \bar{\omega}_s}{\beta_{\shortparallel}}\right)\right] + \bar{k}^2 \left[\left(\frac{b - \bar{\omega}_s}{\beta_{\shortparallel}}\right)^2 - (\bar{\omega}_s^2 - 1)\right] \\
&+ \bar{k}\left[-2(\bar{\omega}_s^2 - 1)\left(\frac{b - \bar{\omega}_s}{\beta_{\shortparallel}}\right)\right] - \frac{\epsilon}{\beta_{\shortparallel}} - (\bar{\omega}_s^2 - 1)\left(\frac{b - \bar{\omega}_s}{\beta_{\shortparallel}}\right)^2 = 0.
\end{aligned}
\tag{B2}
$$

A-18

Since (B1) and (B2) are the same equation, the coefficients must be the same. Thus,

$$-4k_{sr} = 2(b - \bar{\omega}_s)/\beta ,$$ (B3)

$$6k_{sr}^2 + 2k_{si}^2 = \left[\frac{b - \bar{\omega}_s}{\beta_1}\right]^2 - (\bar{\omega}_s^2 - 1) ,$$ (B4)

$$-4k_{sr}(k_{sr}^2 + k_{si}^2) = -2(\bar{\omega}_s^2 - 1)\left[\frac{b - \bar{\omega}_s}{\beta}\right] .$$ (B5)

Dividing (B3) by (B5), we obtain

$$-(\bar{\omega}_s^2 - 1) = k_{sr}^2 + k_{si}^2 .$$ (B6)

Using (B6) and (B3), we express the right hand member of (B4) as

$$\left[\frac{b - \bar{\omega}_s}{\beta_1}\right]^2 - (\bar{\omega}_s^2 - 1) = 5k_{sr}^2 + k_{si}^2 .$$ (B7)

Clearly, (B7) contradicts (B4) if $k_{si} \neq 0$. We conclude then that the assumption that $k_{si} \neq 0$ is false.

Hence at the transition to absolute instability, the wavenumber $\bar{k}_s$ must be real.

APPENDIX C

Detailed Study of Absolute and Convective Instability at the Grazing Condition.

We shall focus our attention to the case where $b = b_0$. The dispersion relation (3) reads

$$D(\omega,k) \equiv [k^2 - (\omega^2 - 1)]\left[k - \frac{\omega - b_0}{\beta_1}\right]^2 = \frac{\epsilon}{\beta_1^2}, \qquad (C1)$$

where, in this Appendix, we have dropped the bar in ω and k for convenience. Since the beam strength ϵ enters only in the RHS of (C1), we shall examine the detailed property of $D(\omega,k)$. In the present study of transition to absolute instability, we need only to consider real values of ω and k. [Cf. Fig. 5]. Since the onset of an absolute instability always occurs at a multiple root of *real* k (Cf. Appendix B), we need only to focus our attention at those values of k in Figs. 5 for which $D(\omega,k)$ is stationary. Moreover, since $\epsilon \geq 0$, only non-negative values of $D(\omega,k)$ are considered.

We first determine the trajectories of the roots in the complex k plane as the imaginary part of ω changes from 0 to $-\infty$. [Cf. Fig. 6a.]* This consideration is necessary to distinguish an absolute from convective instability.[3] As $\omega \rightarrow -i\infty$, among the four roots of k in Eq. (C1), three roots would tend to $-i\infty$ and *only* the fourth root would tend to $+i\infty$. Note that the fourth root (let us designate it to be k_4) corresponds to the waveguide mode which propagates in the opposite direction of the beam velocity. If the movement of the roots is in accordance with that depicted in Fig. (6b), a convective instability sets in when ϵ is slightly increased. On the other hand, if the roots move according to Fig. (6c), an absolute instability would set in when ϵ is raised to a higher level. In other words, an absolute instability sets in only if the merging of roots in the k plane involves the backward wave mode of the waveguide. This result perhaps is anticipated from the outset because the internal feedback, which is required for an oscillation, can be provided for only by the wave supported by the waveguide which propagates in the reverse direction of the beam. This wave can be excited only if the beam strength is so high that all modes are strongly coupled.

---

*We assume that the solutions assume a dependence of $\exp(i\omega t - ikz)$.

From these considerations, we then see that the merging of k roots at $k = \beta_{\shortparallel}/b_o$ in Fig. (5b) must correspond to the outset of a convective instability since the merging roots arise from the beam mode and the *forward* wave mode of the waveguide. This convective instability sets in as long as $\epsilon > 0$, in agreement with the conclusion of Appendix A. As ϵ is raised slightly above zero, we encounter another double root of k [cf. k_4 in Fig. (5c.d)]. This double root of k, however, does *not* correspond to an absolute instability since the merging of the roots does not involve the backward wave of the waveguide mode either.

Examination of Fig. 5 shows that the only multiple root which involves both the backward wave and the (forward) beam mode is k_{sg} as shown in Fig. (5f). Thus the onset of absolute instability occurs when $\epsilon = \epsilon_{cg}$, where ϵ_{cg} is given by [cf. (C1)]

$$\epsilon_{cg} = \beta_{\shortparallel}^2 D(\omega_{sg}, k_{sg}) \qquad (C2)$$

and ω_{sg}, k_{sg} are the *real* root determined from the conditions

$$\left. \frac{\partial D}{\partial k} \right|_{\omega_s, k_s} = 0. \qquad (C3)$$

$$\left. \frac{\partial^2 D}{\partial^2 k} \right|_{\omega_s, k_s} = 0. \qquad (C4)$$

A little algebra yields the relevant solution

$$\omega_{sg} = \frac{b_0 + 6\sqrt{2}\beta_{\shortparallel}^2}{1 + 8\beta_{\shortparallel}^2}. \qquad (C5)$$

$$k_{sg} = \frac{1}{4\beta_{\shortparallel}}(\omega_{sg} - b_0). \qquad (C6)$$

These equations are just in Eqs. (9), (8) of the main text. Substitution of (C5) and (C6) into (C2) gives Eq. (7).

A few remarks concerning our calculations are in order. It can readily be shown from Eq. (9) that $\overline{\omega}_{sg}$ is always less than unity. This fact that oscillation may occur at a frequency lower than the cutoff frequency of the waveguide is hardly a surprising result. It is well-known[12] that when a waveguide is loaded with a plasma, modes with a frequency below the cutoff frequency of the waveguide can exist.

In the present case, the waveguide is partially loaded with the beam, which itself constitutes an active medium. This brings out another point which at first sight may also seem a bit paradoxical. At the grazing condition, one may then ask, how can an absolute instability ever exist as the beam mode and the waveguide mode both propagate in the forward direction? The answer is that at very low beam current, both modes are weakly coupled and indeed no absolute instability exists according to the usual notion of coupling of modes. However, as a sufficiently high current level, both modes are strongly coupled. In fact, *all* modes are coupled, including the waveguide mode which propagates in the opposite direction of the beam. The excitation of the latter modes provides an internal feedback and is the basic reason for the possible excitation of an absolute instability. [Cf. Fig. (5f)].

Table I. The dimensionless frequency $(\bar{\omega}_{sr}$ and wavenumber $(\bar{k}_{sr})$ at the onset of absolute instability $(\epsilon = \epsilon_{sr})$ for various β. Magnetic field is maintained at the grazing condition.

β	b_c	$\bar{\omega}_{sr}$	$\bar{k}_{sr}$	ϵ_{sr}^2
0	1	1	0	0
.1	0.995	0.99985	0.01216	0.00877
.2	0.9798	0.9994	0.0245	0.0250
.3	0.9539	0.9986	0.0372	0.0465
.4	0.9165	0.9974	0.0506	0.0729
.5	0.8660	0.9958	0.0649	0.1046
.6	0.8000	0.9935	0.0806	0.1423
.7	0.7141	0.9902	0.0986	0.1881
.8	0.6000	0.9854	0.1204	0.2455
.9	0.4359	0.9771	0.1503	0.3251

Table II. Data for the transition to absolute instability at various magnetic field strength (b/b_0) with β fixed at 0.266. Shown are the normalized characteristic frequency $(\bar{\omega}_s)$, wavenumber $(\bar{k}_s)$, threshold current (I) and the axial wavelength (λ_z) at the transition.

b/b_0	$\bar{\omega}_s$	$\bar{k}_s$	I (amps)	λ_z (cm)
.92	.990471	.097383	45.42	8.98
.94	.99327	.081894	22.71	10.68
.96	.995634	.065996	9.58	13.25
.98	.997531	.049659	3.07	17.613
1.00	.998920	.032845	0.588	26.625
1.02	.999759	.015514	0.02925	56.377

Table III. Data for transition to absolute instability at various values of wall resistivity (δ/r_w). Here $\beta = .266$, $b/b_0 = .98$. Note that if $\delta \neq 0$, $\bar{k}_s$ is complex, and that $\bar{\omega}_s \leq 1$.

δ/r_w	$\bar{\omega}_s$	$\bar{k}_s$	I (amps)
0	.997531	(.049659, 0)	3.07
.002617	.996291	(.036153, - .05302)	5.567
.005234	.996123	(.02889, - .067291)	7.684
.007851	.996193	(.023109, - .07763)	9.955
.010468	.996391	(.018168, - .08602)	12.391

Fig. 1 — Cross sectional view of the gyro-TWA. The applied magnetic field points out of the paper.

$$\bar{\omega}^2 = \bar{k}^2 + 1 \quad \text{(WAVEGUIDE MODE)}$$

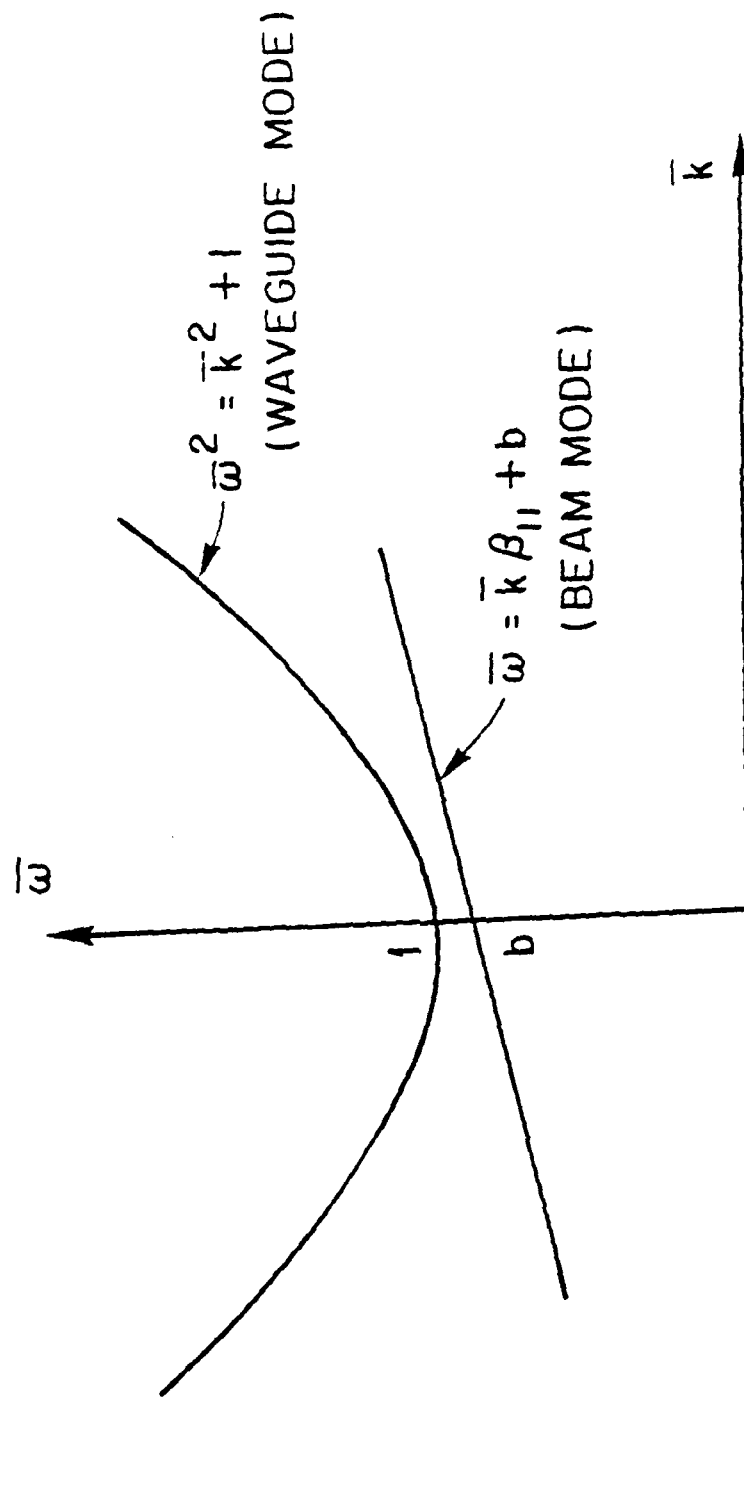$$\bar{\omega} = \bar{k}\beta_{11} + b \quad \text{(BEAM MODE)}$$
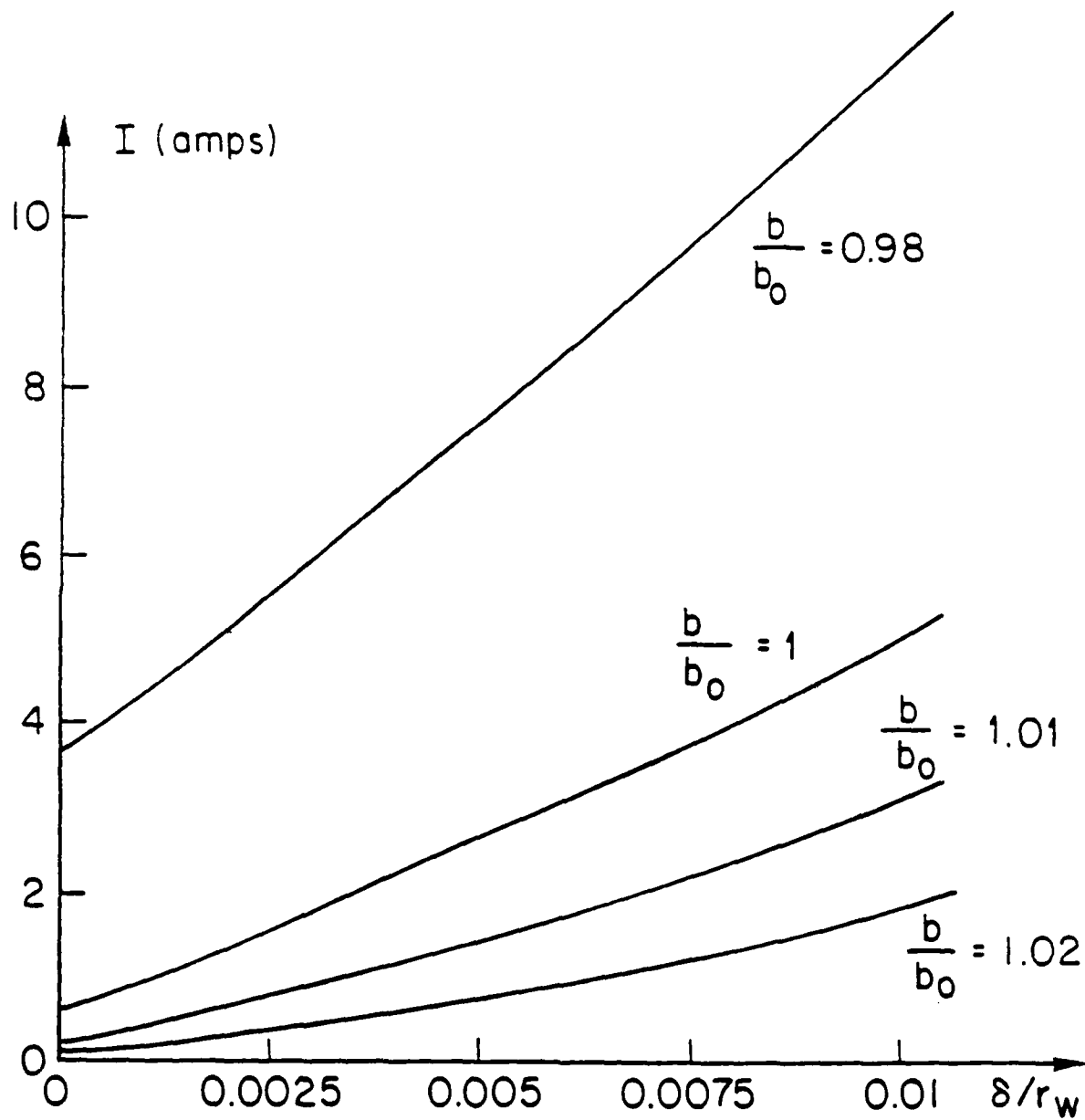
Fig. 2 — The waveguide mode and the beam mode.

A-25

Fig. 3 — Threshold current (I) as a function of skin depth (wall resistivity) at various magnetic field strength (b/b_n). Here $\beta_{11} = 0.266$, $\omega_c/2\pi = 34.3 GHz$ and $r_n = 0.533$ cm.
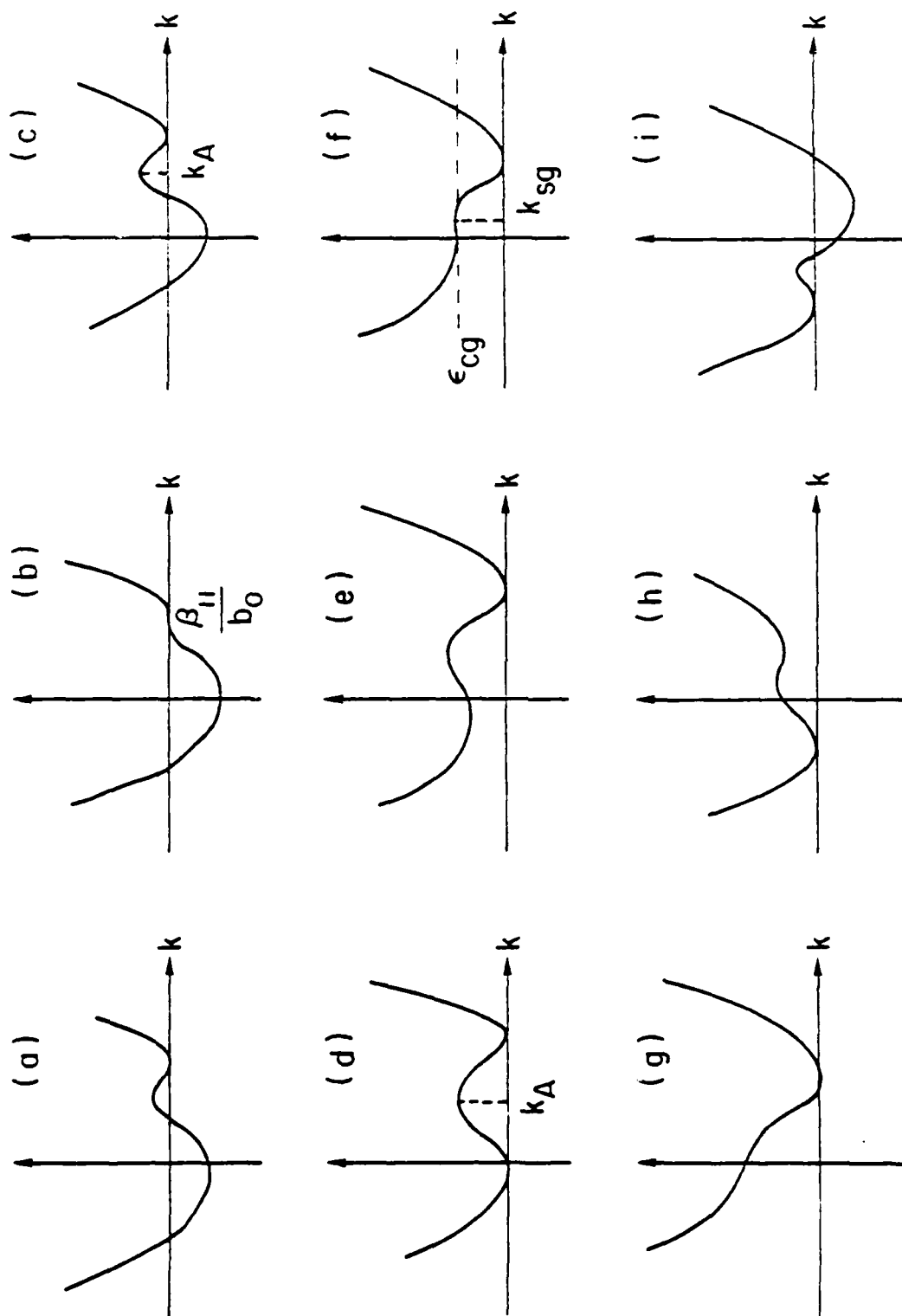
Fig 4 — Sketch of the function $f(y) = (y^2 - 1)(y - a)^2$

A-27

Fig. 5 — Sketches of $\beta_{\parallel}^2 D(\omega, k)$ at various values of ω: (a) $\omega > \frac{1}{b_o}$, (b) $\omega = \frac{1}{b_o}$, (c) $1 < \omega < \frac{1}{b_o}$, (d) $\omega = 1$, (e) $\omega_{sc} < \omega < 1$, (f) $\omega = \omega_{sc}$, (g) $\omega_{sg} < \omega < \omega_{sc}$, (h) $-1 < \omega < \omega_{sg}$, (i) $\omega < -1$. Here, ω_{sc} and k_{sc} are defined in Eqs. ((5) and ((6) and $\omega = (b_o + 6\sqrt{2}\beta_{\parallel})/(1 + 8\beta_{\parallel}^2)$.
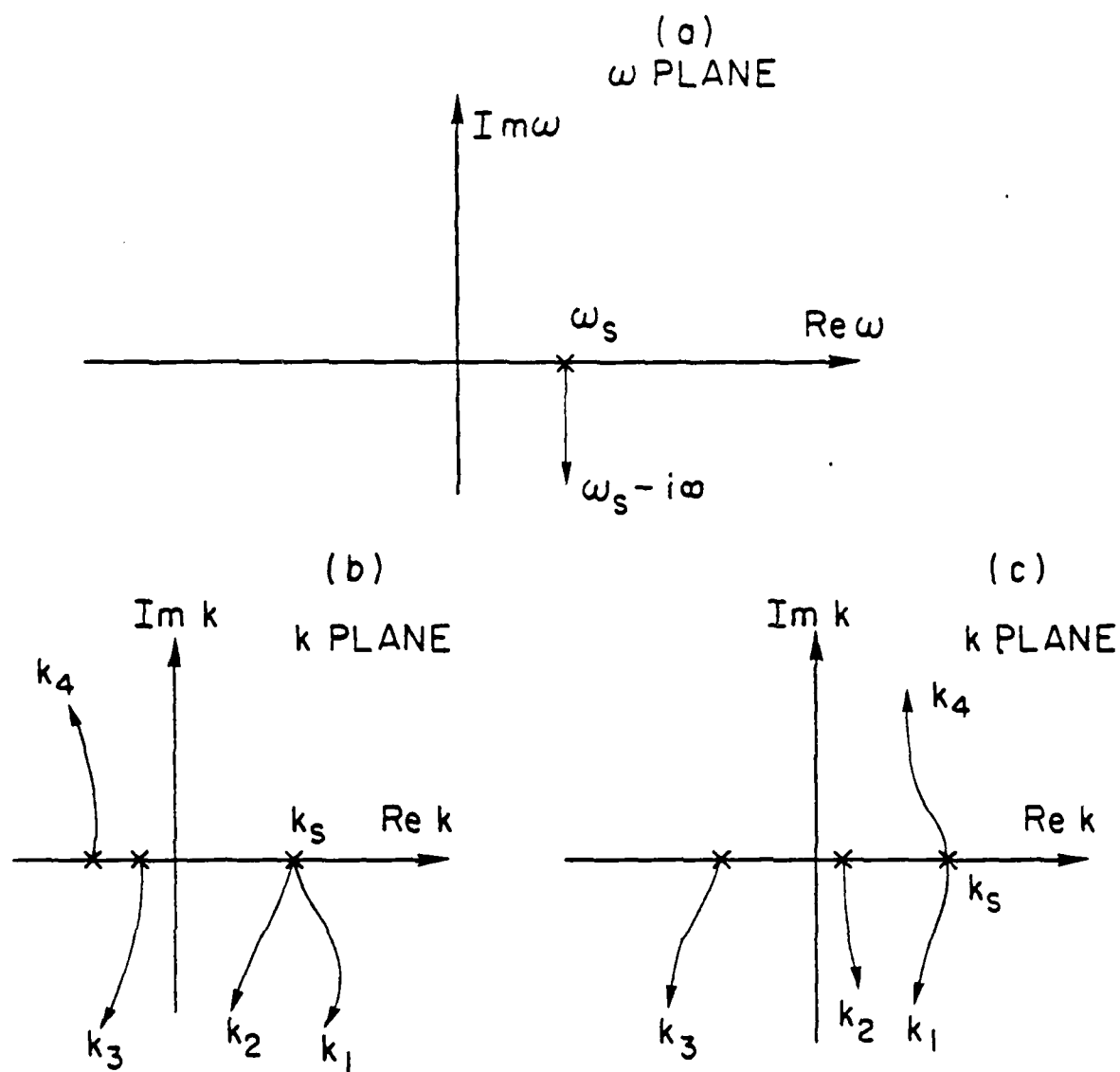
Fig. 6 — Trajectories of the roots in the k plane as ω changes from ω_s to $\omega_s - i\infty$. In (b), a convective instability exists. In (c) k_s corresponds to the onset of an absolute instability.

APPENDIX B

EFFECTS OF VELOCITY SPREAD AND WALL RESISTIVITY
ON THE GAIN AND BANDWIDTH OF THE
GYROTRON TRAVELLING-WAVE AMPLIFIER

Y.Y. LAU
K.R. CHU
L. BARNETT

CONTENTS

EFFECTS OF VELOCITY SPREAD AND WALL RESISTIVITY ON THE GAIN AND BANDWIDTH OF THE GYROTRON TRAVELLING-WAVE AMPLIFIER

I. INTRODUCTION

The onset of oscillations at a relatively low current level remains a major obstacle in the development of high power gyrotron travelling wave amplifier (gyro-TWA)[1,2]. Analogous to the conventional travelling wave tube, it has been experimentally shown that the introduction of wall loss, either in the form of a lumped or distributed loss[3], may render the gyro-TWA stable against oscillations resulted from reflections. Parallel theoretical studies[4] also reveal that a small wall resistivity may reduce the danger of exciting an absolute instability,[5] whose presence can lead to oscillations even in the absence of reflections. While wall resistivity may stabilize the amplifier against both types of oscillations, it may also modify the gain and the bandwidth. On the other hand, there is always the interesting possibility that it may also lead to some type of resistive instability which would not exist if there is no wall resistivity. Thus, in this work, we study in detail the effects of a distributed wall resistivity on the gain and bandwidth of the gyro-TWA, with the velocity spread in the electron beam accounted for. Previously[1,6], the effect of velocity spread has been studied in the absence of wall resistivity. Here, we study the combined effects of the wall resistivity and velocity spread with emphasis on the former.

Under the realistic assumptions that the skin depth δ of the wall material is much less than the wall thickness and the wall radius r_w, we generalize the dispersion relation derived earlier[7] to include the effect of wall resistivity and of velocity spread. We analyze the gain curves over a wide range of parameters. The principal results are summarized as follows.

The presence of a small resistivity (e.g., $\delta/r_w = 0.0026$, as in the NRL experiments), only slightly reduces the gain of the amplifier. More specifically, the reduction in gain is approximately 1/3 of the

cold-tube loss for frequencies in the neighborhood of the grazing intersection. This result may be paraphrased as that the resistive wall is 3 times as effective in damping the backward waves reflected from the end of the waveguide than the forward amplifying waves, leading to the distinct possibility that wall resistivity may stabilize the amplifier without significantly reducing its gain. (Recall in this regard that the resistive wall may also stabilize the absolute instability, as mentioned earlier).

Of equal interest is our finding that wall resistivity can increase the bandwidth for realistic values of δ/r_w. This increase in bandwidth, which is quite substantial when the applied magnetic field is maintained exactly at the grazing value, results primarily from the leveling of the gain curve. The bandwidth is less sensitive to wall resistivity if the magnetic field is below the grazing value. The presence of wall resistivity also broadens the unstable band in the frequency spectrum: growth of waves below the waveguide cutoff frequency is found possible, leading to some optimism that very wide band amplifier may be realized.

A modest amount of velocity spread, say, on the order of 10 per cent, does not reduce the peak gain significantly. However, the bandwidth may be significantly reduced. The reduction in bandwidth is most noticeable when the magnetic field is exactly at the grazing value. For a slightly lower value of magnetic field, the reduction in bandwidth is minimal, even at a current level as high as 10 amps.

The extensive numerical study of gain and bandwidth points to the following optimum design parameters: A beam current on the order of 10 amps, an applied magnetic field about 2% below the grazing value, a wall resistivity with a skin depth about five thousandth of the wall radius. For a gyro-TWA with such design parameters, a gain on the order of 3.5 db/wavelength with a bandwidth of approximately 4 per cent could be achieved. Such an amplifier may operate stably with significant efficiency.

In keeping with the operation of the amplifier, namely, amplification of a signal of frequency ω, in this paper, we shall calculate the complex axial wavenumber k_z as a function of (real) ω from the

dispersion relation. We should remark that in so doing, care must be exercised to obtain and to inter-pret the gain curve, especially when the current exceeds the threshold value for the onset of absolute instabilities.[4] The proper branch of the solution must be chosen [cf. Ref. (5), p. 38]. On the other hand, calculations of complex ω for real values of k_z might easily be misused in connection with amplifiers [cf. Ref. (5), p. 167].

In Section II, we shall formulate the dispersion relation including the effect of wall resistivity and of the velocity spread in the electron beam. The numerical results are presented in Section III. The major results and implication are discussed in Section IV.

II. FORMULATION

The inclusion of a small, but finite wall resistivity in the waveguide requires some modification of the derivation of the dispersion relationship. Considerable simplification results when two assumptions are introduced: (1) The beam is sufficiently tenuous that the wave with which it interacts is primarily the vacuum field supported by the (lossy) waveguide; (2) The thickness, as well as the inner radius r_w of the resistive wall are much larger than the skin depth δ associated with the wall material.

The first assumption was adopted in virtually all literature on gyrotron. The excellent agreement between experiments and the theory developed under this assumption leaves little doubt regarding its validity. Implied also in this assumption is that the beam mode and the waveguide mode are close to synchronism. One should take precaution, therefore, if the present formalism is to be extrapolated to explore the possibility of designing an extremely wideband amplifier, even though such a possibility is potentially attractive. The second assumption is also generally valid for any realistic gyro-TWA experi-ment. For example, in the planned NRL experiments $r_w = .533$ cm, $\delta \simeq 1.4 \times 10^{-3}$ cm at 35 GHz.[3] Thus $\delta/r_w \simeq 2.6 \times 10^{-3}$, an extremely small quantity compared with unity.

Our calculation of the dispersion relationship follows closely with Chu, Drobot, Szu, and Spran-gle.[7] First, the vacuum fields of the TE_{0n} mode in a cylindrical lossy waveguide are

$$B_z^{(1)} = J_0(\alpha_n r) \exp{(ik_z z - i\omega t)} \tag{1}$$

$$B_r^{(1)} = \left(-i\frac{k_z}{\alpha_n}\right) J_1(\alpha_n r) \exp{(ik_z z - i\omega t)} \tag{2}$$

$$E_\phi^{(1)} = -\omega \, B_r^{(1)}/k_z c. \tag{3}$$

Here, J_0 and J_1 are Bessel functions of order zero and one. As will be shown in Appendix A, the characteristic radial wavenumber α_n is given by the equation

$$\frac{\delta}{r_w} \left[\frac{1-i}{2}\right] \zeta J_0(\zeta) = J_1(\zeta), \tag{4}$$

where

$$\zeta \equiv \alpha_n r_w \equiv r_w \sqrt{\frac{\omega^2}{c^2} - k_z^2}. \tag{5}$$

In the limit of small δ/r_w, the approximate solution to Eq. (4) is

$$\zeta = \zeta_{on} \left[1 + \frac{\delta}{r_w} \frac{(1-i)}{2}\right] \tag{6}$$

where ζ_{on} is the n-th non-trivial root of J_1, i.e., $\zeta_{on} = 3.832, 7.016, 10.173$, etc. When we denote $\alpha_{on} \equiv \zeta_{on}/r_w$, the slightly complex radial wavenumber reads

$$\alpha_n = \alpha_{on} \left[1 + \frac{\delta}{r_w} \frac{(1-i)}{2}\right]. \tag{7}$$

Note that

$$J_1(\alpha_n r_w)\begin{cases} = J_1(\alpha_{on} r_w) = 0, & \text{if } \delta = 0 \tag{8} \\[2ex] \neq 0, & \text{if } \delta \neq 0 \ . \tag{9} \end{cases}$$

To make full use of the mathematical property of Bessel functions, let us define

$$r_w^* \equiv \frac{\alpha_{on} r_w}{\alpha_n} \cong r_w \left[1 - \frac{\delta}{r_w} \frac{(1-i)}{2}\right]. \tag{10}$$

Thus

$$J_1(\alpha_n r_w^*) = 0. \tag{11}$$

For ready comparison with the cold tube loss rate resulting from wall resistivity, we calculate the axial wavenumber k_z for the empty waveguide. From Eqs. (5) and (6), we find, for the empty waveguide, $k_z = k_{zE}$ where

$$k_{zE}^2 = k_{zo}^2 - \alpha_{on}^2 (1 - i) \frac{\delta}{r_w},$$
(12)

with

$$k_{zo} \equiv \left[\frac{\omega^2}{c^2} - \alpha_{on}^2 \right]^{1/2}$$
(13)

being the axial wavenumber of the corresponding lossless waveguide. Note that Eq. (12) is valid even if $k_{zo} = 0$. It will be used to calculate the attenuation rate of the waves in the cold tube due to the wall loss. On the other hand, measurements of attenuation rate for the cold tube at various frequencies may be used to determine the skin depth of the wall material by Eq. (12).

We now consider the interaction of the electron beam with the above electromagnetic waves. In the typical configuration of a gyro-TWA (Fig. 1), the electrons, forming an annular beam, are guided by a uniform magnetic field $(B_o \, e_z)$. They move along helical trajectories. Ideally, all electrons have the same perpendicular velocity $v_{\perp o}$ and the same parallel velocity v_{zo}, with their guiding centers uniformly distributed on a surface of constant radius r_o (Fig. 1). The electromagnetic fields represented by Eqs. (1)-(3) induce a current perturbation in the beam. This response in the current has been computed by Chu[8] for the lossless waveguide by solving the linearized Vlasov equation. His calculation can readily be extended to the present case of a lossy waveguide because the field solutions $J_0(\alpha_n r)$ and $J_1(\alpha_n r)$ in Eqs. (1)-(3) are entire functions of $\alpha_n r$. In order that this perturbation current $J^{(1)}$ be consistant with the field solutions (1)-(3), they must be related by the Maxwell equations as follows:

$$\frac{1}{r} \frac{\partial}{\partial r} \left[r \frac{\partial B_z^{(1)}}{\partial r} \right] - k_z^2 B_z^{(1)} + \frac{\omega^2}{c^2} B_z^{(1)} = - \frac{1}{r} \frac{\partial}{\partial r} (r J_\theta^{(1)}),$$
(14)

where $J_\theta^{(1)}$ is the θ component of the perturbation current. Strictly speaking, Eq. (14) is an integral-differential equation since $J_\theta^{(1)}$ is a function of the fields which are to be solved self-consistently.

B-7

The first assumption introduced at the beginning of this section can now be used to simplify the formulation. By this assumption $B_z^{(1)}$ is given by Eq. (1). Multiply equation (14) by $r J_s(\alpha_n r)$ and integrate the resultant equation from $r = 0$ to r_w^*. We then obtain

$$\left[\frac{\omega^2}{c^2} - k_z^2 - \alpha_n^2\right] = \frac{8\pi\alpha_n\, e^{-ik_z z - i\omega t}}{c\, r_w^{*2}\, J_0^2(\zeta_{on})} \int_0^{r_w^*} dr\; r\, J_\theta^{(1)}\, J_1(\alpha_n r) \tag{15}$$

where we have used equation (11) and α_n, r_w^* are given by equations (7) and (10) respectively. This procedure is justified as all quantities in equation (14) are entire functions of r. For the same reason, the modified dispersion relation now reads

$$\frac{\omega^2}{c^2} - k_z^2 - \alpha_n^2 = \frac{-8\pi\nu}{\zeta_{on}^2 J_0^2(\zeta_{on})} \int_0^\infty p_\perp\, dp_\perp \int_{-\infty}^\infty dp_z\, g(p_\perp, p_z)$$
$$\cdot \left\{ \frac{(\omega^2 - k_z^2 c^2) p_\perp^2 H_s(\alpha_n r_0, \alpha_n r_L)}{\gamma^3 m^2 c^2 (\omega - k_z v_z - s\Omega_c)^2} \right.$$
$$\left. - \frac{(\omega - k_z v_z) Q_s(\alpha_n r_0, \alpha_n r_L)}{\gamma(\omega - k_z v_z - s\Omega_c)} \right\} \tag{16}$$

where $\Omega_c = eB_0/\gamma mc$, $r_L = v_\perp/\Omega_c$, $\nu \equiv Ne^2/mc^2$ is the dimensionless beam density parameter, N is the number of electrons per axial length, and the functions H_s and Q_s are defined by

$$H_s(x,y) \equiv [J_s(x) J_s'(y)]^2$$

and

$$Q_s(x,y) \equiv 2H_s(x,y) + y J_s'(y) J_s''(y) \{ J_s^2(x)(1 + s^2/x^2)$$
$$- [J_s'(x)]^2 \} + 2s^2 J_s(x) J_s'(x) J_s'(y) [y J_s'(y)$$
$$- J_s(y)]/xy.$$

In Eq. (16), $g(p_\perp, p_z)$ is an arbitrary function of the momentum $p_\perp$ and p_z satisfying $\int g(p_\perp, p_z)\, d^3p = 1$. The most suitable electron beams for the gyrotrons are those generated from a magnetron-type electron gun. Typically, such beams are characterized by a negligible energy spread, hence the velocity spread comes primarily from the pitch angle spread of the electron velocity. To model this kind of beam, we let

$$g(p_\perp, p_z) = K\, \delta(\gamma - \gamma_0) \exp\left[\frac{-(p_z - p_{zo})^2}{(\Delta p_z)^2}\right].$$

B-8

where K is a normalization constant and Δp_z is the mean axial velocity spread, and δ is the delta function of Dirac.

Equation (16) is identical in form with that for the lossless waveguide[1,6] except that α_n now has a small imaginary part, and that we have neglected the azimuthal modes. It incorporated two obvious physical effects of the wall resistivity: (a) its modification of the waveguide mode and hence (b) the modified beam-wave interaction as a result of the modification in the electromagnetic field. The first effect is represented by the complex α_n appearing in the LHS of Eq. (16) and the second effect by that in the RHS. In Appendix B, we show that the second effect is negligible in comparison with the first effect. Thus we may replace α_n by α_{on} in the right hand side of Eq. (16).

It is anticipated that wall resistivity should reduce the forward gain of the amplifier. Actually, the reduction in the gain is considerably less than that expected of the vacuum waveguide. In Appendix B, we estimate that the reduction in the gain by wall resistivity is approximately 1/3 of the cold tube loss (by resistivity) at the same frequency. This analytic result is supported by our numerical results. It may be regarded significant since it means that wall resistivity may stabilize the amplifier, by damping out any reflected signal from the end of the waveguide, without sacrificing the forward gain as significantly.

In Section III, we shall present numerical results for various combinations of δ/r_w, velocity spread, beam current and the applied magnetic field. The results are obtained from the full dispersion relationship (16), and from its modified form when velocity spread is present.

III. NUMERICAL EXAMPLES

The general dispersion relationship (16) is applicable to all cyclotron harmonics (s) and to all radial mode numbers (n). Thus, a huge parameter space needs to be explored for an exhaustive investigation of the performance of the gyro-TWA. To limit our studies of the effects of wall resistivity and

of velocity spread, we shall only examine the lowest cyclotron harmonic of the TE_{0} mode. Even then, four parameters need to be specified to obtain the gain curve. They are:

(a) the magnetic field B_0, in units of the grazing value B_G.

(b) the current I.

(c) the wall resistivity, measured by δ/r_w, and

(d) the velocity spread, measured by $\Delta p_z/p_{zo}$.

The magnetic field is said to assume the grazing value when the non-relativisitic electron cyclotron frequency equals to the cut-off frequency of the waveguide. The numerical examples obtained may then be used, after properly scaled, to predict the performance of the amplifier operated at higher harmonics and at higher order modes.

To facilitate comparison of results, at the expense of some duplications, we shall present our numerical calculations in three subsections. In each subsection, gain curves are given in which three of the four parameters mentioned above are held fixed and only the remaining one is allowed to vary. All gain curves are drawn with the same scale. The individual effects are thus placed in sharp focus. In Subsection a, in each graph of the gain curves, only the wall resistivity is varied. In Subsection b, only the velocity spread is varied and in Subsection c, only the current is varied. In all cases studied, we assume that $\beta_{\parallel} = 0.266$, $v_{\perp 0}/v_{\parallel 0} = 1.5$ and that the beam energy is 70 keV. These assumptions closely represent the NRL experiments.[1] We shall postpone to the next section for some general discussion of the role of resistivity in instabilities.

a. The Effect of Wall Resistivity

In this subsection, we present the gain curves in which the wall resistivity (δ/r_w) is allowed to vary. We shall plot the normalized spatial growth rate $\bar{k}_i \equiv -k_i r_w$ as a function of normalized frequency $\bar{\omega} \equiv \omega \, r_w/c$. For a lossless waveguide, $\bar{\omega}$ assumes the value 3.832 at the cutoff frequency and 3.975 at the grazing frequency. In both Figs. (2) and (3), we set $B/B_G = 1$ and $\Delta p_z = 0$. In Fig. (2),

$I = 1$ amp and in Fig. 3. $I = 3$ amps. Also shown in parentheses in these figures are the bandwidths, which represent the frequency range inside which the gain is within 85% of the peak value. It is seen from these two figures that the gain is not reduced by a significant amount as δ/r_w is raised from 0 to 0.0025 (again, in the NRL experiments, $\delta/r_w \simeq 0.0025$). If δ/r_w is further raised from 0.0025 to 0.01, amounts to an increase of wall resistivity by a factor of 16, we see that the bandwidth significantly increases [c.f. Fig. 3] while the gain is not substantially reduced. In fact, if we compare the numerical value of this reduction in gain with the cold tube loss as determined from Eq. (12) [c.f. Fig. 4] the former is approximately 1/3 of the latter, over the useful bandwidth in the vicinity of the grazing frequency. This result is in qualitative agreement with the analytical study given in Appendix B. The sharp peak in the $\delta/r_w = 0$ curve in Fig. 3 is indicative of the presence of an absolute instability[4] in that case.

In Figs. 5-7, we include the effect of the velocity spread while the magnetic field is still maintained at the grazing level. It is again seen that the bandwidth increases with wall resistivity, and the forward gain is not reduced significantly.

In Fig. 8, we set $B/B_G = 0.98$, $I = 7$ amps, and $\Delta p_z = 0$. The bandwidth also increases with wall resistivity, but its dependence on resistivity is less sensitive than that in the case of exact grazing magnetic field. The slight decrease in bandwidth as δ/r_w changes from 0.005 to 0.01 as shown in this figure suggest the presence of resistive damping.

It is of interest to point out that even though the peak gain is reduced by wall resistivity, the unstable band of the amplifier is enlarged. Virtually, in all cases, the unstable band extends to frequencies below the cut-off frequency of the waveguide if wall resistivity is included, thus suggesting the presence of some resistive wall-induced instability. We shall comment on this dual role of resistivity in Section IV.

b. The Effect of Velocity Spread

In this subsection, we evaluate the effect of velocity spread on the gain and bandwidth of the gyro-TWA. In each figure, all parameters are held fixed except the velocity spread $\Delta p_z / p_{zo}$. We take the values of $\Delta p_z / p_{zo}$ to be 0, 7% and 15%. It is found that the velocity spread reduces the gain and bandwidth significantly when the magnetic field is maintained at the grazing level. On the other hand, when $B/B_G < 1$, velocity spread does not seem to reduce the gain nor the bandwidth to as a great extent, even at a high current level. [Of course, one might also worry that at a high current level, the beam quality may deteriorate and the velocity spread may increase].

In Figs. 9-11, we set $B/B_G = 1$, $I = 1$ amp. and let $\delta/r_w = 0$, 0.0025 and 0.1 respectively. We see that at this low current level, the presence of velocity spread reduces the gain and bandwidth quite significantly [c.f. Fig. 11]. This remains to be the case when the current is raised to 3 amps, as shown in Figs. 12-14, where we still set $B = B_G$.

If we lower the magnetic field, so that $B/B_G = 0.98$, [c.f. Figs. (15)-(17)], then the velocity spread has a lesser influence in the gain and in the bandwidth. In these figures, we have set $\delta/r_w = 0.0025$. A higher value of δ/r_w, such as 0.01 as used in Figs. 18-21, would permit the amplifier to operate stably at substantially higher current.[4] It is apparent from these figures that the bandwidth, as well as the gain, again does not greatly suffer from the presence of velocity spread.

c. The Effect of Increasing Current

Finally, we examine the dependence of gain and bandwidth on the current. When the current is sufficiently high, an absolute instability sets in. There would then be some ambiguity[5] regarding the proper solutions of the amplifying waves. Such an ambignity arises from the intersection of the branch cut in the ω plane with the real ω axis. It does not seem to pose a serious problem in the present study when the beam current exceeds the threshold current only by a moderate factor, such as 1.5. We have

exercised some care in choosing the correct solution, and we may refer to Ref. (4) for a detailed discussion of the absolute instability and for the calculation of the threshold current in the gyro-TWA.

Here, we report that while the gain increases with the current, as expected, the bandwidth decreases once the current exceeds the threshold value for the onset of absolute instability. This may be intepreted as the tendency of the system to respond mostly to a particular frequency, namely, the natural frequency of oscillation when the absolute instability is present, thereby leading to a narrow bandwidth that results from the sharp peak in the gain curve in the neighborhood of that natural frequency. These statements are corroborated in Figs. 22 and 23, where the gain curves tend to peak at the cutoff frequency (i.e., $\bar{\omega}_c = \omega_c r_w/c = 3.832$), which also is the frequency[4] for the onset of the absolute instability. From Ref. (4) the threshold current for parameters shown in Fig. 22 is 1.5 amps and that for Fig. 23 is 5.0 amps.

On the other hand, if the current is below the threshold value, then increasing the current would lead to the increase of both gain and bandwidth, as clearly indicated in Figs. 24-27. In these figures, we set $B/B_G = 0.98$ so that the threshold current is high[4]. The threshold current for both Figs. 24 and 25 is 5.5 amps and that for both Figs. 26 and 27 is 12 amps. The velocity spread in Fig. 24 is 7% and that in Fig. 25 is 15%. Figure 26 and Fig. 27 differ also only in velocity spread. The curves in Fig. 26 are hardly modified if the velocity spread in 7% instead of zero [c.f. Figs. 15-21].

IV. DISCUSSIONS

One thing that stands out among the numerical results is the dual role played by electrical resistivity: (a) in its reduction of the gain of the cyclotron maser instability and (b) in its excitation of amplifying waves in a regime where such amplification would have been impossible if the resistivity is absent. Such a dual role of dissipative effects is of common occurrence in physical systems with available free energy. If in such a system an instability of the reactive type[5] is already present even in the absence of dissipative effects, the introduction of dissipation would reduce the growth rate because it

takes away the free energy that drives the instability. On the other hand, if there is no instability in such a system in the absence of dissipation, the introduction of dissipative effects would lead to growth of waves, as dissipation would induce relaxation of the system which is on the verge of becoming unstable to begin with. Numerous examples of these phenomena can be found in the literature of classical mechanics, hydrodynamics, plasma physics, electron beam devices, astrophysics, etc.

The major results and their implication of the present study may then be summarized as follows:

(1) In terms of power, gain, bandwidth, efficiency, and stability, the gyro-TWA would achieve best overall performance when the magnetic field is maintained just slightly (say, 2%) below the grazing value. Stable operation with significant gain and bandwidth (such as 3-4 db per wavelength in gain and 4% in bandwidth) may be achieved at a current of 10 amps, or even higher, if $\delta/r_w \geq 0.005$.

(2) Wall resistivity leads to a reduction in gain by an amount on the order of 1/3 of the cold tube loss. It leads to an *increase in bandwidth* when the magnetic field is maintained at the grazing value. If the magnetic field is below the grazing value, and if the current is low, the presence of wall resistivity may actually reduce the bandwidth. The latter may be regarded as an example of resistive damping.

(3) Velocity spread typical of present electron guns ($\Delta p_z/p_{zo} \approx 5-10\%$) does not significantly reduce the peak gain. The underlying reason is that its effect enters in the combination $k_z^2(\Delta p_z)^2$ qualitatively and the amplifier reaches a peak gain when $\omega \approx \omega_c$, at which k_z is small. At higher frequencies, k_z becomes sizable and the effect of velocity spread would then be important. Thus, the bandwidth may be significantly reduced, especially if the magnetic field is maintained at the grazing value.

(4) The gain and bandwidth of the amplifier are less sensitive to velocity spread or to resistivity when the magnetic field is below the grazing value. Thus, for stability of the

amplifier, we need a wall resistivity whose skin depth is on the order of $5 \times 10^{-3}\ r_w$. To reduce the deteriorating influence of the velocity spread on the bandwidth, the magnetic field should be maintained slightly below the grazing value. The current should be on the order of 10 amps, which is sufficiently high for gain and power, yet low enough to avoid oscillations. These arguments form the basis of the parameters quoted in the Abstract.

ACKNOWLEDGEMENT

REFERENCES

*   Science Applications, Inc.

**   B.-K. Dynamics

1.   J.L. Seftor, V.L. Granatstein, K.R. Chu, P. Sprangle and M.E. Read, "The Electron Cyclotron Maser as a High-Power Travelling Wave Amplifier of Millimeter Waves," IEEE J. Quantum Electronics, Vol. QE-15, pp. 848-853 (1979).

2.   L.R. Barnett, K.R. Chu, J.M. Baird, V.L. Granatstein, and A.T. Drobot, "Gain, Saturation, and Bandwidth Measurements of the NRL Gyrotron Travelling Wave Amplifier," IEDM Technical Digest, pp. 164-167 (Dec., 1979).

3.   L.R. Barnett, et al., to be published. R.S. Symons, H.R. Jory, and S.T. Hegii, to be published.

4.   Y.Y. Lau, K.R. Chu, L.R. Barnett and V.L. Granatstein, "Analysis of Oscillations in the Gyrotron Travelling-Wave Amplifier," to be published.

5.   R.J. Briggs, *Electron Stream Interaction with Plasma*, MIT Press, Cambridge, Mass. (1964).

6. H.S. Uhm and R.C. Davidson, "Influence of Energy and Axial Momentum Spreads on the Cyclotron Maser Instability in Intense Hollow Electron Beams," Phys. Fluids, Vol. 22, pp. 1804-1810 (1979).

7. K.R. Chu, A.T. Drobot, H.H. Szu, and P. Sprangle, "Theory and Simulation of the Gyrotron Travelling Wave Amplifier Operating at Cyclotron Harmonics," IEEE Trans. MTT (April, 1980).

8. K.R. Chu, "Theory of Electron Cyclotron Maser Interaction in a Cavity at the Harmonic Frequencies," Phys. Fluids, Vol. 21, pp. 2354-2364 (1978).

Appendix A

DERIVATIONS OF FIELD PATTERNS IN A CYLINDRICAL

LOSSY WAVEGUIDE

In this Appendix, we calculate the field patterns of the TE_{on} modes in an empty, cylindrical waveguide with a lossy wall. We shall assume that the skin depth δ of the wall is much less than the wall radius r_w, the wall thickness, and the free space wavelength c/ω. Thus, we consider two regions. Region I is the free space region: $0 < r < r_w$, inside which the electrical conductivity σ is zero. Region II is the wall region: $r_w < r < \infty$, where σ is large but finite.

It is well known that the z component of the magnetic field of the TE_{on} mode is governed by the Bessel equation

$$\left[\frac{1}{r}\frac{\partial}{\partial r}\left(r\frac{\partial}{\partial r}\right) + k_n^2\right] B_z^{(1)} = 0. \tag{A1}$$

In region I, $k_n^2 = k_{n1}^2$ where

$$k_{n1}^2 = \frac{\omega^2}{c^2} - k_z^2. \tag{A2}$$

Thus, the solution which is regular in this region is

$$B_z^{(1)}(r) = A \; J_0(k_{n1}r), \quad 0 \leqslant r < r_w, \tag{A3}$$

where A is an arbitrary constant and J_0 is the Bessel function of order zero.

In Region II, $k_n^2 = k_{n2}^2$, where

$$k_{n2}^2 = \frac{\omega^2}{c^2}\left[1 - \frac{\sigma}{i\omega\epsilon_0}\right] - k_z^2 \approx i\omega\mu_0\sigma. \tag{A4}$$

Here, ϵ_0 and μ_0 are the permittivity and permeability of free space. In writing the last expression in (A4), we have assumed that the skin depth

$$\delta = \sqrt{\frac{2}{\omega\mu_0\sigma}} \tag{A5}$$

is much less than the free space wavelength c/ω. Using (A4) into (A1), and introducing the transformation

$$B_z^{(1)} = r^{-1/2} \phi, \tag{A6}$$

we rewrite equation (A1) for Region II as

$$\frac{d^2\phi}{dr^2} + \left[i\omega\mu_0\sigma + \frac{1}{4r^2} \right] \phi = 0, \quad r_w < r < \infty. \tag{A7}$$

The last term $1/4r^2$ is clearly small in comparison with $\omega\mu_0\sigma$ for all $r > r_w$ and hence is neglected. In order that the solution to (A7) is bounded as $r \to \infty$, we have

$$B_z^{(1)}(r) = r^{-1/2} \phi(r) \simeq B \, r^{-1/2} \, e^{-(1-i)r/\delta}; \quad r > r_w \tag{A8}$$

where B is an arbitrary constant. Two conditions are now imposed on the solutions (A3) and (A8) at the boundary $r = r_w$ separating the two regions:

$$B_z^{(1)}(r)\Big|_{r=r_w^-} = B_z^{(1)}(r)\Big|_{r=r_w^+} \tag{A9}$$

$$\frac{dB_z^{(1)}(r)}{dr}\Bigg|_{r=r_w^-} = \frac{dB_z^{(1)}(r)}{dr}\Bigg|_{r=r_w^+}. \tag{A10}$$

Condition (A9) assures the continuity of the magnetic field and (A10) the continuity of the tangential electric field. Observe from Eq. (A8) that the variation of the magnetic field in the wall region $(r > r_w)$ is dominated by the exponential factor since $\delta \ll r_w$. Thus, in imposing condition (A10), we can ignore the geometrical factor $r^{-1/2}$ in Eq. (A8). It can then immediately be shown that (A9) and (A10) lead to the dispersion relationship

$$\frac{\delta}{r_w} \left[\frac{1-i}{2} \right] (k_{n1}r_w) \, J_0(k_{n1}r_w) = J_1(k_{n1}r_w) \tag{A11}$$

which is reproduced as Eq. (4) in the main text. Of course, this dispersion relation can also be obtained by first formulating the field solutions in the wall region in terms of Bessel functions (with complex arguments), to be followed by the use of asymptotic formulas of the Bessel functions when $\delta/r_w \ll 1$. The formulation presented above illustrates clearly the nature of such approximations.

With $\zeta \equiv k_{n1} r_w$ and $\delta/r_w \ll 1$, Eq. (A11) admits the approximate solution

$$\zeta = \zeta_{on} + \Delta\zeta \qquad (A12)$$

where $J_1(\zeta_{on}) = 0$ and $\Delta\zeta$ is given by

$$\Delta\zeta = \frac{(\delta/r_w) \left[\frac{1-i}{2}\right] \zeta_{on} J_0(\zeta_{on})}{(\partial J_1(\zeta)/\partial\zeta)_{\zeta = \zeta_{on}}}. \qquad (A13)$$

Equation (A12) reduces to Eq. (6) of the main text after we use in (A13) the formula $\partial J_1(\zeta)/\partial\zeta = J_0(\zeta)$ at the roots ζ_{on} of J_1.

We summarize by stating that the vacuum fields of the TE_{on} mode in a lossy waveguide are given by Eqs. (1)-(3) in the main text. The radial wavenumber α_n in these expressions is given by Eq. (7). The influence of the wall resistivity on the beam dynamics will be discussed in Appendix B.

Appendix B

EFFECTS OF RESISTIVE WALL ON THE DYNAMICS OF

THE ELECTRON BEAM

In this Appendix, we assess the influence on the electron beam dynamics by a small, but finite, wall resistivity. We shall show (a) that the loss in the forward gain of the amplifier is approximately 1/3 of the cold tube loss and (b) that the electron beam essentially experiences the vacuum field inside a *lossless* waveguide. Again, our estimates will be based on the smallness of δ/r_w and we shall consider complex roots of k_z for real values of ω.

Near synchronism, $\omega^2 - k_z^2 c^2 - \alpha_n^2 c^2 \simeq 0$ and $\omega - k_z v_{z0} - s\Omega_c \simeq 0$. The second term in the right hand member of Eq. (16) can be ignored compared with the first term. We can further approximate $\omega^2 - k_z^2 c^2$ by $\alpha_n^2 c^2$ in the right hand side of (16). Thus, Eq. (16) is simplified to read

$$(\omega^2 - k_z^2 c^2 - \alpha_n^2 c^2)(\omega - k_z v_{z0} - s\Omega_c)^2 = -\frac{4\nu\alpha_n^4 c^4 \beta_{z0}^2}{\gamma_o \zeta_{on}^2 J_0^2(\zeta_{on})} H_s(\alpha_n r_o; \alpha_n r_L) \tag{B1}$$

where, for analytical tractability, we have set $\Delta p_z = 0$.

With $\overline{\omega} \equiv \omega r_w/c$, $\overline{k} \equiv k_z r_w$, Eq. (B1) becomes

$$\left\{ \overline{k}^2 - \overline{\omega}^2 + \zeta_{on}^2 \left[1 + \frac{\delta}{r_w}(1-i) \right] \right\} \left[\overline{k} - \frac{\overline{\omega} - \overline{\Omega}_c}{\beta_{\parallel}} \right]^2 = E \equiv E_r + iE_i \tag{B2}$$

where we have used Eq. (7) and $\overline{\Omega}_c \equiv s\Omega_c r_w/c$. In Eq. (B2), the parameter E, whose real and imaginary parts are denoted E_r and E_i, is proportional to the right hand member of Eq. (B1). It is clear from (7) and (B1) that

$$\frac{E_i}{E_r} = 0\left(\frac{\delta}{r_w} \right). \tag{B3}$$

Thus, both sides of (B2) are modified by wall resistivity through the introduction of a term of order δ/r_w. The statement (b) at the beginning of this Appendix claims that E_i can be neglected. The argument supporting this claim will be given later in the Appendix. We shall now prove the statement (a).

In the absence of the beam. $E \to 0$, and the wave inside the lossy waveguides attenuates at a rate given by the imaginary part of $\bar{k}_w$, where

$$\bar{k}_w = \bar{\omega}^2 - \zeta_{on}^2 \left[1 + \frac{\delta}{r_w}(1 - i) \right]^{1/2} \simeq (\bar{\omega}^2 - \zeta_{on}^2)^{1/2} \left[1 + \frac{\zeta_{on}^2 (i - 1)\delta/r_w}{2(\bar{\omega}^2 - \zeta_{on}^2)} \right]. \tag{B4}$$

The last expression is valid once $\bar{\omega}/\zeta_{on} - 1 > \delta/r_w$, i.e.. once the frequency ω exceeds the cut-off frequency ω_c by the (small) amount $(\delta/r_w)\omega_c$. Thus the normalized attenuation rate of the cold tube is

$$Im(\bar{k}_w) \cong \zeta_{on}^2 \left| \frac{\delta_c}{2r_w} \right| \bigg/ (\bar{\omega}^2 - \zeta_{on}^2)^{1/2}. \tag{B5}$$

To estimate the reduction of the gain by the wall resistivity. we neglect E_i in (B2) and rewrite (B2) as

$$(\bar{k} - \bar{k}_w)(\bar{k} - \bar{k}_B)^2 = \frac{E}{(\bar{k} + \bar{k}_w)} \tag{B6}$$

where

$$\bar{k}_B = \frac{\bar{\omega} - \bar{\Omega}_c}{\beta_{\parallel}}, \tag{B7}$$

which is real for real values of $\bar{\omega}$. If we consider the vicinity of the grazing condition. at which

$$\bar{k}_B \equiv \frac{\bar{\omega} - \bar{\Omega}_c}{\beta_{\parallel}} \simeq (\bar{\omega}^2 - \zeta_{on}^2)^{1/2}, \tag{B8}$$

then we may rewrite Eq. (B6) as

$$\bar{k}'^2 [\bar{k}' + (\bar{k}_B - \bar{k}_w)] = \frac{E}{(\bar{k} + \bar{k}_w)} \simeq \frac{E}{2\bar{k}_g} \equiv E_1 \tag{B9}$$

where we have defined

$$\bar{k}' \equiv \bar{k} - \bar{k}_B \tag{B10}$$

and $\bar{k}_g \equiv \zeta_{on}\beta_{\parallel}(1 - \beta_{\parallel}^2)^{-1/2}$ is the characteristic wavenumber at the grazing condition. Note that $Im(\bar{k}') = Im(\bar{k})$. Upon using (B8) and (B4), we have

$$\bar{k}_B - \bar{k}_w \simeq -\frac{\zeta_{on}^2}{2} \left(\frac{\delta}{r_w} \right) \frac{(i - 1)}{(\bar{\omega}^2 - \zeta_{on}^2)^{1/2}}. \tag{B11}$$

Equation (B11) may now be used in Eq. (B9) to estimate the effect of a small (δ/r_w) on the gain per unit length, which is measured by the imaginary part of $\bar{k}'$. We represent the solutions to Eq. (B9) as

B-21

$$\bar{k}' = \bar{k}'_0 - \bar{k}'_1. \tag{B12}$$

where $\bar{k}'_0$ is the solution to (B9) when wall resistivity is absent, (i.e., $\delta = 0$). Thus, $\bar{k}'_0$ satisfies

$$\bar{k}'^3_0 = E_1 \tag{B13}$$

and the imaginary part of $\bar{k}'_1$ represents the reduction of the forward gain by the wall loss. By substituting (B12) into (B9) and by assuming $\bar{k}'_1 \ll \bar{k}'_0$, we obtain

$$\bar{k}'_1 \cong -\frac{1}{3} \ (\bar{k}_B - \bar{k}_w) \cong \frac{\zeta^2_{0n}}{6} \ \frac{(\delta/r_w) \ (i-1)}{\sqrt{\bar{\omega}^2 - \zeta^2_{0n}}} \tag{B14}$$

whose imaginary part is approximately 1/3 of $\mathrm{Im}(\bar{k}_w)$ by Eq. (B4). These qualitative estimates are confirmed by detailed numerical calculations (c.f. Fig. (4)). Thus, the reduction in the forward gain because of the wall resistivity is only one third of the cold tube loss.

We finally show that a small imaginary part in the RHS of the dispersion relationship (B2) [or (B9)] has a negligible influence on the gain. To this end, let us consider Eq. (B9) and add a small imaginary part to its right hand side. Then (B9) becomes

$$\bar{k}'^2 \ [\bar{k}' + \delta_1] = \bar{k}'^3_0 (1 + i\delta_2) \tag{B15}$$

where δ_1 and δ_2 are both of the order of δ/r_w and $\bar{k}'^3_0 = E_1$. Again, expressing the approximate solution to (B15) in the form of (B12), we find

$$\bar{k}'_1 \cong -\frac{1}{3} \ [\delta_1 - i\bar{k}'_0 \ \delta_2]. \tag{B16}$$

Since δ_1 and δ_2 are of the same order and $\bar{k}'_0 = E_1^{1/3}$ is a small quantity whose order of magnitude is typically in the range between 0.01 and .1, we conclude that the introduction of a small imaginary part in the RHS of the dispersion relation (16) has a much smaller effect than that appearing on the LSH of (16). In physical terms, the modified fields by the wall resistivity does not significantly affect the beam current perturbation in response to these fields.

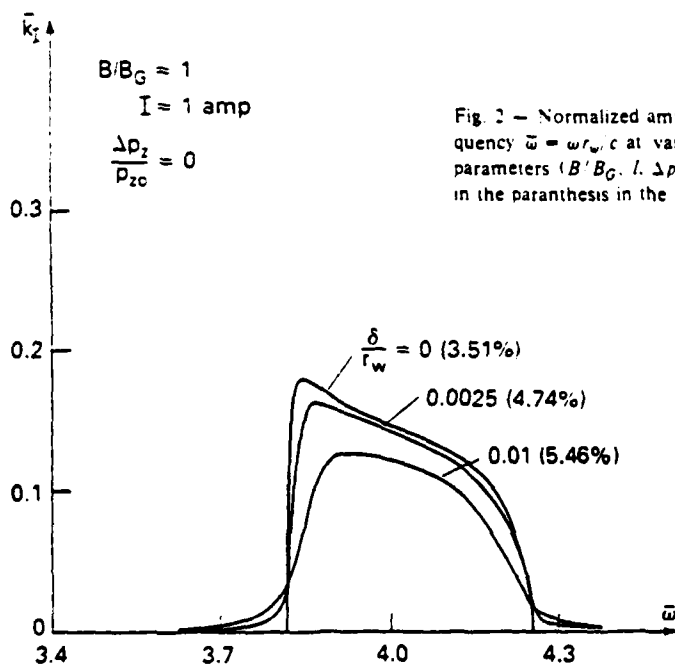Fig. 1 — Cross sectional view of the gyro-TWA. The applied magnetic field points out of the paper.

Fig. 2 — Normalized amplification rate $\bar{k}_i = k_i r_w$ versus normalized frequency $\bar{\omega} = \omega r_w / c$ at various values of wall resistivity (δ/r_w). All other parameters $(B/B_G, I, \Delta p_z, p_{zo})$ are fixed as indicated. The numbers shown in the paranthesis in the figure denote the bandwidths
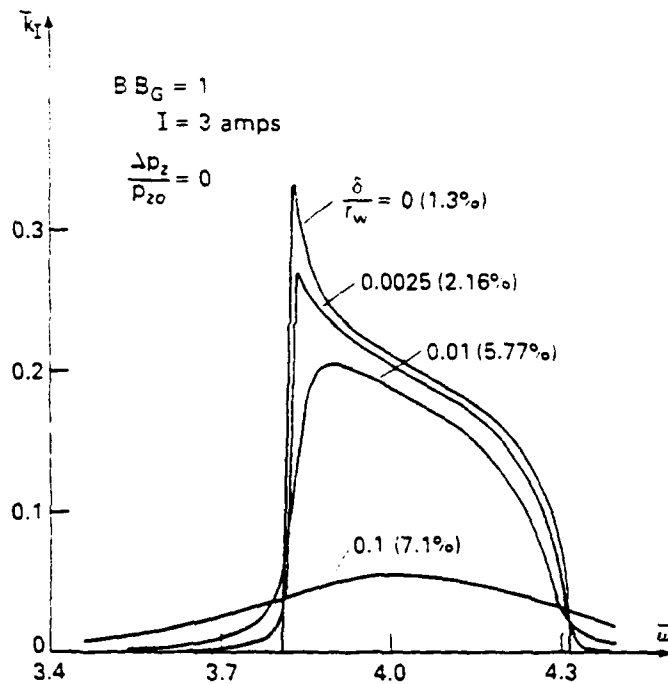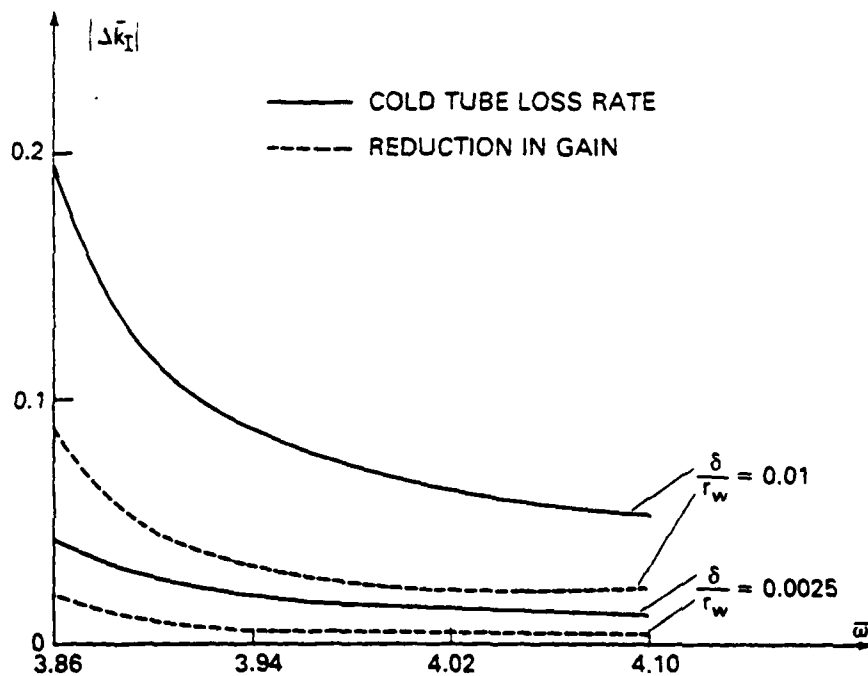
Fig. 3 — Same as in Fig. 2.

Fig. 4 — Cold tube loss rate (solid curves) and the reduction in the amplification rate (dashed curves) due to wall resistivity. The parameters for the dashed curves are $B/B_G = 1$, $\Delta p_z = 0$, $I = 1$ amp. The same dashed curves are obtained if I is raised to 3 amps.

Fig. 5 — Same as in Fig. 2.

Fig. 6 — Same as in Fig. 2.

B-25

Fig. 7 — Same as in Fig. 2

Fig. 8 — Same as in Fig 2.

Fig. 9 — Normalized amplification rate $\bar{k}_I$ versus normalized frequency $\bar{\omega}$. Here, only the velocity spread $\Delta p_z/p_{zo}$ is allowed to vary, all other parameters $(B/B_G, I, \delta/r_w)$ are fixed at the values as indicated in the figure. The numbers in paranthesis denote the bandwidth.
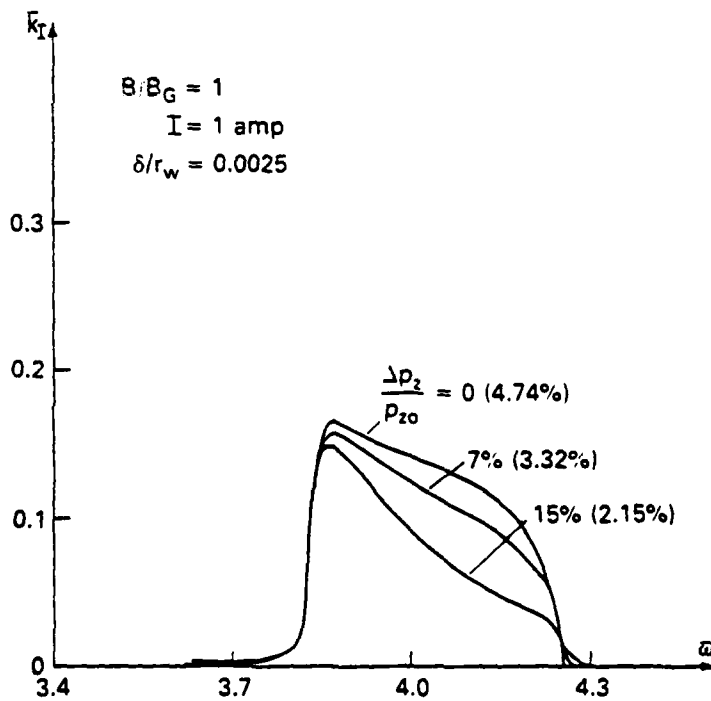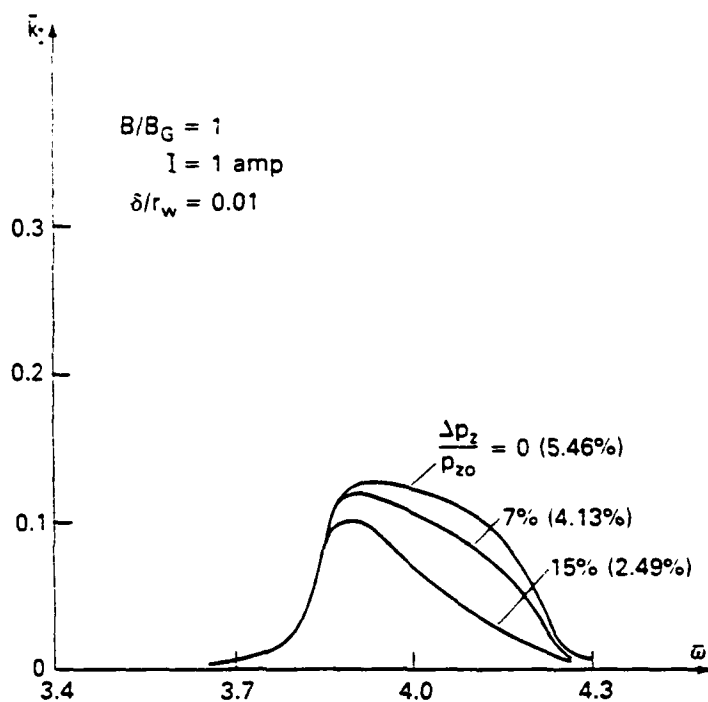
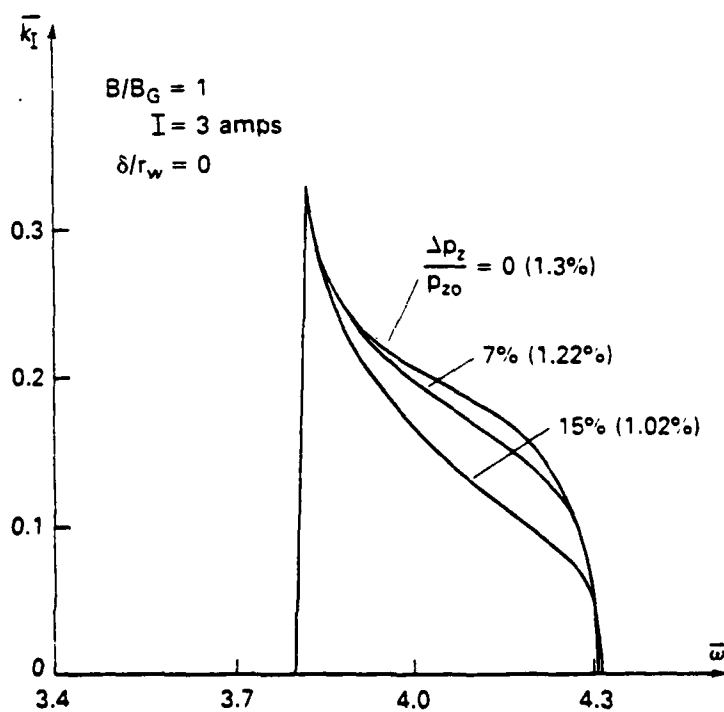

Fig. 10 — Same as in Fig. 9

Fig. 11 — Same as in Fig. 9.

$B/B_G = 1$
$I = 1$ amp
$\delta/r_w = 0.01$

$\frac{\Delta p_z}{p_{zo}} = 0$ (5.46%)

7% (4.13%)

15% (2.49%)

Fig. 12 — Same as in Fig. 9.

$B/B_G = 1$
$I = 3$ amps
$\delta/r_w = 0$

$\frac{\Delta p_z}{p_{zo}} = 0$ (1.3%)
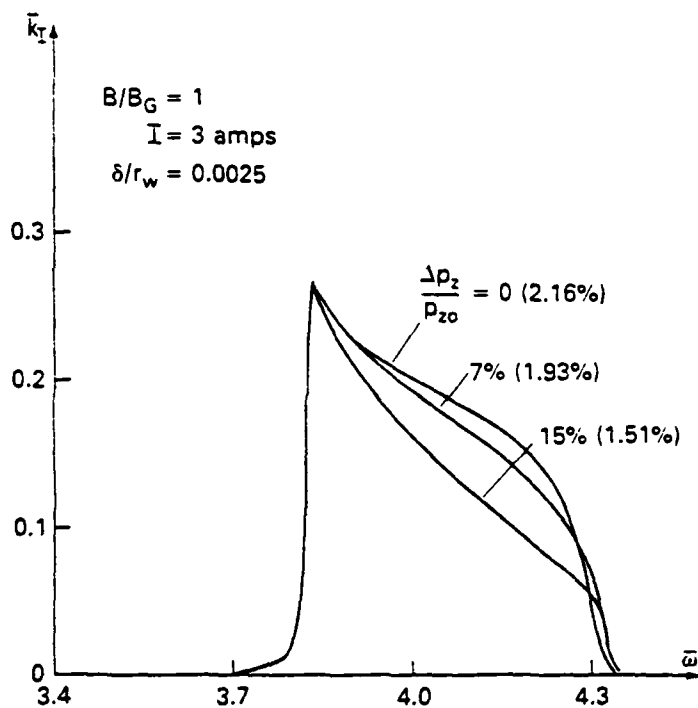
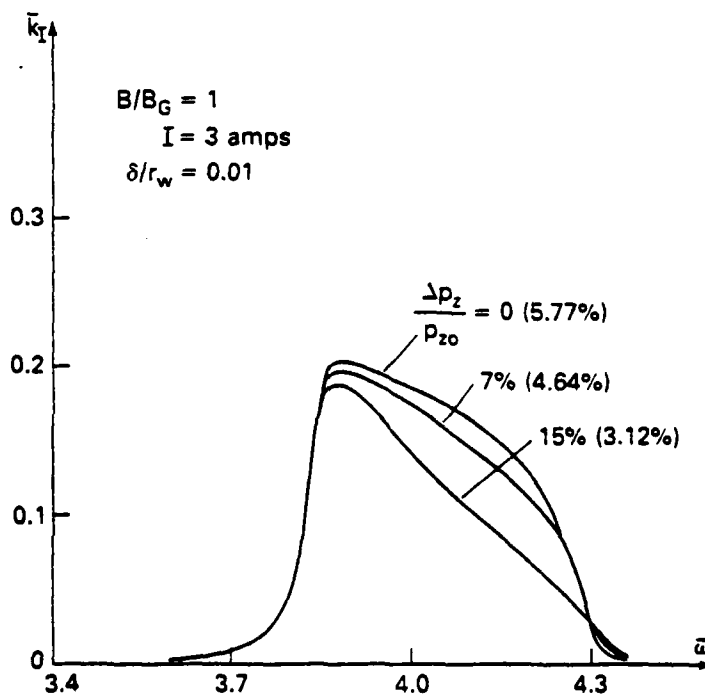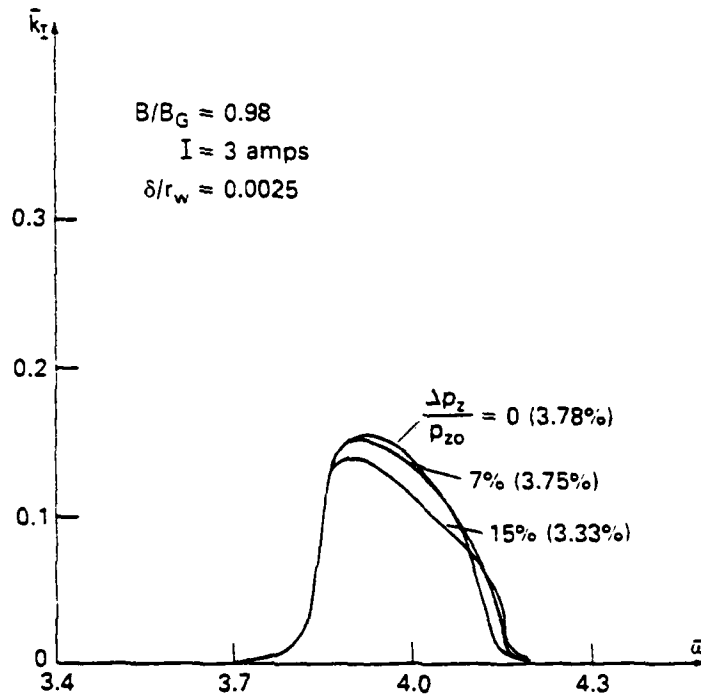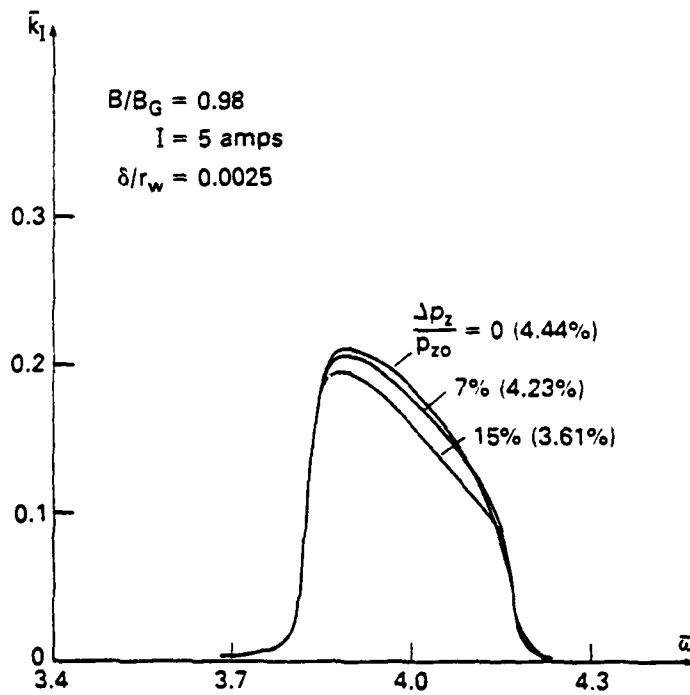7% (1.22%)

15% (1.02%)

Fig. 13 — Same as in Fig. 9.

Fig. 14 — Same as in Fig. 9.

B-29

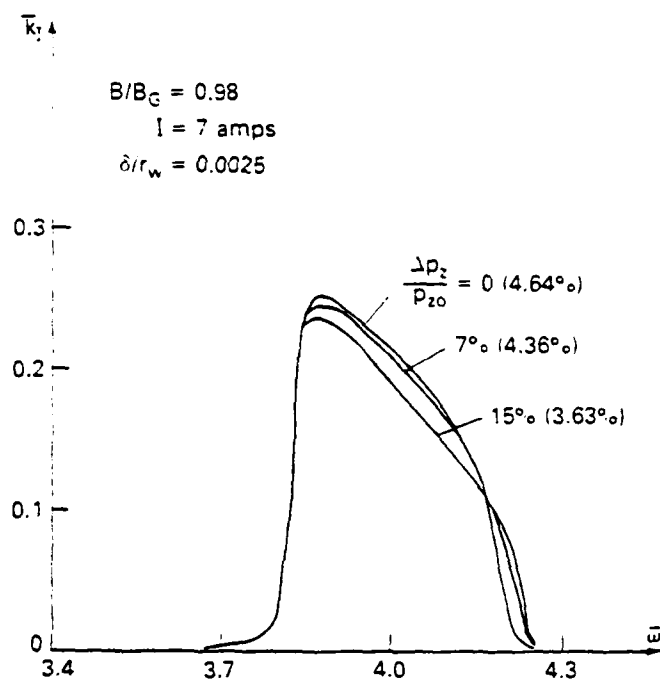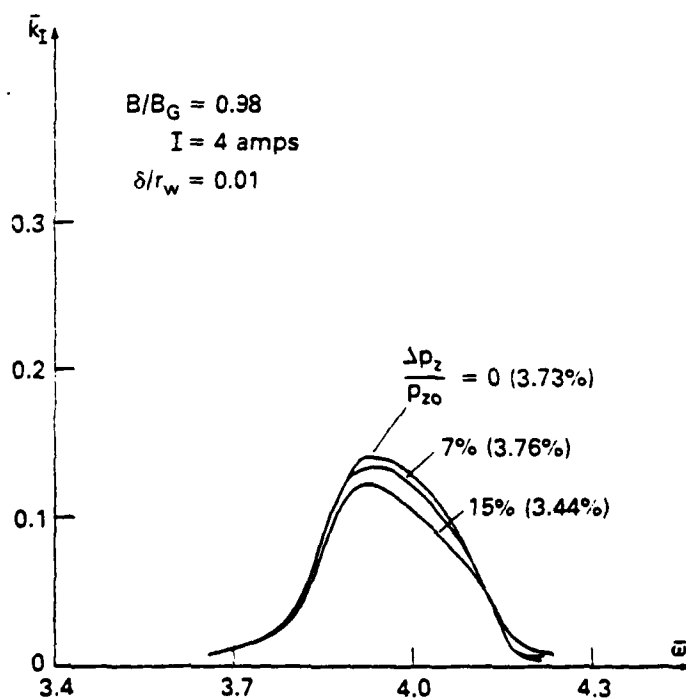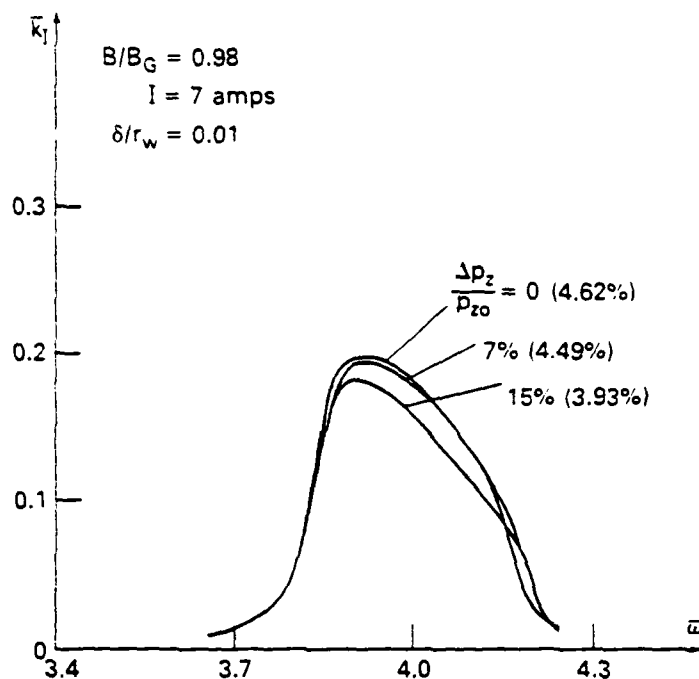Fig. 15 — Same as in Fig. 9

Fig. 16 — Same as in Fig. 9.

B-30

$\overline{k}_I$

$B/B_G = 0.98$
$I = 7$ amps
$\delta/r_w = 0.0025$

0.3

$\frac{\Delta p_z}{p_{zo}} = 0 \ (4.64\%)$

0.2

$7\% \ (4.36\%)$

$15\% \ (3.63\%)$

0.1

0

3.4   3.7   4.0   4.3 $\overline{\omega}$

Fig. 17 — Same as in Fig. 9.

$\overline{k}_I$

$B/B_G = 0.98$
$I = 4$ amps
$\delta/r_w = 0.01$

0.3

0.2

$\frac{\Delta p_z}{p_{zo}} = 0 \ (3.73\%)$

$7\% \ (3.76\%)$

$15\% \ (3.44\%)$

0.1

0

3.4   3.7   4.0   4.3 $\overline{\omega}$

Fig. 18 — Same as in Fig. 9.

B-31

B/B_G = 0.98
I = 7 amps
δ/r_w = 0.01

$\frac{\Delta p_z}{p_{zo}} = 0$ (4.62%)

7% (4.49%)

15% (3.93%)

Fig. 19 — Same as in Fig. 9.

B/B_G = 0.98
I = 10 amps
δ/r_w = 0.01

$\frac{\Delta p_z}{p_{zo}} = 0$ (4.97%)
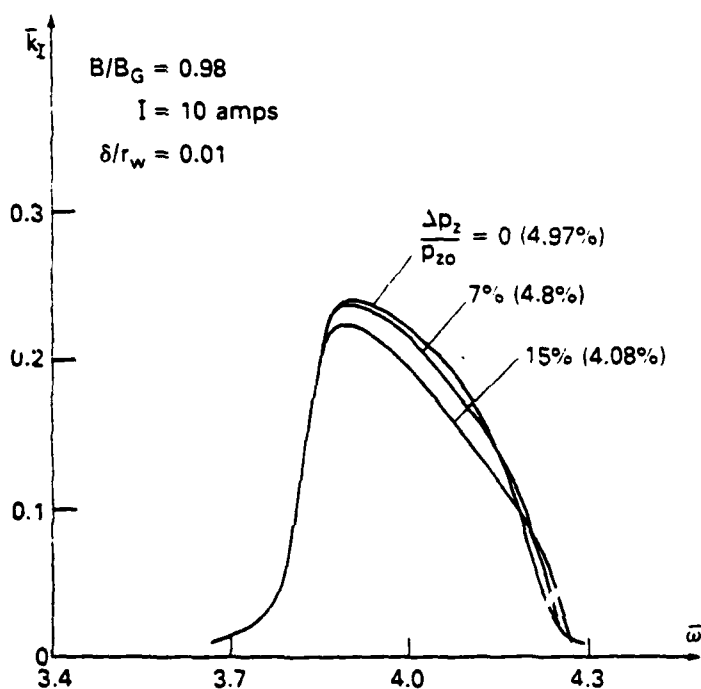
7% (4.8%)

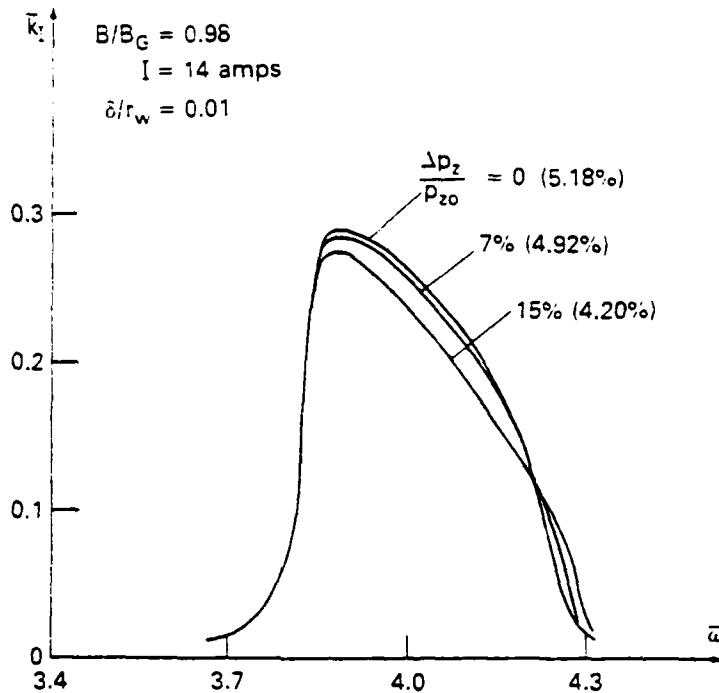15% (4.08%)

Fig. 20 — Same as in Fig. 9.
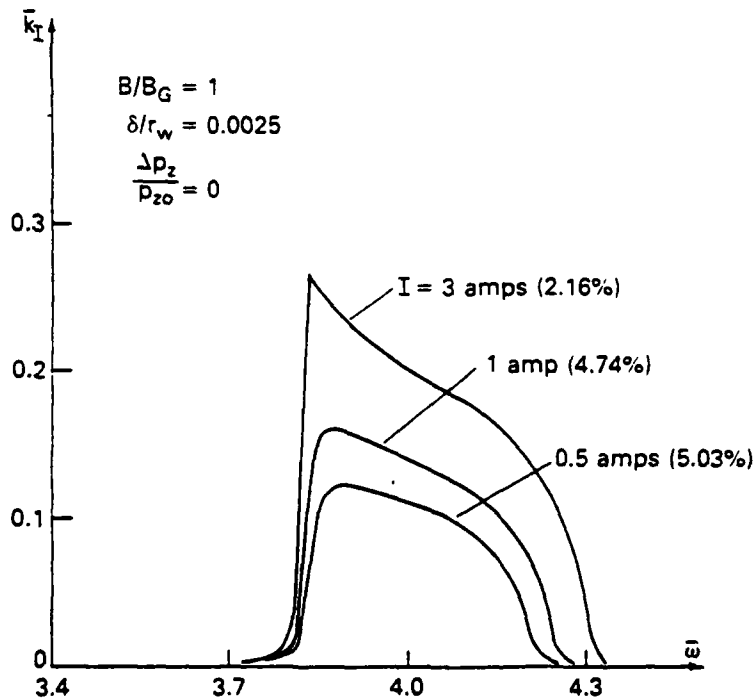
Fig. 21 — Same as in Fig. 9.

Fig. 22 — Normalized amplification rate $\bar{k}_I$ versus normalized frequency $\bar{\omega}$. Here, only the current I is allowed to vary, all other parameters B/B_G, δ/r_w, $\Delta p_z/p_{zo}$, are fixed at the values as indicated in the figure. The numbers in paranthesis denote the bandwidths.
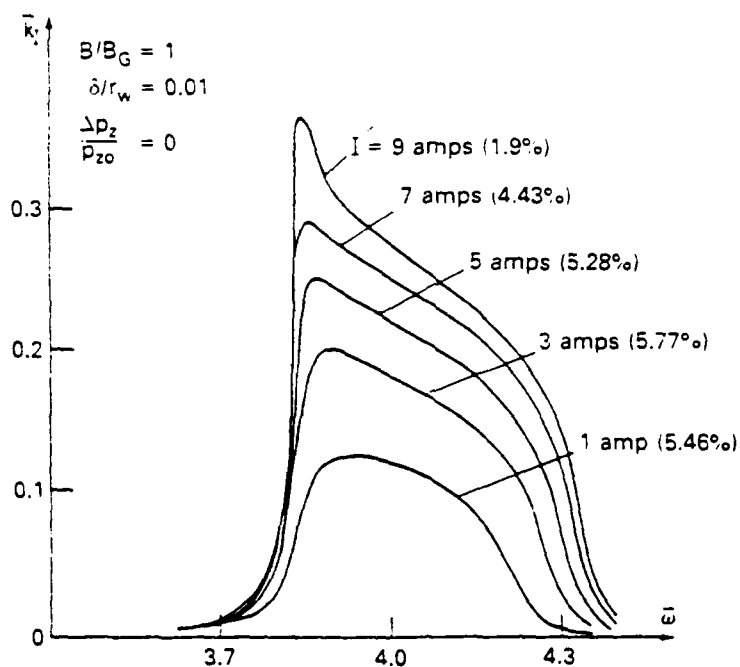
Fig. 23 — Same as Fig. 22.

Fig. 24 — Same as Fig. 22.

$B/B_G = 0.98$

$\delta/r_w = 0.0025$

$\dfrac{\Delta p_z}{p_{zo}} = 15\%$

$I = 7$ amps (3.63%)

5 amps (3.61%)

3 amps (3.33%)

Fig. 25 — Same as Fig. 22.

$B/B_G = 0.98$

$\delta/r_w = 0.01$

$\dfrac{\Delta p_z}{p_{zo}} = 0$

$I = 14$ amps (5.18%)

10 amps (4.97%)

7 amps (4.49%)

4 amps (3.73%)

Fig. 26 — Same as Fig. 22.

B-35

Fig. 27 — Same as Fig. 22.

APPENDIX C

MODE COMPETITION IN A
GYROTRON CAVITY

THE MODEL

r_w

Cavity of length L

Tv_{z0}

r_o

r_L

$$T = \frac{2\pi}{\omega_2 - \omega_1}$$

Case of 3 rings

ASSUMPTIONS

1. Initially, all the electrons have the same $v_{\perp 0}$ and v_{z0} (i.e. cold beam)

2. Initially, all electrons have the same guiding center position r_0 (i.e. thin annular beam)

3. Mode frequency and spatial structure are unperturbed by the presence of the beam (i.e. tenuous beam)

4. There is a steady state in the presence of many modes in the cavity.

5. The equations of motion of each electron are independent of the other electrons (i.e. no space charge effects)

EQUATIONS OF MOTION FOR EACH ELECTRON

$$\frac{d\underline{P}}{dt} = - e\left[\sum_{i=1}^{M} \underline{E}_i + \frac{1}{c}\underline{v} \times (\underline{B}_O + \sum_{i=1}^{M} \underline{B}_i)\right]$$

$$\frac{d\Delta\gamma_i}{dt} = - \frac{e}{mc^2}\underline{v} \cdot \underline{E}_i \quad , \; i = 1, 2, \ldots, M$$

where

$$\gamma = \left[1 + \underline{P}^2/m^2c^2\right]^{\frac{1}{2}}$$

$$\underline{v} = \underline{P}/\gamma m = \frac{d\underline{x}}{dt}$$

Initial values of $\Delta\gamma_i(t_O) = 0$.

For the mode $TE_{on\ell}$, the EM field is equal to:

$$E_\theta = E_O J_1(k_n r) \; \sin k_z z \; \cos(\omega t + \phi_O)$$

$$B_r = \frac{k_z}{\omega} E_O J_1(k_n r) \; \cos k_z z \; \sin(\omega t + \phi_O)$$

$$B_z = - \frac{k_n}{\omega} E_O J_0(k_n r) \; \sin k_z z \; \sin(\omega t + \phi_O)$$

where

$$J_1(k_n r_w) = 0$$

$$k_z = \frac{\pi\ell}{L}, \; \ell = 1, 2, \ldots$$

$$\omega = \left[k_n^2 + k_z^2\right]^{\frac{1}{2}} c$$

MAIN QUANTITIES EVALUATED

$$\Delta W_i(\phi_r, R_s) \equiv -\Delta \gamma_i \, mc^2, \quad i = 1, 2, \ldots M$$

i.e. the energy deposited to the ith mode by each electron traversing the cavity.

ϕ_r: initial phase angle of electron

R_s: ring on which electron is located initially

DEFINITION OF EFFICIENCY FOR EACH MODE

$$\eta_i = \frac{1}{N W_b} \sum_{r,s}^{N} \Delta W_i(\phi_r, R_s)$$

N: Total number of electrons

W_b: Initial energy of each electron

The efficiency for each mode depends on the amplitudes E_{01}, E_{02}, ..., E_{0M} of all the modes, i.e.

$$\eta_i = f_i(E_{01}, E_{02}, \ldots, E_{0M})$$

$$i = 1, 2, \ldots, M.$$

TEST OF CONVERGENCE

The efficiency for each mode converges to a fixed value as the number of rings increases. (This value is independent of the constant phase for each mode.)

TEST OF CONVERGENCE

Modes: TE_{011}, TE_{012}

$\overline{L} = 8$ $s = 1$

$\overline{r}_o = 0.48$ $\Delta_i = 3.5$

$\gamma = 1.14$ $\overline{E}_1 = 0.1$

$\alpha = 1.5$ $\overline{E}_2 = 0.05$

Efficiency (%)

25

20

10

5

Mode TE_{011}

6 rings chosen for the runs

Mode TE_{012}

1   2   3   4   5   6   7   8

Number of rings

TEST OF CONVERGENCE

Modes: TE_{021} TE_{022}

$\overline{L}$ = 5   s = 2

$\overline{r}_o$ = 0.51 $\triangle_1$ = 3.0

γ = 1.14 $\overline{E}_1$ = 0.1

α = 1.5 $\overline{E}_2$ = 0.05

Mode TE_{021}

5 rings chosen for the runs

Mode TE_{022}

Efficiency (%)

Number of Rings

TEST OF CONVERGENCE

Modes:	TE_{011}	TE_{012}
$\overline{L} = 8$	$\alpha = 1.5$	
$\overline{r}_o = 0.48$	$s = 1$	$\overline{E}_1 = 0.1$
$\gamma = 1.14$	$\triangle_1 = 3.5$	$\overline{E}_2 = 0.05$

Number of Rings	Phase Difference	$\eta_1 (\%)$	$\eta_2 (\%)$
1	0	24.481	4.968
2	0	23.173	0.534
4	0	24.566	1.646
5	0	23.877	1.865
6	0	24.384	1.812
6	3.1415	24.410	1.798
7	0	24.321	1.959
8	0	24.183	1.766

TEST OF CONVERGENCE

Modes: TE_{021} TE_{022}

$\bar{L} = 5$ $\alpha = 1.5$ $\bar{E}_1 = 0.1$

$\bar{r}_o = 0.51$ $s = 2$ $\bar{E}_2 = 0.05$

$\gamma = 1.14$ $\ell_1 = 3.0$

Number of Rings	Phase Difference	$\eta_1(\%)$	$\eta_2(\%)$
1	0	4.046	1.071
2	0	2.523	0.587
3	0	2.512	0.630
4	0	2.513	0.628
4	3.1415	2.473	0.630
5	0	2.493	0.645
5	3.1415	2.495	0.644
6	0	2.511	0.629
6	3.1415	2.475	0.631
7	0	2.511	0.629
8	0	2.495	0.625

DEFINITION OF STEADY STATE

Let

$$F_i(E_{01}, E_{02}, \ldots, E_{0M}, P_b) \equiv r_i P_b - \frac{\omega_i W_{fi}}{Q_i}$$

for $i = 1, 2, \ldots, M$.

$r_i P_b \equiv P_{di}$: Power deposited to the ith mode by the beam

$\dfrac{\omega_i W_{fi}}{Q_i} \equiv P_{fi}$: Wave power of the ith mode
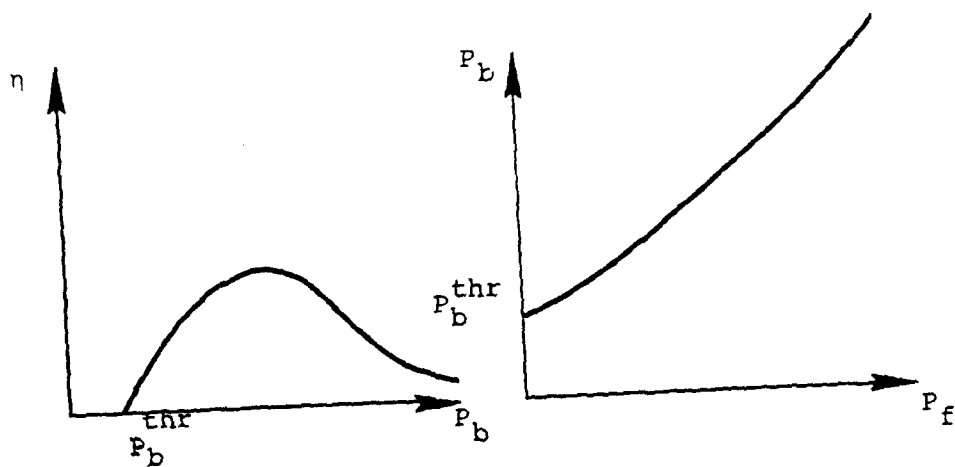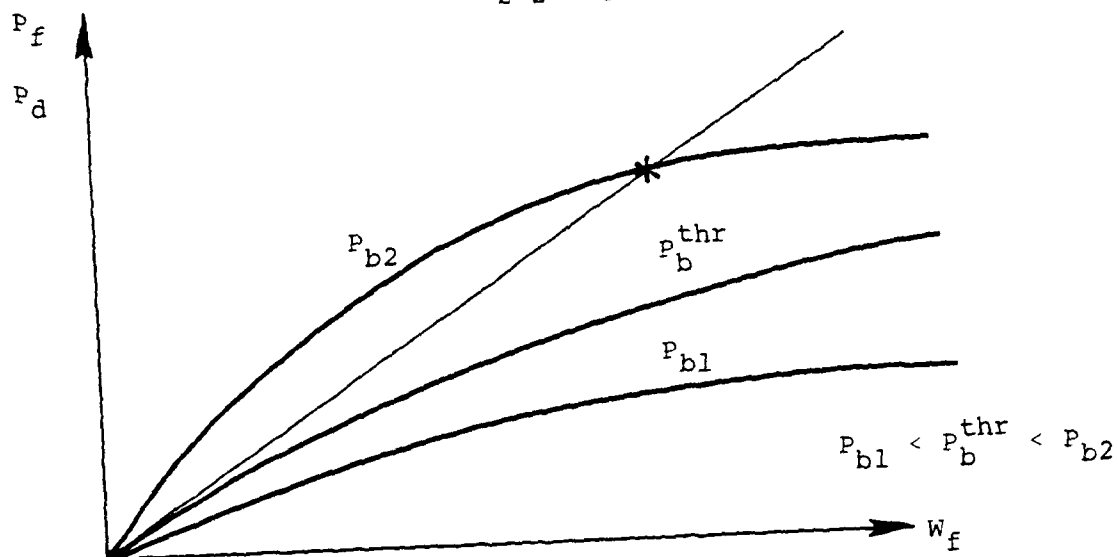
- The M nonlinear equations

$$F_i(E_{01}, E_{02}, \ldots, E_{0M}, P_b) = 0, \quad i = 1, 2, \ldots, M$$

  define the steady state for each value of the beam power P_b.
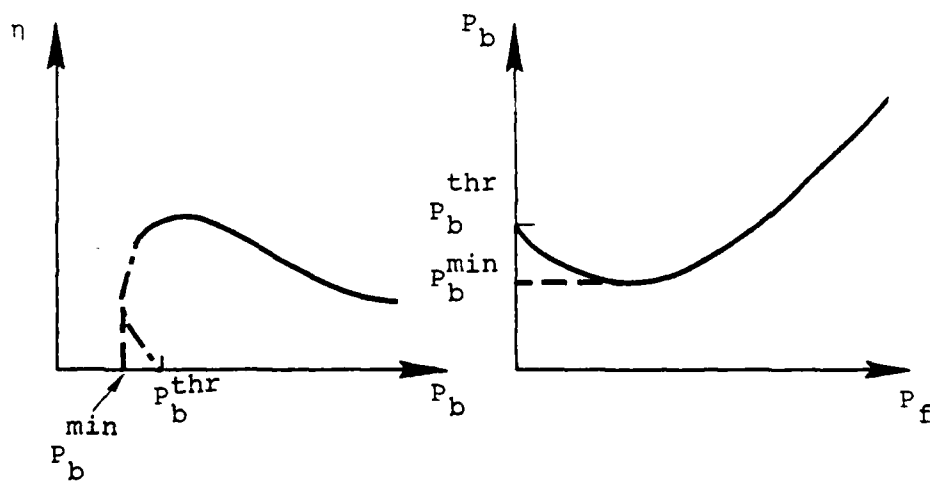
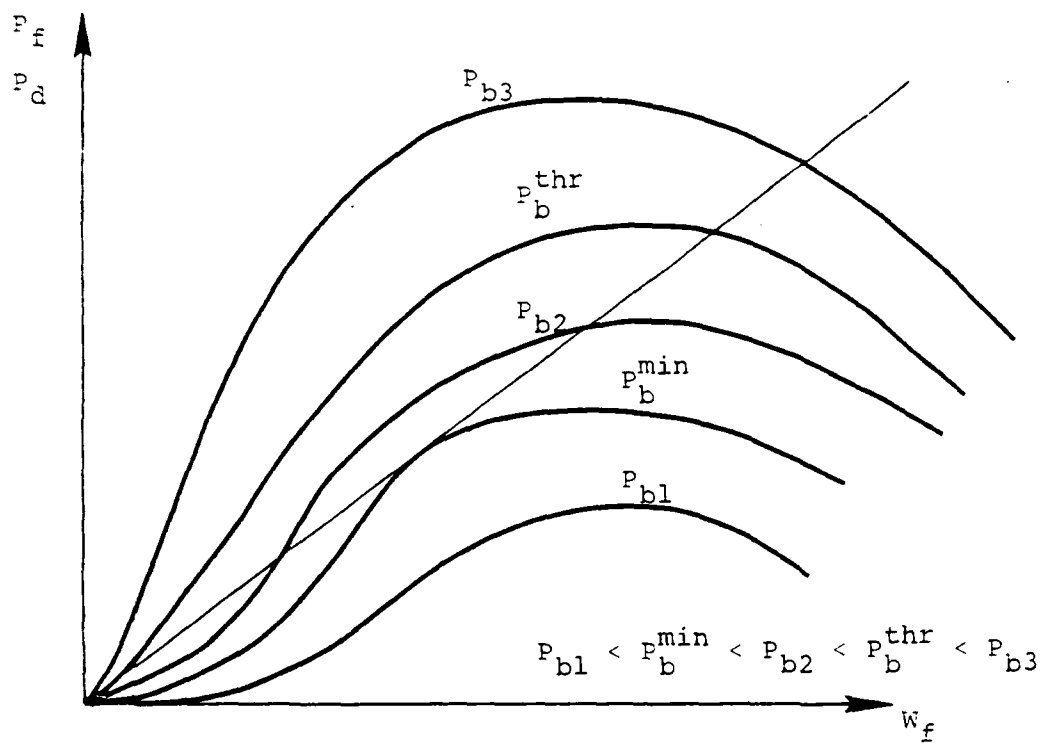- At the steady state, there is a balance of power for each mode.

For a single mode, the steady state can be described
as follows:

I. $\bar{L}$ or $\bot$ small: $\bot \equiv (\omega - k_z v_z - s\hat{\Omega}_e/\gamma)\tau$

$$P_{b1} < P_b^{thr} < P_{b2}$$

II. $\bar{L}$ or $\underline{L}$ large

a) The threshold P_b^{thr} exists

$P_{b1} < P_b^{min} < P_{b2} < P_b^{thr} < P_{b3}$

b) The threshold P_b^{thr} does not exist

$P_{b1} < P_b^{min} < P_{b2} < P_{b3}$

AD-A124 072   RADIATION SOURCES AT ELECTRON CYCLOTRON HARMONIC
                FREQUENCIES(U) SCIENCE APPLICATIONS INC MCLEAN VA
                Y Y LAU ET AL. 28 JAN 83 SAI-83-134-WA N00173-79-C-0450
UNCLASSIFIED   F/G 14/2   NL

2/2

END
DATE
FILMED

DTIC

MICROCOPY RESOLUTION TEST CHART

NATIONAL BUREAU OF STANDARDS 1963 A
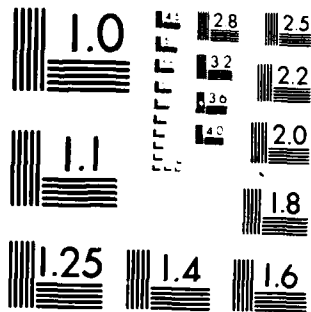
BASIC ASSUMPTION OF MODE EXCITATION

- The beam voltage is fixed.

- As the beam current (or P_b) is increased from zero to a certain value, the system traces a sequence of steady states (as defined above).

- The mode with the lowest threshold is excited first.

- As the beam current is increased, a new mode is excited if this is allowed by the presence of the other modes in the cavity.

- The above assumption is valid since:

  Rising (or decay) time of fields $\sim$ nsec

  Rising time of beam current $\sim$ μsec

- A nonlinear algebraic system may have more than a single real solution for given P_b, and only one of these solutions is physically acceptable.

O Basic results will be presented for two modes as plots of the form
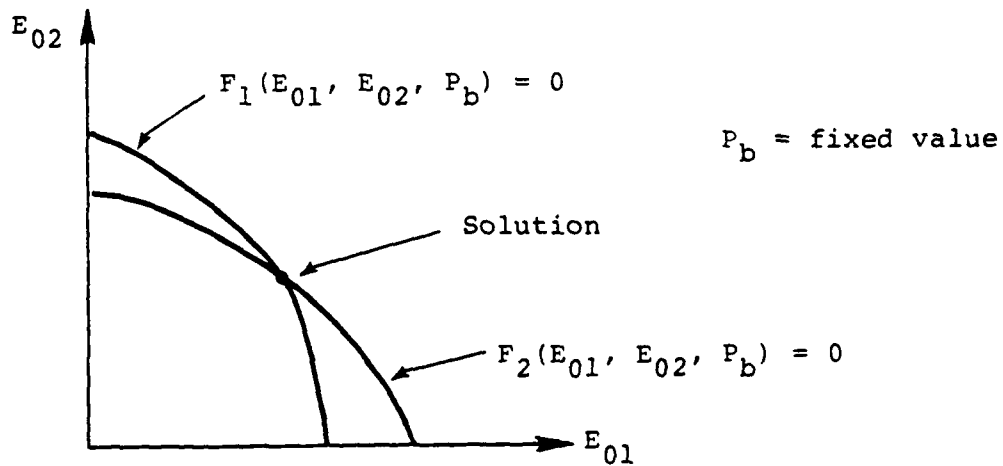

- - - Mode 1

——— Mode 2

● Each point in the above plots is obtained by solving the nonlinear algebraic equations

$$F_1(E_{01}, E_{o2}, P_b) = 0$$

$$F_2(E_{01}, E_{02}, P_b) = 0$$

for given P_b.

$F_1(E_{01}, E_{02}, P_b) = 0$

P_b = fixed value

Solution
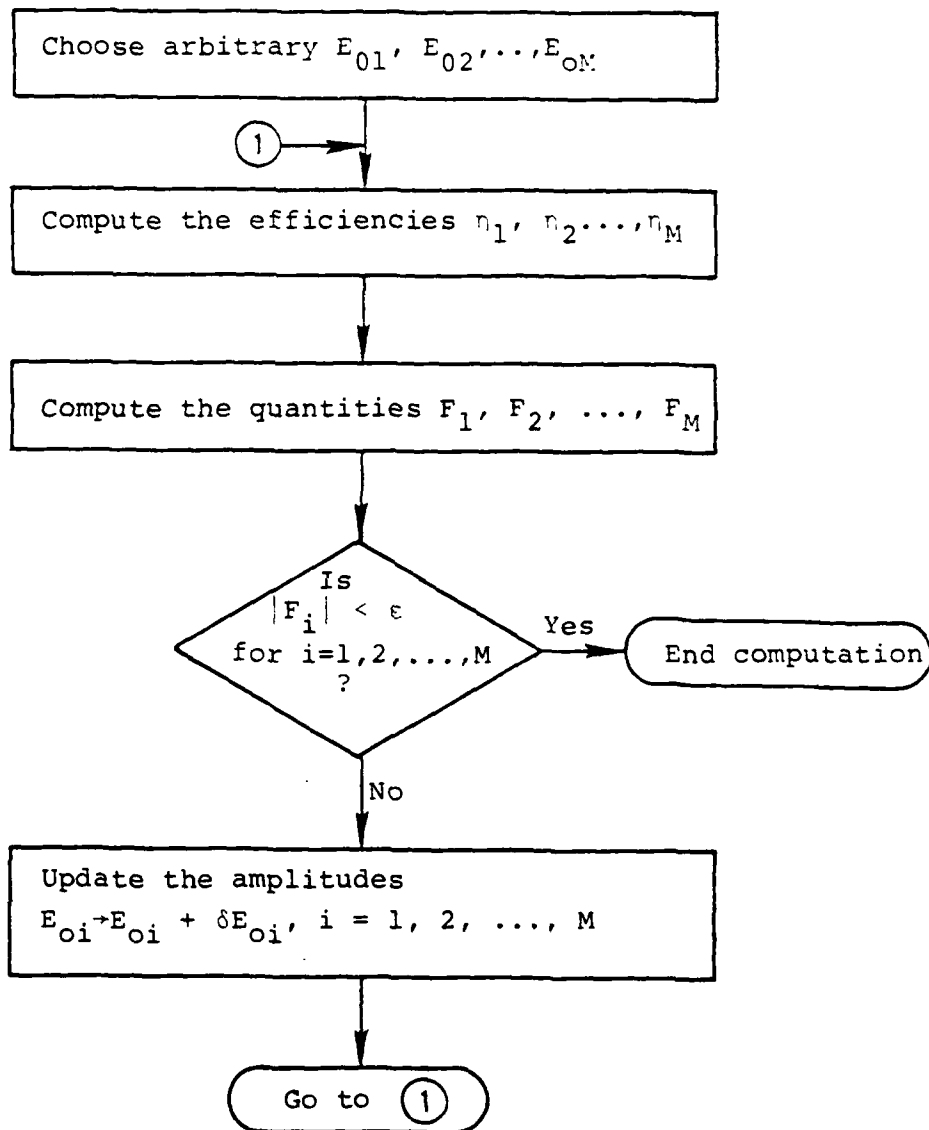
$F_2(E_{01}, E_{02}, P_b) = 0$

C-15

Iteration algorithm for solving the M nonlinear algebraic equations

$$F_i(E_{01}, E_{02}, \ldots, E_{OM}, P_b) = 0, \quad i = 1, 2, \ldots, M$$

for given P_b.

```
        ┌─────────────────────────────────────┐
        │  Choose arbitrary E₀₁, E₀₂,...,E_OM  │
        └─────────────────────────────────────┘
                          │
            ①──────▶      ▼
        ┌─────────────────────────────────────┐
        │  Compute the efficiencies n₁, n₂...,n_M │
        └─────────────────────────────────────┘
                          │
                          ▼
        ┌─────────────────────────────────────┐
        │  Compute the quantities F₁, F₂, ..., F_M │
        └─────────────────────────────────────┘
                          │
                          ▼
                      ◇ Is
                   |F_i| < ε        Yes
                  for i=1,2,...,M  ──────▶  ( End computation )
                        ?
                          │ No
                          ▼
        ┌─────────────────────────────────────┐
        │  Update the amplitudes               │
        │  E_oi→E_oi + δE_oi, i = 1, 2, ..., M │
        └─────────────────────────────────────┘
                          │
                          ▼
                  (  Go to  ①  )
```

- Another approach to the same problem, which provides information in selecting the physically acceptable solution, is the following:

Define:

$$X_i(E_{01}, E_{02}, \ldots, E_{0M}) \equiv \frac{\eta_i W_{fi}}{\eta_i}, \quad i = 1, 2, \ldots, M$$

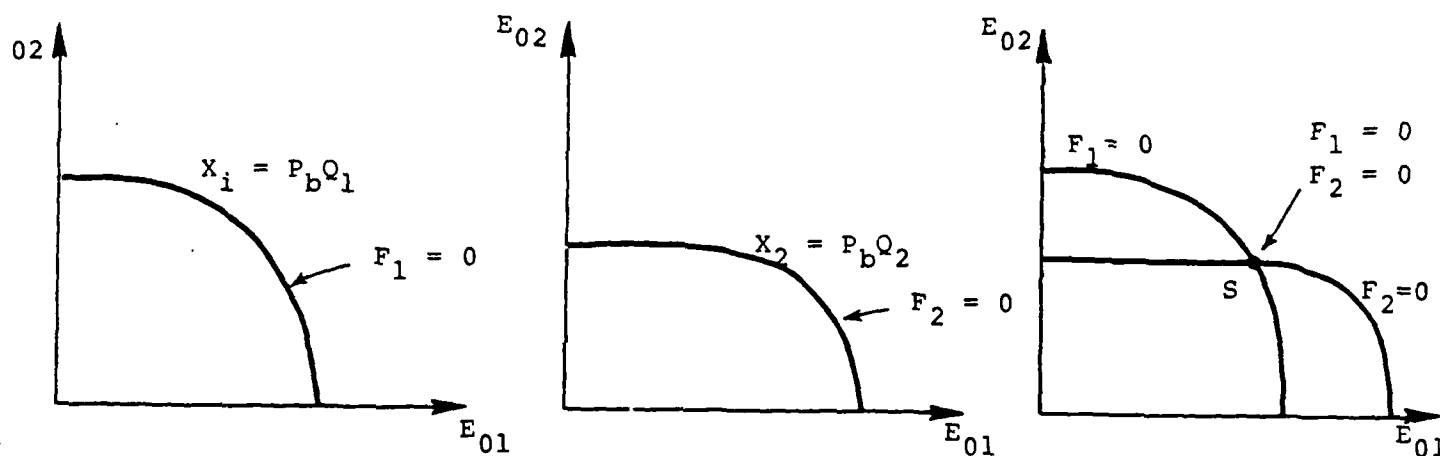$$K_i(E_{01}, E_{02}, \ldots, E_{0M}) \equiv \frac{X_i}{X_1}, \quad i = 1, 2, \ldots, M$$

Provide contour plots of X_i, K_i, η_i as functions of $E_{01}, E_{02}, \ldots, E_{0M}$. Notice that X_i, K_i are independent of P_b.

- From the definition of X_i, it follows that

$$F_i = \frac{\eta_i}{Q_i} \left[P_b Q_i - X_i \right], \quad i = 1, 2, \ldots, M$$
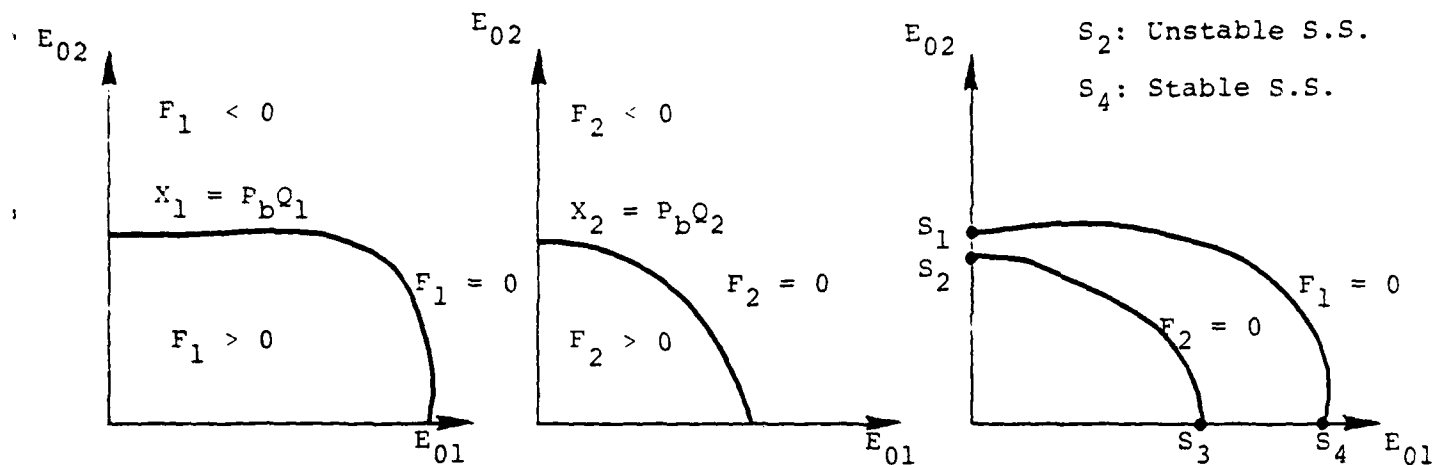
- Therefore, for a given cavity (Q_i fixed) and for given P_b, the relation $F_i = 0$ holds on the contour $X_i = P_b Q_i$ for each $i = 1, 2, \ldots, M$.

Example 1: Two modes P_b = given value

The amplitudes E_{01}, E_{02} at S determine the steady state efficiencies $\eta_1(E_{01}, E_{02})$, $\eta_2(E_{01}, E_{02})$ for the given value of P_b.

Example 2: Two modes P_b = given value

E_{02}

$F_1 < 0$

$X_1 = P_b Q_1$

$F_1 = 0$

$F_1 > 0$

E_{01}

E_{02}

$F_2 < 0$

$X_2 = P_b Q_2$

$F_2 = 0$

$F_2 > 0$

E_{01}

E_{02}

S_2: Unstable S.S.

S_4: Stable S.S.

S_1
S_2

$F_1 = 0$

$F_2 = 0$

S_3 S_4 E_{01}

● Contour $F_1 = 0$ ($F_2 = 0$) divides plane into two regions where $F_1 > 0$
  ($F_2 > 0$) and $F_1 < 0$ ($F_2 < 0$).

● When $F_1 > 0$ ($F_2 > 0$) the mode 1 (2) amplifies
  When $F_1 < 0$ ($F_2 < 0$) the mode 1 (2) decays.

● At S_1: $F_2 < 0 \rightarrow E_{o2}$ decays to S_2
  At S_2: $F_1 = 0$, $F_2 = 0$. For infinitesimal E_{01} (noise) $F_1 > 0 \rightarrow E_{01}$
          amplifies to S_4 (Unstable steady state)
  At S_3: $F_1 > 0 \rightarrow E_{01}$ amplifies to S_4
  At S_4: $F_1 = 0$, $F_2 = 0$. For infinitesimal E_{02} (noise) $F_2 < 0 \rightarrow E_{02}$
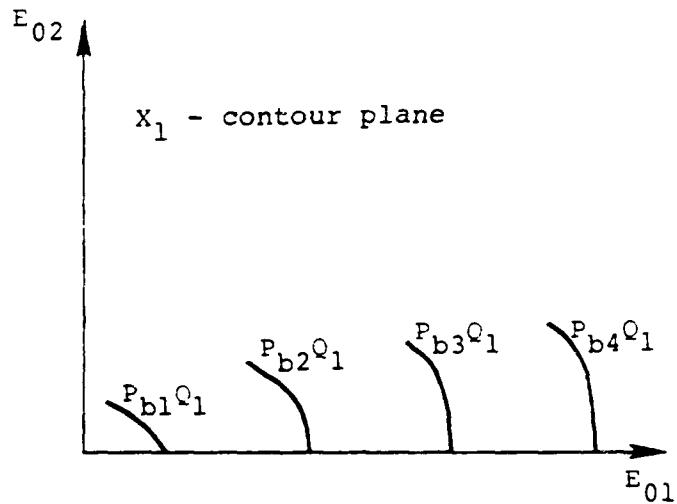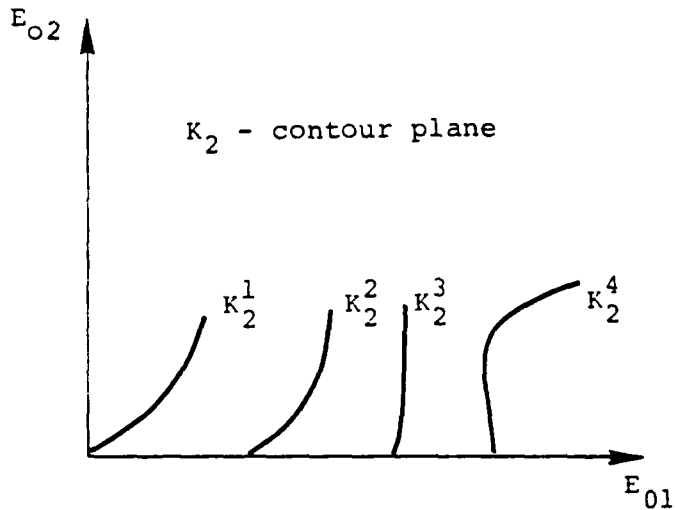   decays back to S_4 (Stable steady state)

- From the definition of F_i, it follows that, for all P_b, at a steady state (i.e. $F_i = 0$, $i = 1, 2, \ldots, M$) the relation

  $$F_i(E_{01}, E_{02}, \ldots, E_{0M}) = \frac{Q_i}{Q_1}, \quad i = 1, 2, \ldots, M$$

  holds.

- Therefore, for a given cavity (Q_i fixed) the contours $F_i = Q_i/Q_1$, $i = 1, 2, \ldots, M$, provide the sequence of steady states in the cavity as the beam power P_b increases, <u>if that is also the case (i.e. P_b increases) as we move along these contours</u>.
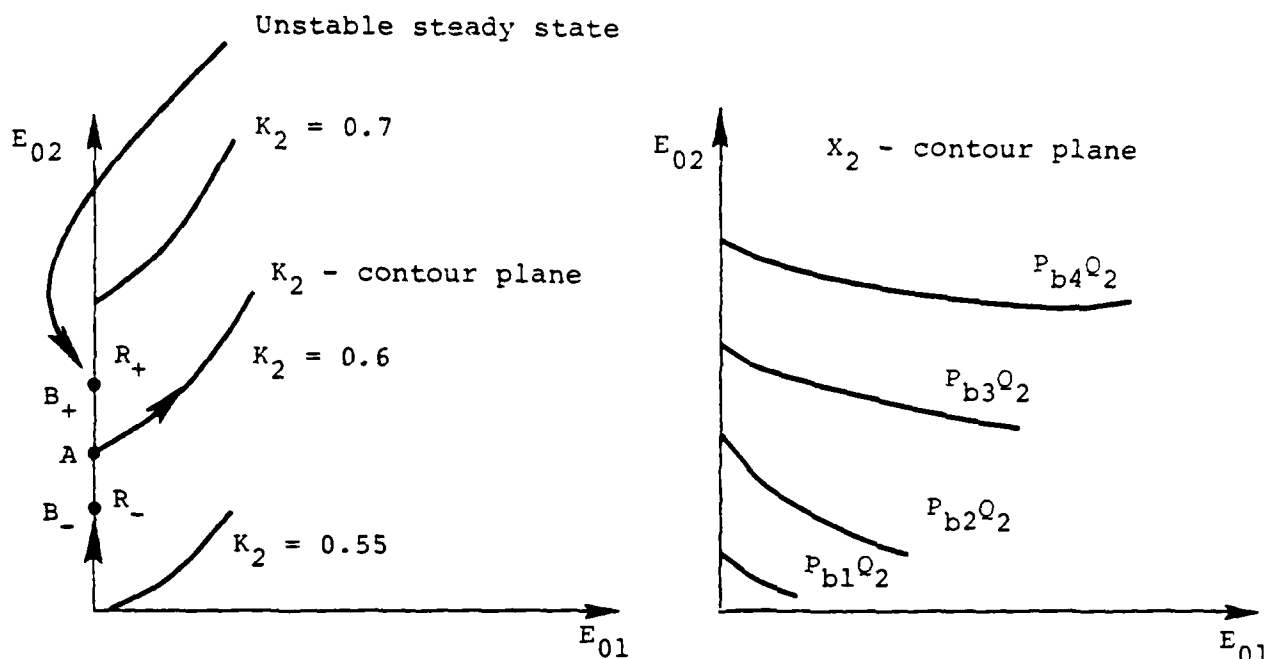
Example 3:   Two modes, $Q_2/Q_1 = 0.5$

Assume:

a) $K_2^n > 0.5$, all n

b) $P_{b1} < P_{b2} < P_{b3} < \ldots$

c) $P_{b1}^{thr} < P_{b2}^{thr}$

● Easy to show that if $F_1 = 0$, then

$$F_2 = \eta_2 P_b Q_2 \left[1 - \frac{K_2}{Q_2/Q_1} \right]$$

● It follows (since $K_2/(Q_2/Q_1) > 1$ for all K_2) that for infinitesimal E_{o2}, the relation $F_2 < 0$ holds. Thus, mode 2 will never be excited, as the beam power increases.

Example 4: Two modes, $Q_2/Q_1 = 0.6$

Unstable steady state

$K_2 = 0.7$

K_2 - contour plane

$K_2 = 0.6$

$K_2 = 0.55$

E_{02}

E_{01}

X_2 - contour plane

$P_{b4}Q_2$

$P_{b3}Q_2$

$P_{b2}Q_2$

$P_{b1}Q_2$

E_{02}

E_{01}

Assume:

a) In region R_- : $K_2 < 0.6$
    In region R_+ : $K_2 > 0.6$

b) $P_{b1} < P_{b2} < P_{b3} < \cdots$

c) $P_{b2}^{thr} < P_{b1}^{thr}$

● Easy to show that if $F_2 = 0$, then

$$F_1 = \eta_1 P_b Q_1 \left[1 - \left[\frac{Q_2/Q_1}{K_2} \right] \right]$$

For infinitesimal E_{01}, it follows that
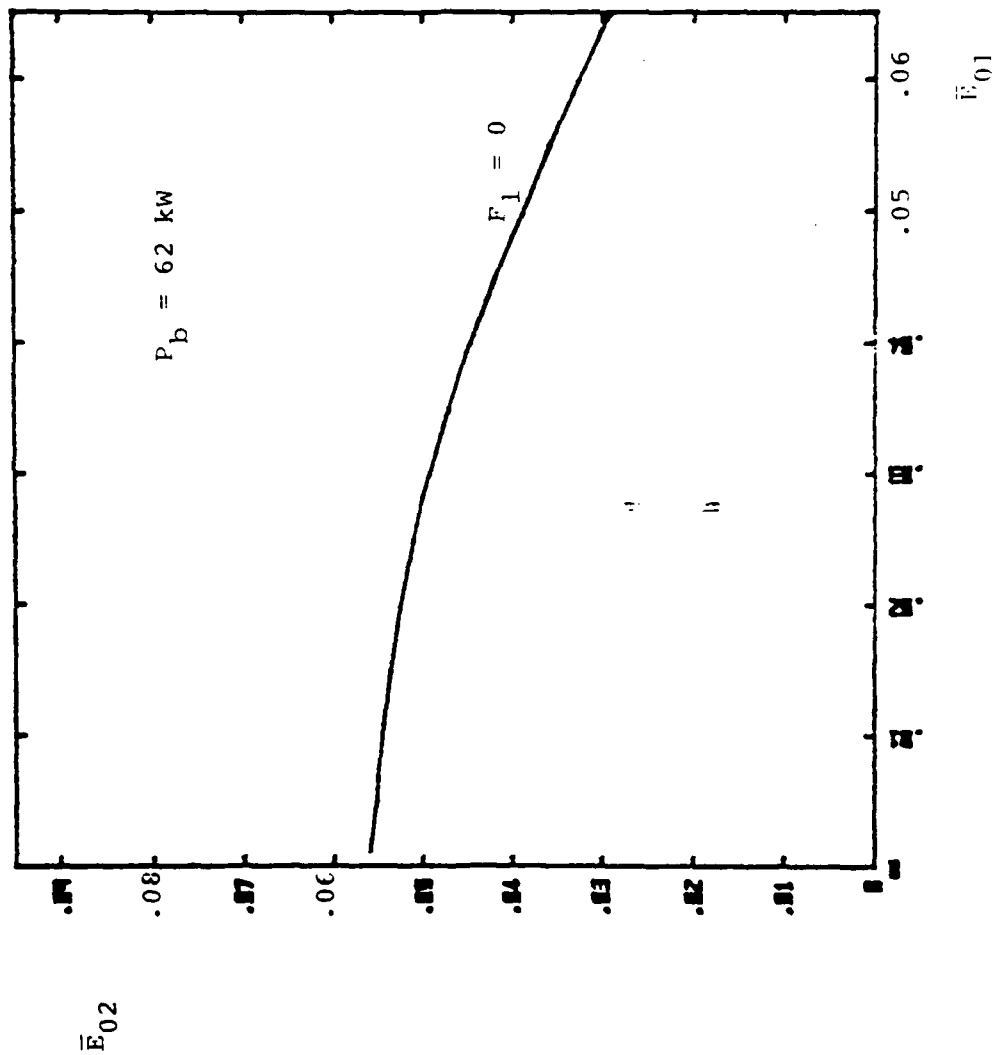$F_2 < 0$ for points B_- in region R_-
$F_2 > 0$ for points B_+ in region R_+
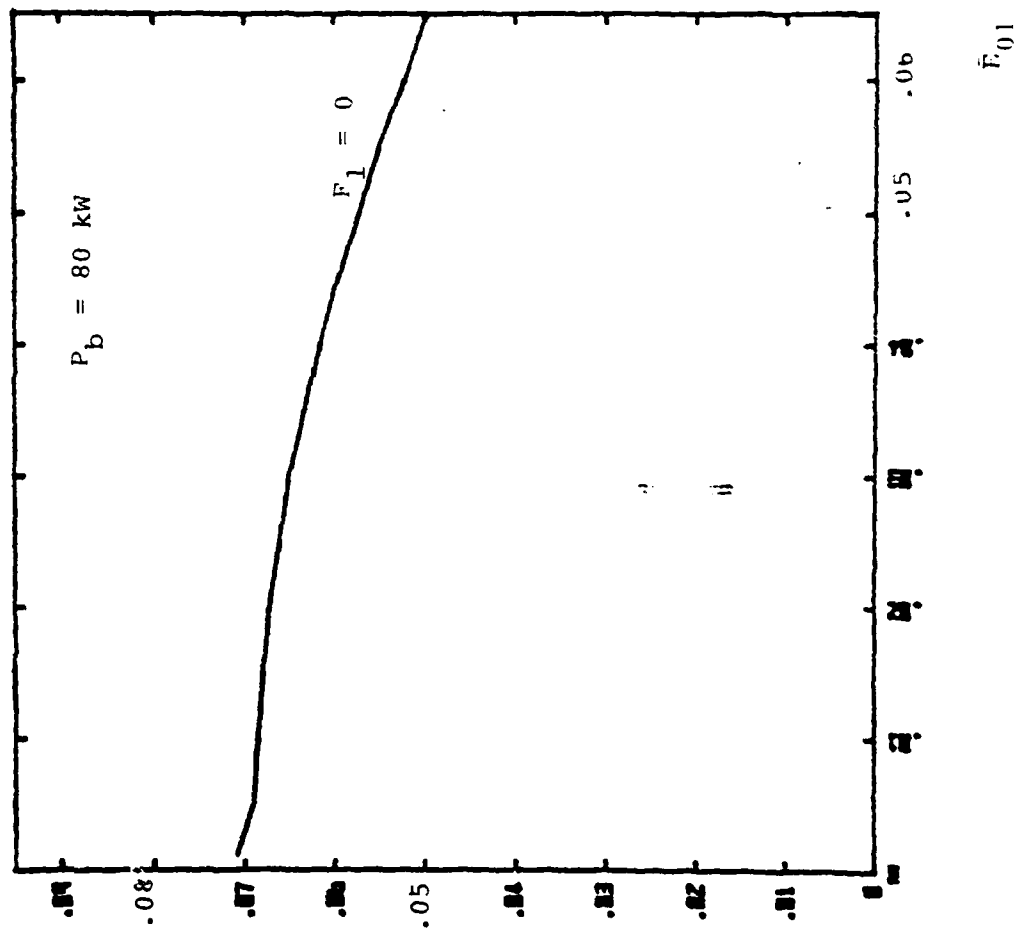Thus, as the beam power increases, the sequence of s.s. will be along
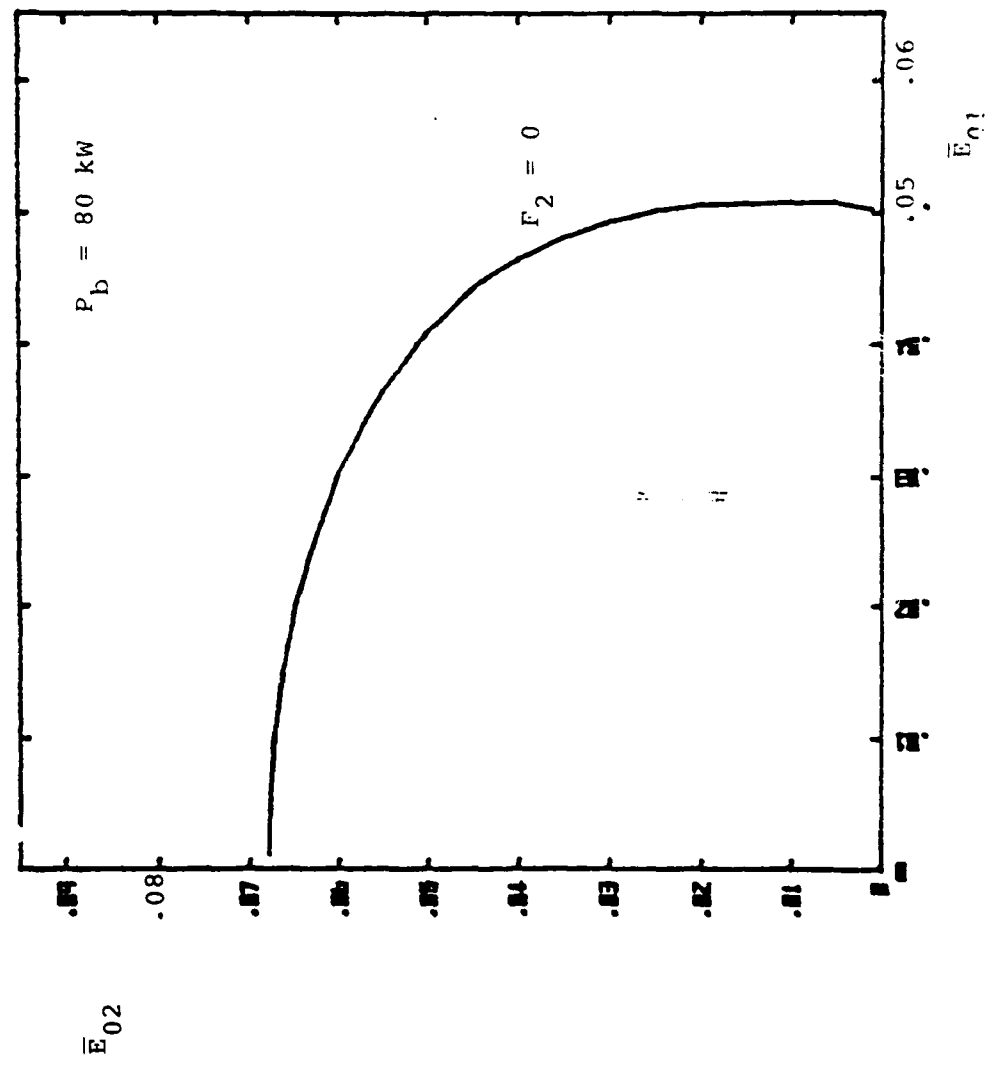contour $K_2 = 0.6$.

Mode 1, Mode 2

Modes: TE_{011}, TE_{012}

$\bar{E}_{02}$

$P_b = 62$ kw

$F_1 = 0$

$\bar{E}_{01}$

$\bar{L} = 8$

$\bar{r}_C = 0.48$

$\gamma = 1.14$

$\alpha = 1.5$

$s = 1$

$\Lambda_1 = 3.5$

$Q_1 = 1000$

$Q_2 = 800$

Mode 1, Mode 2

Modes: TE_{011}, TF_{012}

$P_b = 80$ kW

$F_1 = 0$

$\bar{E}_{02}$

$\bar{F}_{01}$

$\bar{L} = 8$

$\bar{r}_o = 0.48$

$f = 1.14$

$\alpha = 1.5$

$s = 1$

$\Lambda_1 = 3.5$

$Q_1 = 1000$

$Q_2 = 800$

C-23

Modes: Mode 1, Mode 2

modes: TE_{011}, TE_{012}

$\bar{L} = 8$

$\bar{r}_0 = 0.48$

$\gamma = 1.14$

$\alpha = 1.5$

$s = 1$

$\Lambda_1 = 3.5$

$Q_1 = 1000$

$Q_2 = 800$

$P_b = 80$ kW

$\Gamma_2 = 0$

$\bar{E}_{02}$

$\bar{E}_{01}$

.06

.05

- The contour plots of X_i, K_i provide information on the threshold beam power for each mode.

- In the linear regime (i.e. $\overline{E}_{oi} \ll 1$, $i = 1, 2, \ldots, M$):

$$X_{i,\text{lin}} \equiv \frac{\gamma_i W_{fi}}{\nu_i} = P_{bi}^{\text{thr}} Q_i$$

Thus $P_{bi}^{\text{thr}} Q_i$ is computed from the value of X_i at the origin. (Since $\gamma_i \sim E_{oi}^2$, $W_{fi} \sim E_{oi}^2$ in the linear regime, $X_{i,\text{lin}}$ is independent of E_{oi}).
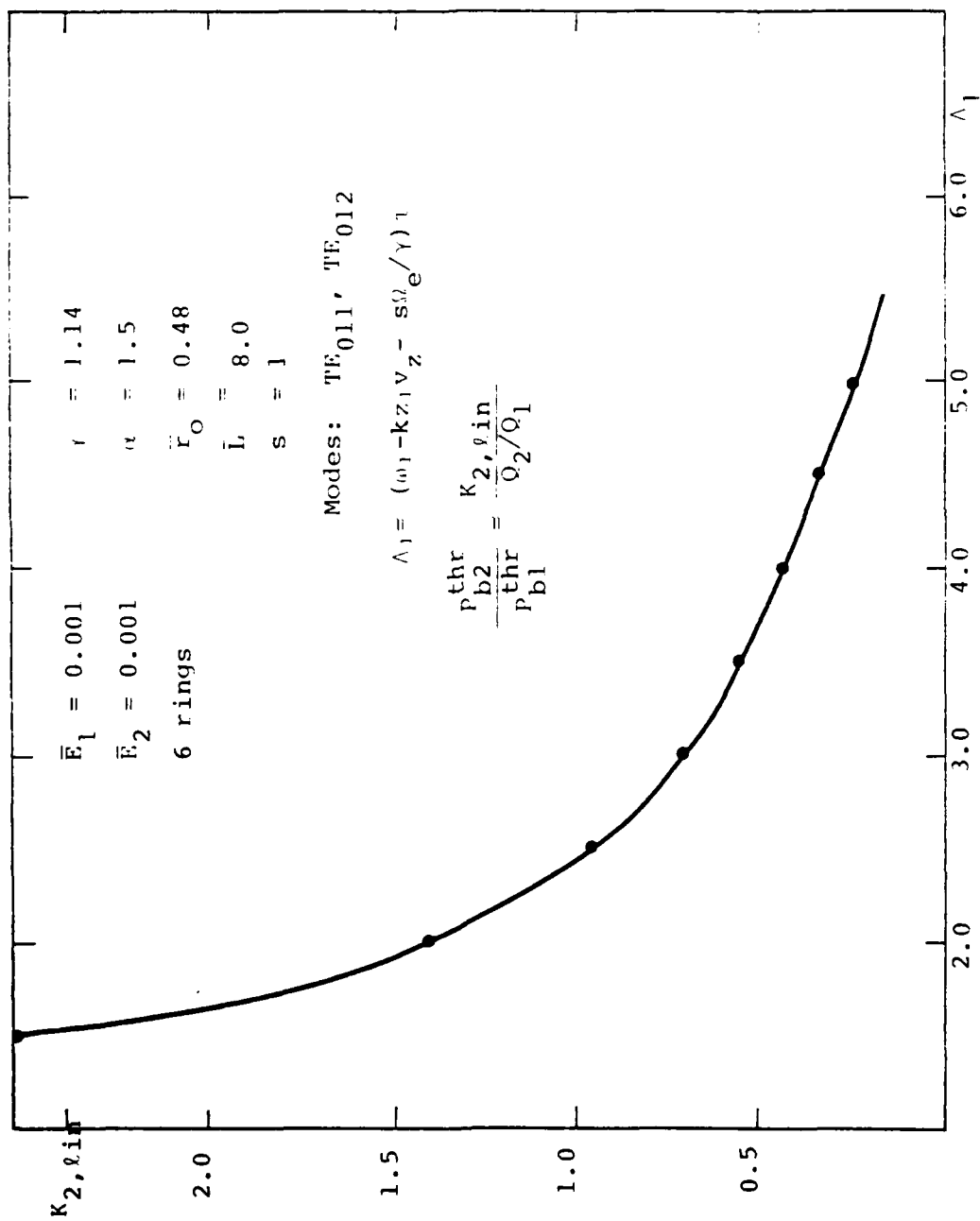
- The relation

$$\frac{P_{bi}^{\text{thr}}}{P_{b1}^{\text{thr}}} = \frac{K_{i,\text{lin}}}{Q_i/Q_1} \text{ holds.}$$

- For two modes:

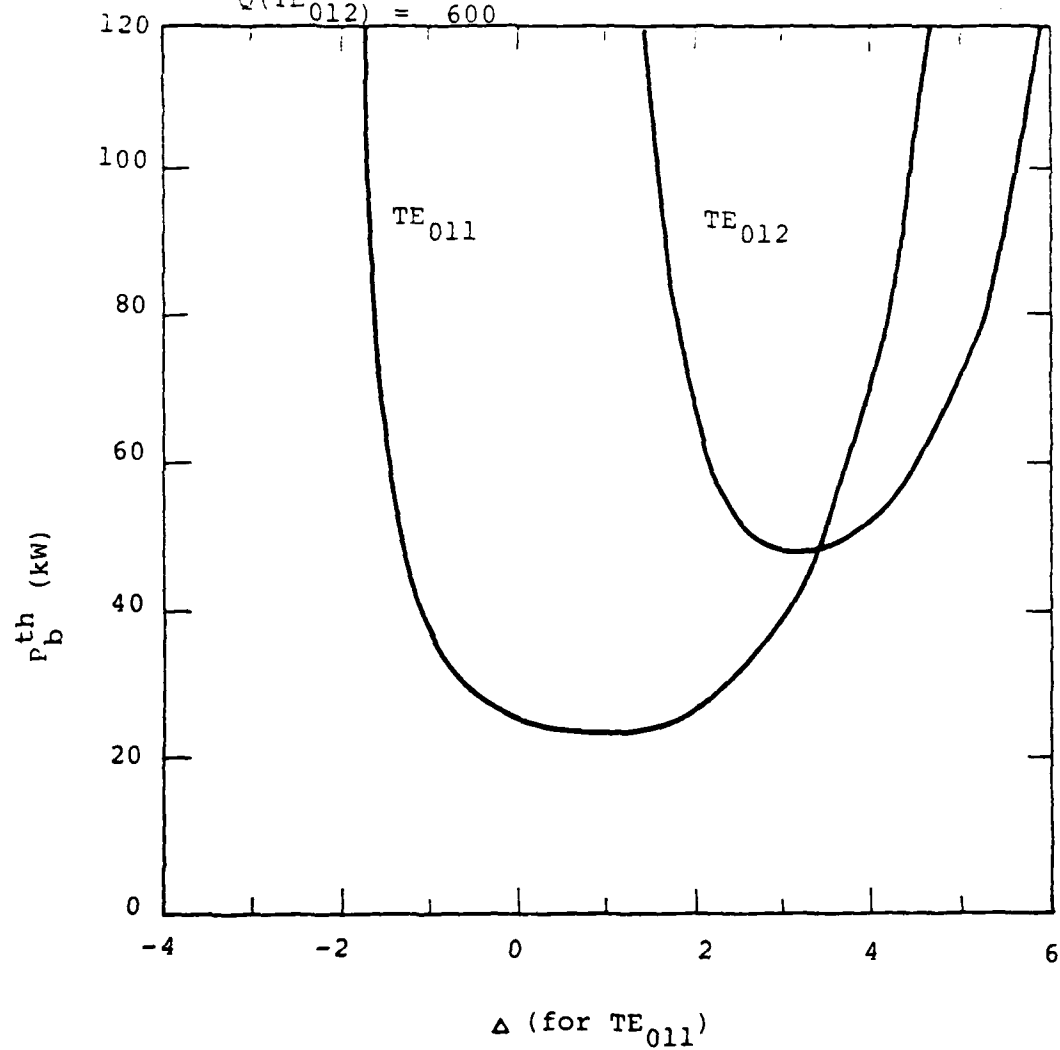If $Q_2/Q_1 < K_{2,\text{lin}} \rightarrow P_{b2}^{\text{thr}} > P_{b1}^{\text{thr}}$

If $Q_2/Q_1 > K_{2,\text{lin}} \rightarrow P_{b2}^{\text{thr}} < P_{b1}^{\text{thr}}$

$$\bar{E}_1 = 0.001$$

$$\bar{E}_2 = 0.001$$

6 rings

$$r = 1.14$$

$$\alpha = 1.5$$

$$\bar{r}_0 = 0.48$$

$$\bar{L} = 8.0$$

$$s = 1$$

Modes: TE_{011}, TE_{012}

$$\Lambda_1 = (\omega_1 - kz_1 v_z - s\Omega_e/\gamma)\tau$$

$$\frac{P_{b2}^{thr}}{P_{b1}^{thr}} = \frac{K_{2,\ell in}}{Q_2/Q_1}$$

$K_{2,\ell in}$ (vertical axis): 2.0, 1.5, 1.0, 0.5

Λ_1 (horizontal axis): 2.0, 3.0, 4.0, 5.0, 6.0

$\overline{L} = .8,\quad = 1.14,\ a = 1.5,\ \overline{r}_O = 0.48,\ s = 1$

$Q(TE_{011}) = 1000$

$Q(TE_{012}) = 600$

The plot shows P_b^{th} (kW) on the vertical axis (0 to 120) versus Δ (for TE_{011}) on the horizontal axis (−4 to 6), with two curves labeled TE_{011} and TE_{012}.

C-27

Mode 1, Mode 2

Modes: TE$_{011}$, TE$_{012}$

$$L = 8$$
$$r_0 = 0.48$$
$$r = 1.14$$
$$? = 1.5$$
$$s = 1$$
$$? = 3.5$$

$$? = x_2$$
$$? = x_1$$
$$x_1 = \frac{?_1 w_{f1}}{?_1}$$
$$x_2 = \frac{?_2 w_{f2}}{?_2}$$

$\bar{E}_{02}$

r_2

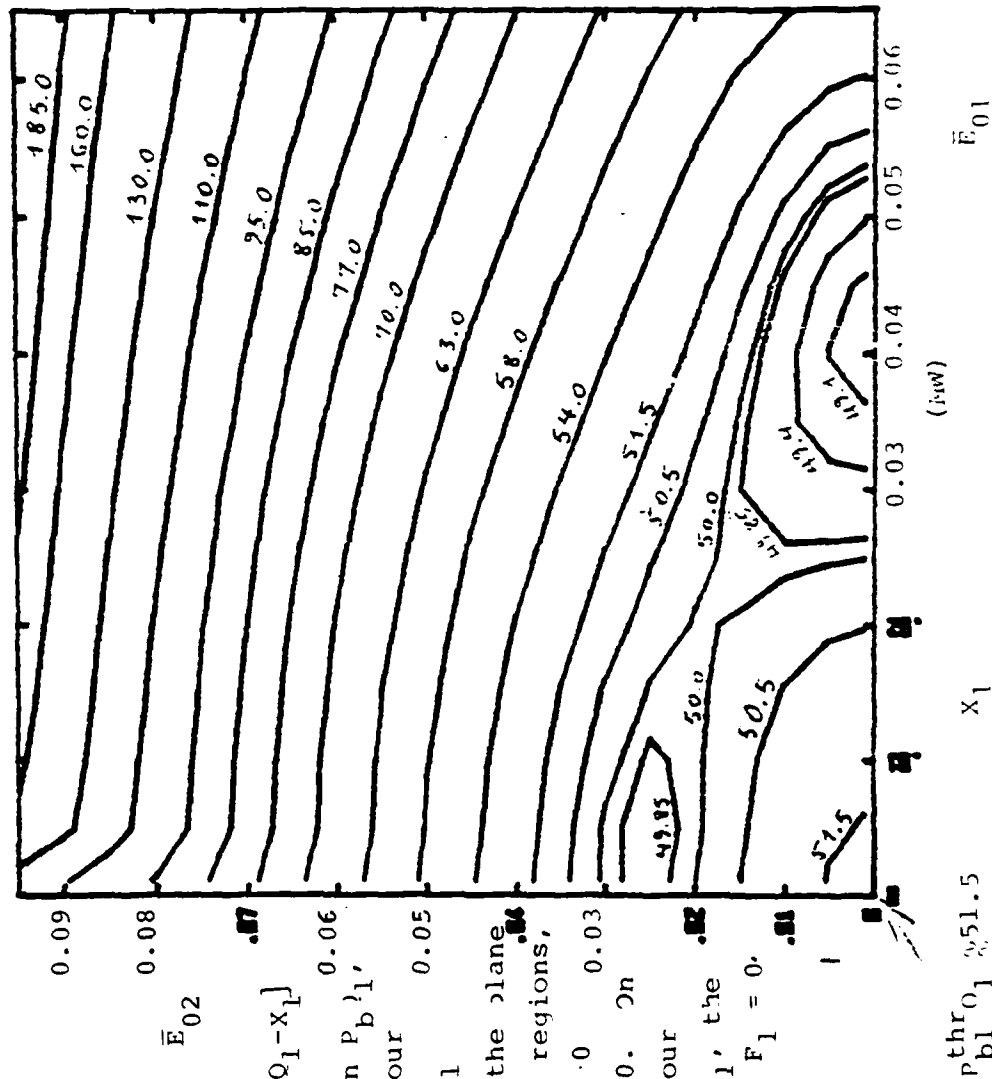E_{01}

Contour plots of K_2 as a function of E_{01}, E_{02}

For given Q_1, Q_2 if there is a continuous sequence of steady states as the beam power increases, then it must lie on the contour $K_2 = Q_2/Q_1$, when the two modes coexist in the cavity.

$$\frac{P_{b2}^{thr}}{P_{b1}^{thr}} = \frac{0.55}{Q_2/Q_1}$$

Mode 1, Mode 2

Modes: TE_{011}, TE_{012}

$F_l = \eta_l Q_l [P_b Q_l - x_l]$

For given $P_b Q_l$,
the contour
$x_l = P_b Q_l$
divides the plane
into two regions,
where $F_l > 0$
and $F_2 < 0$. On
the contour
$x_l = P_b Q_l$, the
relation $F_l = 0$.
holds.

$P_{bl}^{thr} Q_l \approx 51.5$

X_l

Contour plots of X_l (MW)

$L = 8$
$r_o = 0.48$
$\cdots = 1.14$
$\cdots = 1.5$
$s = 1$
$\cdots = 3.5$
$x_l = \cdots$

Mode 1, Mode 2

Modes: TE_{011}, TE_{012}

$\bar{L} = 8$

$\bar{r}_0 = 0.48$

$\gamma = 1.14$

$\alpha = 1.5$

$s = 1$

$\ell_1 = 3.5$

$x_2 = \omega_2 W_{f2}/n_2$

Contour plots of x_2 (MW)
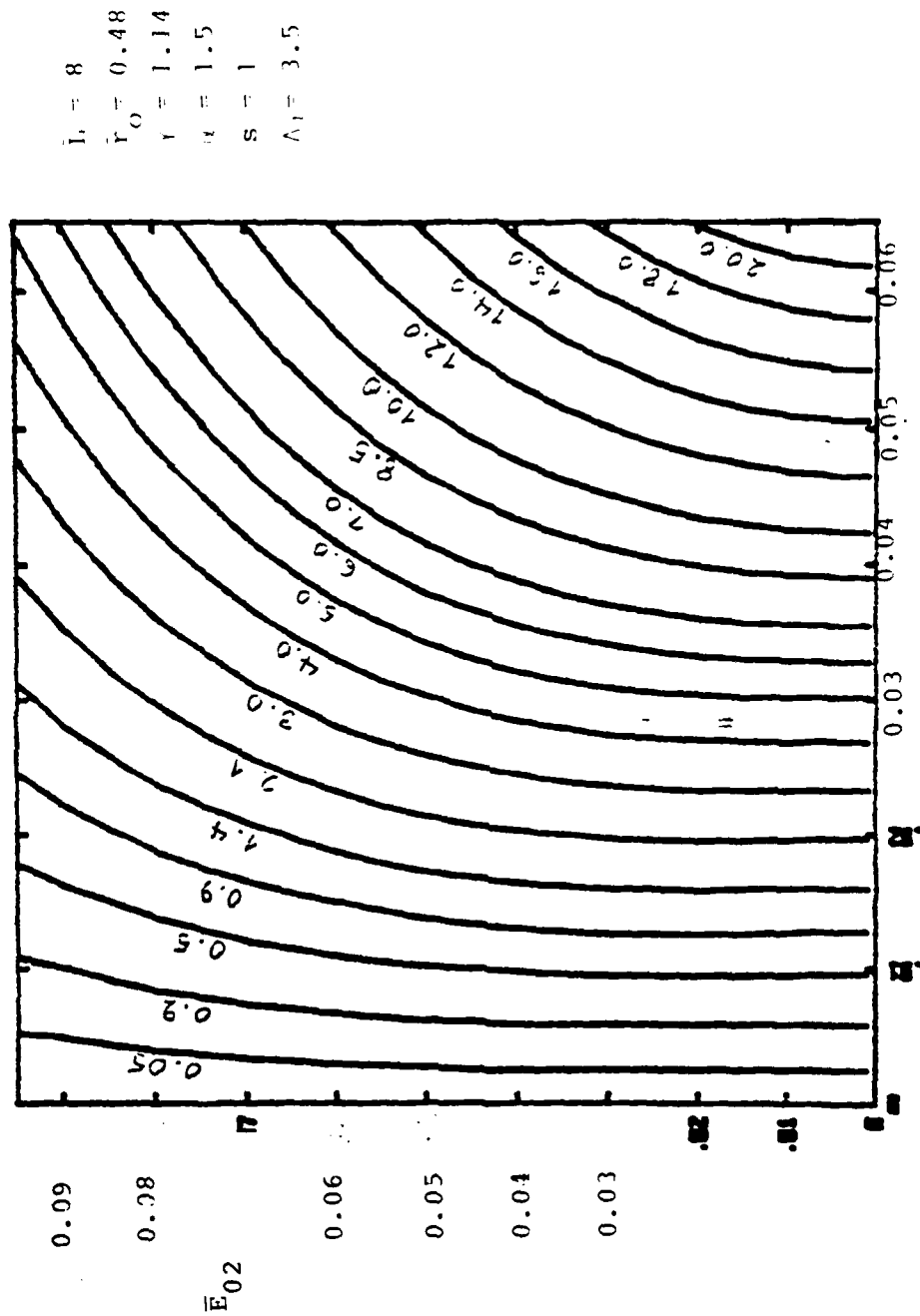
$F_2 \equiv \frac{n_2}{Q_2}[P_b Q_2 - x_2]$

For given $P_b Q_2$, the contour $x_2 = P_b Q_2$ divides the plane into two regions, where $F_2 > 0$ and $F_2 < 0$. On the contour $x_2 = P_b Q_2$, the relation $F_2 = 0$ holds.
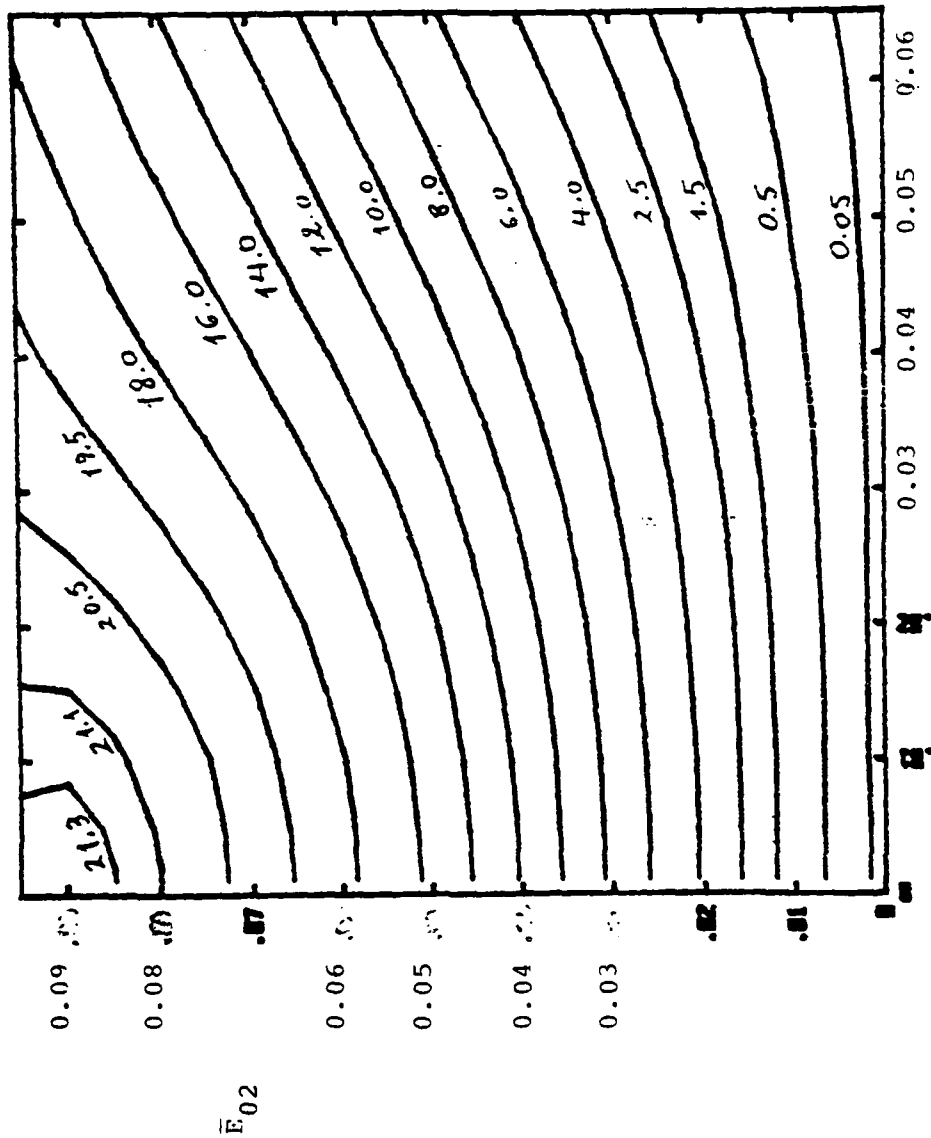
$P_{b2}^{thr} Q_{2c}$: 28.5

Mode 1, Mode 2

Modes: TE_{011}, TE_{012}

Contour Plot of Efficiency for Mode 1 (%) $\bar{r}_{01}$

$L = 8$
$\bar{r}_0 = 0.48$
$\gamma = 1.14$
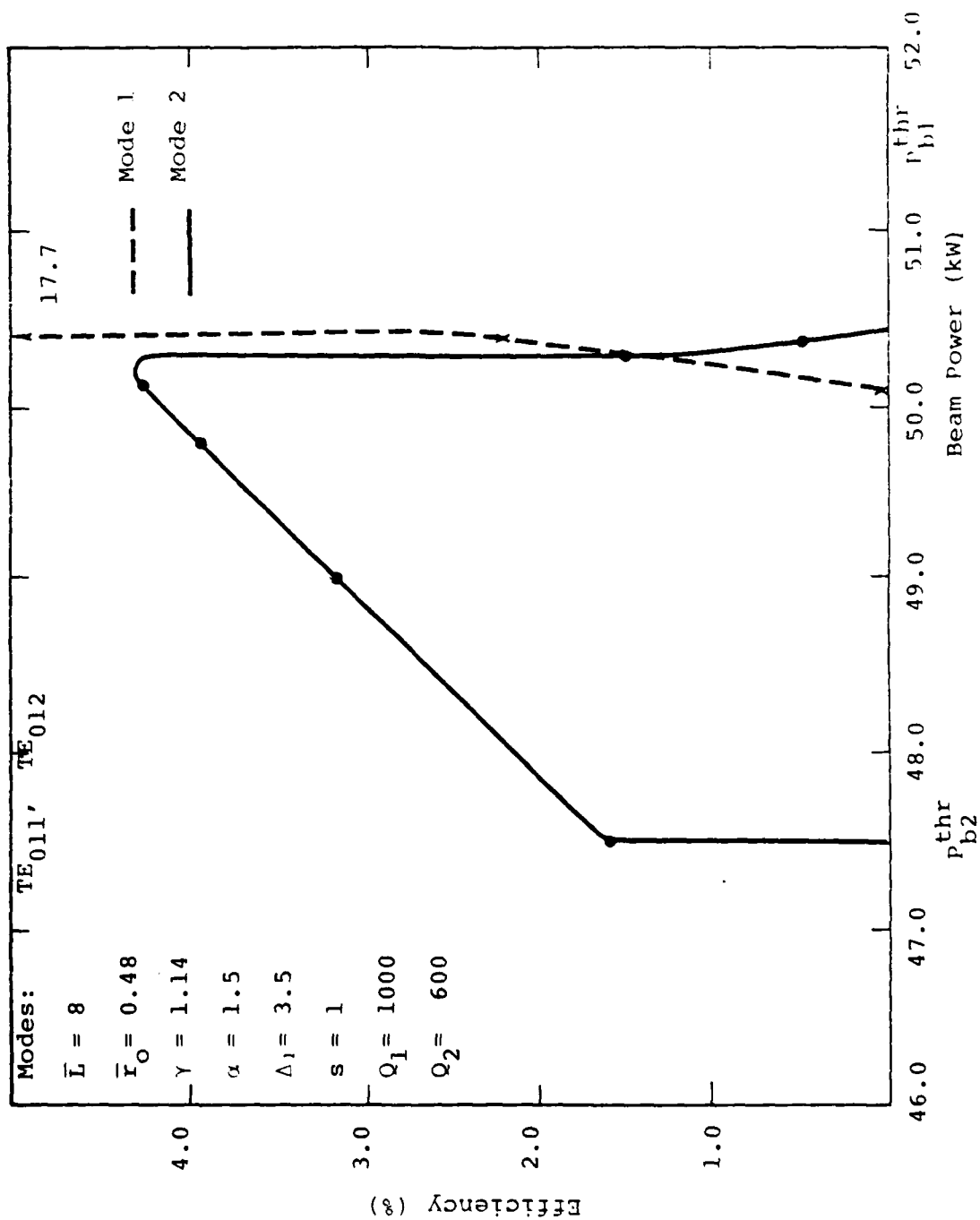$\alpha = 1.5$
$s = 1$
$A_1 = 3.5$

Mode 1, Mode 2

Modes: TE_{011}, TE_{012}

$L = 8$
$\bar{r}_O = 0.48$
$\gamma = 1.14$
$q = 1.5$
$s = 1$
$A_1 = 3.5$

Contour Plot of Efficiency for Mode 2 (%) $\bar{E}_{01}$

$\bar{E}_{02}$

Mode 1, Mode 2

Modes: TE$_{011}$, TE$_{012}$

$\bar{L} = 8$
$\bar{r}_o = 0.48$
$\gamma = 1.14$
$\alpha = 1.5$
$\Delta_1 = 3.5$
$s = 1$
$Q_1 = 1000$
$Q_2 = 600$

17.7

Mode 1
Mode 2

P_{b2}^{thr}
P_{b1}^{thr}

Beam Power (kW)

Efficiency (%)

C-33

Mode 1, Mode 2

Modes: TE_{011}, TE_{012}

$\bar{L} = 8$
$\bar{r}_o = 0.48$
$\gamma = 1.14$
$\alpha = 1.5$
$\Lambda_1 = 3.5$
$s = 1$

$Q_1 = 1000$
$Q_2 = 600$

———— Mode 1

———— Mode 2

Efficiency (%)

40.0
30.0
20.0
10.0

40.0   60.0   80.0   100.0   120.0   140.0   160.0

Beam power (kw)

Mode 1, Mode 2

Modes: TE_{011}, TE_{012}

$\overline{L} = 8$ $\Delta_1 = 3.5$

$\overline{r}_o = 0.48$ $s = 1$

$\gamma = 1.14$ $Q_1 = 1000$

$\alpha = 1.5$ $Q_2 = 600$

- - - Mode 1

——— Mode 2

P_{b1}^{thr}

P_{b2}^{thr}

Wave power (kW)

Mode 1, Mode 2

Modes: TE_{011}, TE_{012}

$\bar{L} = 8$

$\bar{r}_O = 0.48$

$\gamma = 1.14$

$\alpha = 1.5$

$\bar{\omega}_1 = 3.5$

$s = 1$

$Q_1 = 1000$

$Q_2 = 600$

Wave power (kW)

- - - Mode 1

——— Mode 2

C-36

Mode 1, Mode 2

Modes: TE_{021}, TE_{022}

Contour Plot of Efficiency for Mode 1 (%)

$L = 5$
$r_c = 0.51$
$Y = 1.14$
$\alpha = 1.5$
$s = 2$
$\Lambda_1 = 3.0$

Mode 1, Mode 2

Modes: TE_{021}, TF_{022}

Contour Plot of Efficiency for Mode 2 (%)

$\bar{E}_{02}$

$\bar{E}_{01}$

Mode 1, Mode 2

Modes: TE_{021}, TE_{022}

Contour Plot of K_2 as a Function of $\bar{E}1,\bar{E}2$

$\dfrac{P_{b2}^{thr}}{P_{b1}^{thr}} = \dfrac{0.575}{Q_2/Q_1}$

Mode 1, Mode 2

Modes: TE_{021}, TE_{022}

Contour Plot of K_2 as a Function of $E1,E2$

$\bar{E}_{02}$

$$\frac{P_{b2}^{thr}}{P_{b1}^{thr}} = \frac{0.575}{Q_2/Q_1}$$

Mode 1, Mode 2

modes: TE_{021}, TE_{022}

$L = 5$
$r_0 = 0.51$
$\cdot = 1.14$
$\cdot = 1.5$
$s = 2$
$\cdot = 3.0$

Contour Plot of X_1 (MW)

$\bar{E}_{02}$

$\bar{E}_{01}$

$p_{b1}^{thr} Q_1 = 667.67$

Mode 1, Mode 2

Modes: TE_{021}, TE_{022}

L = 5
F_0 = 0.51
f = 1.14
q = 1.5
s = 2
A_t = 3.0

$\bar{E}_{02}$

$\bar{E}_{01}$

Contour Plot of x_2 (MW)

725
700
675
650
625
600
585
565
550
540
520
500
400

P_{b2}^{thr} Q_2 = 383.94

Mode 1, Mode 2
Modes: TE$_{011}$, TE$_{012}$

P_b = 62 kW

F_2 = 0

$\bar{E}_{02}$

$\bar{E}_{01}$

.06 .05

$\bar{L}$ = 8
r_0 = 0.48
γ = 1.14
α = 1.5
s = 1
A_1 = 3.5
Q_1 = 1000
Q_2 = 800
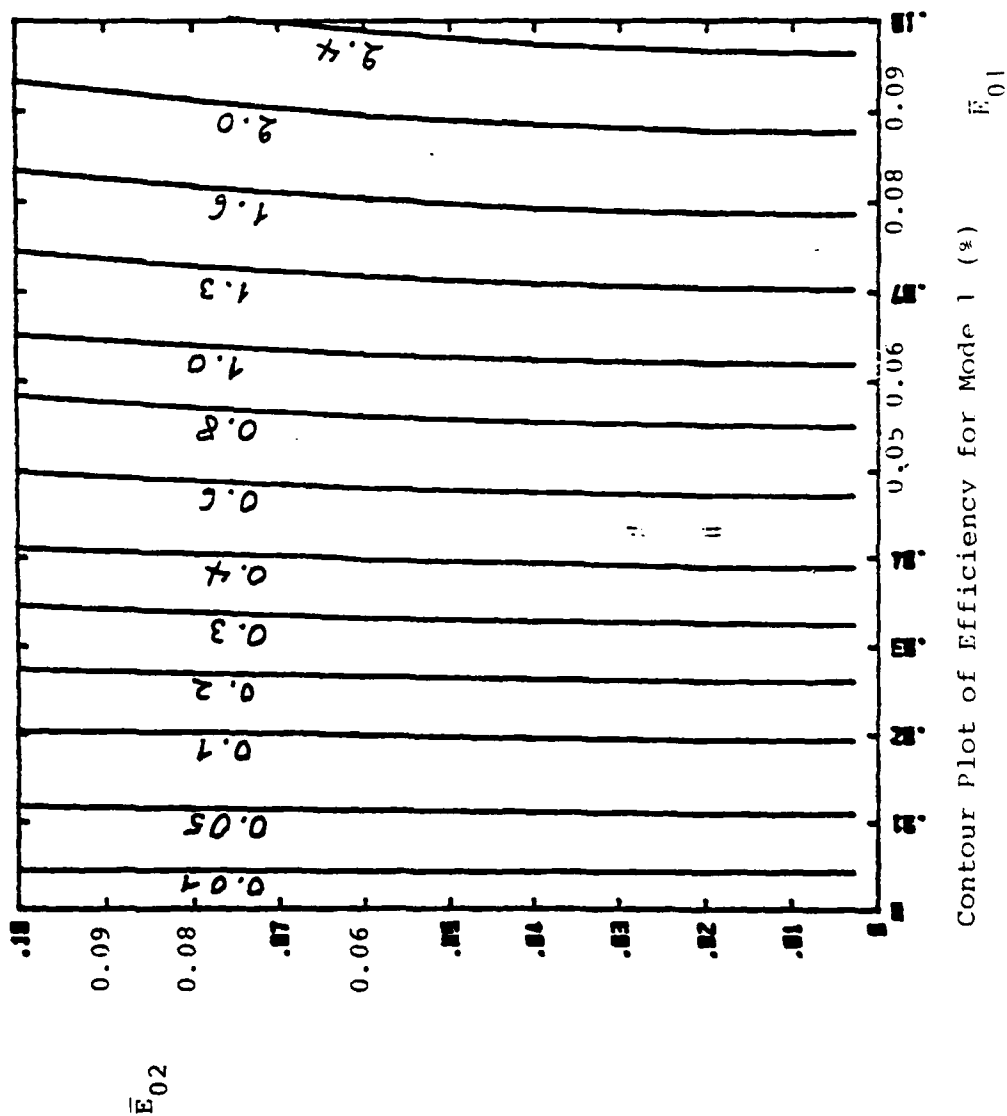
Mode 1, Mode 2

Modes: TE_{021}, TE_{022}

$L = 5$
$r_0 = 0.51$
$r = 1.14$
$u = 1.5$
$s = 2$
$\Lambda_1 = 3.0$

Contour Plot of Efficiency for Mode 1 (%)

$\bar{E}_{01}$

$\bar{E}_{02}$

Mode 1, Mode 2

Modes: TE_{021}, TE_{022}

$\bar{L} = 5$
$r_0 = 0.51$
$\gamma = 1.14$
$\alpha = 1.5$
$s = 2$
$A_1 = 3.0$

$\bar{E}_{02}$

2.4
2.0
1.6
1.3
1.0
0.8
0.6
0.4
0.3
0.2
0.1
0.05
0.01

0.08
0.06
0.05
0.06 0.08 0.09

$\bar{E}_{03}$

Contour Plot of Efficiency for Mode 2 (%)

Mode 1, Mode 2

Modes: TE_{021}, TE_{022}

$Q_2 = 3400$

$\overline{L} = 5$
$\overline{r}_o = 0.51$
$Y = 1.14$
$\alpha = 1.5$
$\Delta_1 = 3.0$
$s = 2$
$Q_1 = 4000$

Mode 1

Mode 2

Beam power (kW)

Efficiency (%)

30.0

20.0

10.0

200 600 1000 1400 1800 2200

Beam power (kW)

2200

1800

1400

1000

600

200

Modes: TE_{021}, TE_{022}

$\overline{L}$ = 5
$\overline{r}_O$ = 0.51
γ = 1.14
α = 1.5
Δ_1 = 3.0
s = 2
Q_1 = 4000
Q_2 = 3400

- - - Mode 1
——— Mode 2

100   200   300   400

Wave power (kW)

$s = 1$, $TE_{04\ell}$, $\overline{L} = 2.43$, $\gamma = 1.14$, $\omega = 1.5$, $\overline{r}_o = 0.138$

$Q_\ell = Q_1/\ell$

$W_b = 70$ keV, $v_o/v_{zo} = 1.8$, $L/r_w = 12$, $r_o/r_w = 0.48$

Constant magnetic field profile $Q_\zeta = Q_1/\zeta$
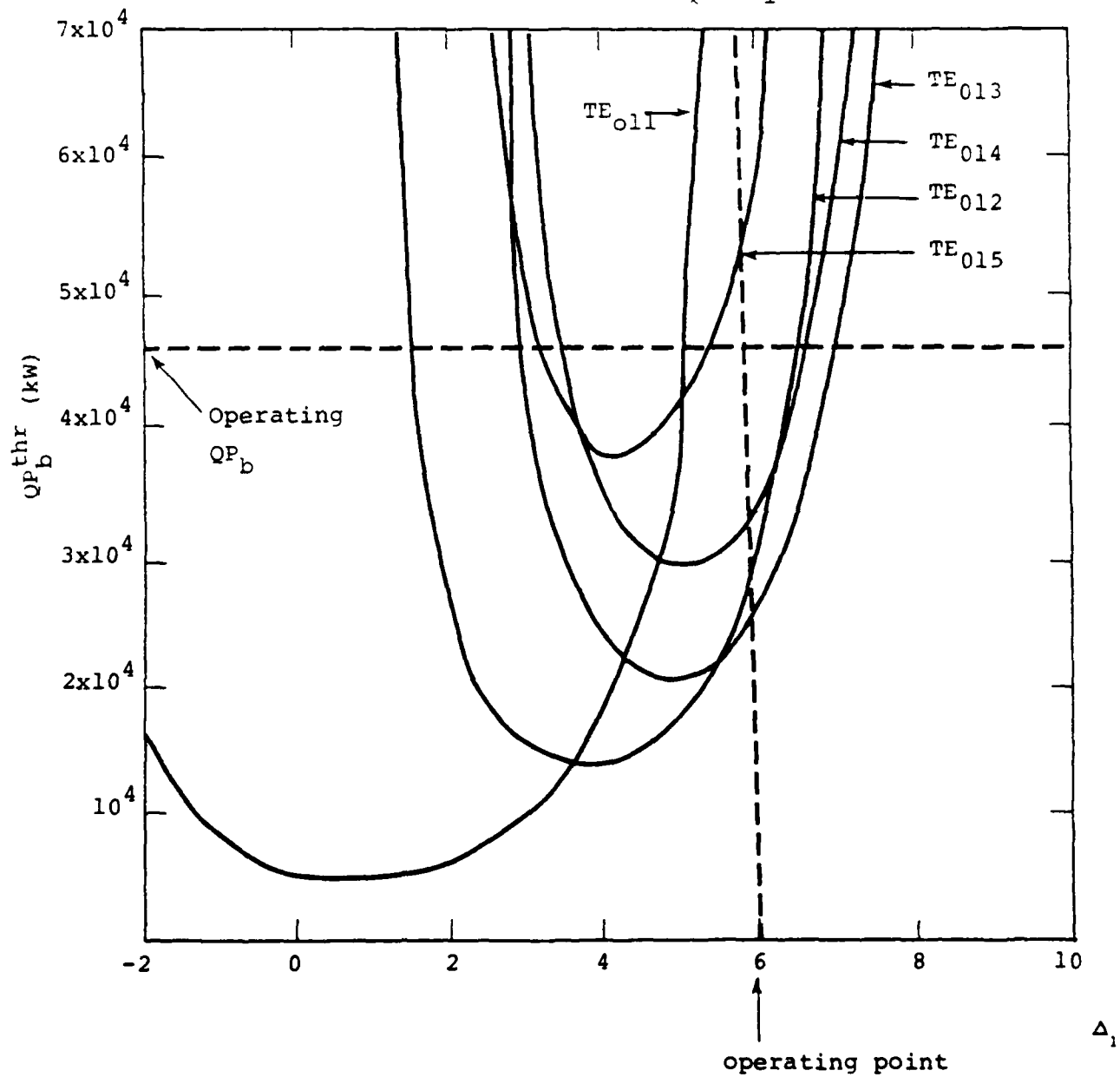
PUBLISHED CHARACTERISTICS OF EXPERIMENTAL GYROTRONS IN U.S.S.R.

	REF	POWER (kW)	FREQ., GHz (WAVE-LENGTH)	BEAM VOLTAGE (kV)	EFF. (%)	OPERATION	FIELD MODE	HARMONIC $s = \omega/\omega_c$	NOTES
OSCILLATORS									
1.	15	19	30 (8.9 mm)	-19	40	CW	π_{021}	2	
2.	15	39	36 (8.9 mm)	22	43	S.m.	π_{021}	2	Same device as above with pulsed operation
3.	10	230	38 (7.9 mm)	?	40	pulse	?	?	Possibly a second generation of device above
4.	16 10	12	103 (2.73 mm)	27	30	CW	π_{021}	2	
5.	3 10	22	150 (2.0 mm)	40	22	CW	π_{021}	2	
6.	17	10-30	138 (2.2 mm)	35	18	pulsed (2.5 ms)	π_{031}	?	
7.	17	10-20	153 (1.9 mm)	35	10	pulsed (2.5 ms)	π_{161}	?	Pulsed magnetic field
8.	18	10	60 (5 mm)	?	?	pulsed (2.5 ms)	π_{131}	?	Used for π_{13} to π_{11} mode converter units
9.	18	7	154 (1.95 mm)	25	11	pulsed	π_{231}	2	
10.	16	2.4	157 (1.91 mm)	13	9.5	CW	π_{031}	2	Same tube as above with different tuning
11.	16 10	1.5	333 (0.92 mm)	27	6	CW	π_{231}	2	Ref 16 reports field mode as π_{031}
12.	19	180	15 (2 cm)	40	45	?	π_{521}	?	Whispering gallery mode
13.	19	300	15 (2 cm)	40	30	?	π_{521}	?	Same as above tuned for optimum power
14.	19	300	15 (2 cm)	40	30	?	π_{911}	?	Coaxial cavity resonator
15.	18	1250	45 (6.7 mm)	65	35	pulsed 1-5 ms	?	1	
16.	10	1100	100 (3.0 mm)	48	34	pulsed 120 ns	?	1	
17.	14	300	86 (3.5 mm)	65	39	Long pulse ~100 ms	?	?	Long pulse version of above device for ICRH Plasma heating
Amplifier	10	"several kW"	"X-band"	?	70*	CW	?	?	*Stated efficiency of this gyroklystron is believed to be the transverse efficiency only

TABLE II

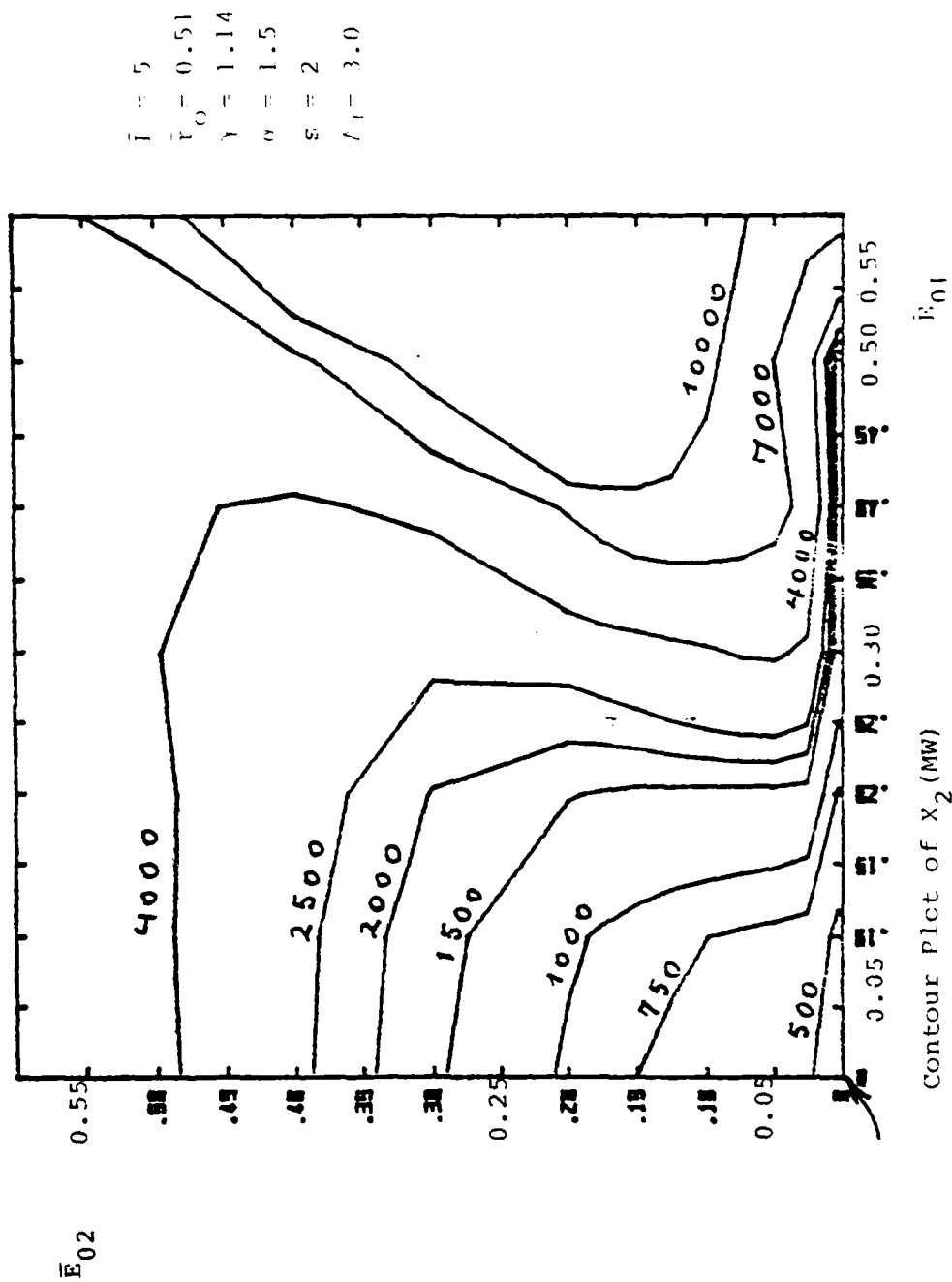PUBLISHED CHARACTERISTICS OF EXPERIMENTAL GYROTRONS IN U.S.A.

	REF	POWER (kW)	FREQ. GHz (WAVE-LENGTH)	BEAM VOLTAGE (kV)	EFF. (%)	OPERATION	FIELD MODE	HARMONIC s = ...	NOTES
OSCILLATORS	20	200	28	80	37	300 µs pulse (low duty)	π_{02}	1	Varian monotron (opt. power output)
	30	200	28	80	38	1 ms pulse (10 kW Ave.)	π_{02}	1	Long pulse (power supply limited)
	20	105	28	80	39	CW	Mixed	1	For ECRH
	31	150	35	70	31	pulse 150 ms	π_{011}	1	NRL Oscillator. Line width < 1.5 MHz.
AMPLIFIERS	31	18-20	35	71	8? max	pulse 1.5 µs	π_{01}	1	NRL Gyro-TWT, 32 dB maximum gain. Single section waveguide circuit.
	20	65	28	80	9	pulse 1 ms	π_{02}	1	Varian gyroklystron amplifier 40 dB gain
	28	20	10		8	pulse	π_{01}	2	Varian 3 cavity gyroklystron 10 dB small signal gain 6 dB saturated gain
	22	50	5		17	pulse	π_{11}	1	Gyro-TWT, 18-26 dB gain, 6% bandwidth

PRELIMINARY CONCLUSIONS

● The Q's for each mode are important in the determination of mode competition.

● For modes with azimuthal symmetry, there is indication that, as the beam power builds up, the mode with axial eigennumber $\ell = 1$ will eventually exclude all other higher order modes in the cavity.

● There is indication that a mode with infinite threshold beam power may be excited through the excitation of other modes first and subsequent mode conversion.
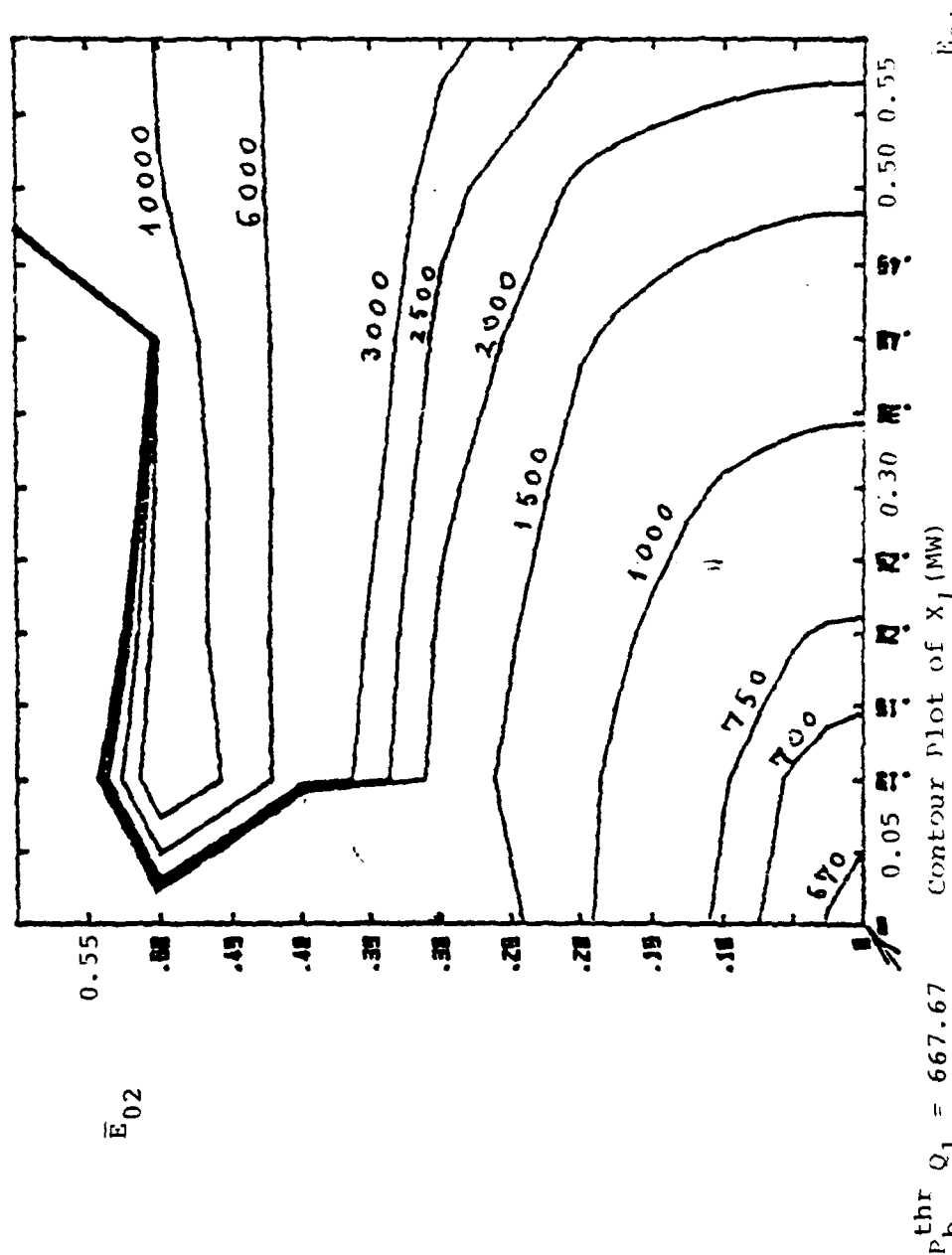
Mode 1, Mode 2

Modes: TE_{021}, TE_{022}

Contour Plot of X_2 (MW)

P_{b2}^{thr} $Q_2 = 383.94$

Mode 1, Mode 2

Modes: TF_{021}, TF_{022}

Contour Plot of X_1 (MW)

$\bar{E}_{02}$

$P_{b_1}^{thr} Q_1 = 667.67$

C-54

END

DATE
FILMED

2-83

DTIC